RICE UNIVERSITY

Electrophysiological investigation of prestin function: Impact of cysteine replacement and characterization of self-association during voltage stimulation
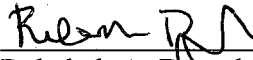
by

Ryan M. McGuire

A THESIS SUBMITTED
IN PARTIAL FULFILLMENT OF THE
REQUIREMENTS FOR THE DEGREE
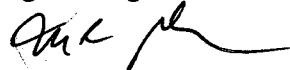
Doctor of Philosophy

APPROVED, THESIS COMMITTEE:

Robert M. Raphael
Associate Professor
Bioengineering

Rebekah A. Drezek
Associate Professor
Bioengineering, Electrical and Computer
Engineering

Michael C. Gustin
Professor
Biochemistry and Cell Biology

Fred A. Pereira
Assistant Professor
Huffington Center on Aging, Department of
Otolaryngology – Head and Neck Surgery,
Department of Molecular and Cellular Biology
Baylor College of Medicine

HOUSTON, TEXAS
MAY, 2009

UMI Number: 3362355

INFORMATION TO USERS

The quality of this reproduction is dependent upon the quality of the copy
submitted. Broken or indistinct print, colored or poor quality illustrations
and photographs, print bleed-through, substandard margins, and improper
alignment can adversely affect reproduction.
In the unlikely event that the author did not send a complete manuscript
and there are missing pages, these will be noted. Also, if unauthorized
copyright material had to be removed, a note will indicate the deletion.

UMI®

ABSTRACT

Electrophysiological investigation of prestin function: Impact of cysteine replacement

and characterization of self-association during voltage stimulation

By

Ryan M. McGuire

Almost 25 years ago unique piezoelectric activity was discovered in neuroepithelial cells of the mammalian cochlea. These cells, outer hair cells (OHCs), are mechanoelectrical transducers capable of converting changes in membrane potential into whole cell axial deformations. This so called reverse transduction allows OHCs to impart force upon surrounding structures that comprise the cochlear sensory organ, the organ of Corti. Electromotility has been suggested to serve as the cochlear amplifier since it provides cycle by cycle positive feedback that enhances basilar membrane motion. Without this active process, hearing sensitivity and frequency discrimination are profoundly diminished. The motor protein prestin has recently been identified as a critical component of OHC electromotility and thought to populate the 11 nm particles observed in freeze-fractured OHC lateral membranes as either oligomers or complexes with accessory proteins. The mechanism for prestin activity is unknown and a common method of study has involved mutation of the protein, expression in a surrogate system, and characterization of function using electrophysiology. Our mutational study of

prestin, involving replacement of cysteine residues, demonstrates that disulfide bonding is not required for oligomerization or function. Cysteine residues 196 and 415 are however critical to prestin activity, and might be important structural determinants of the protein's putative chloride binding pocket. We provide the first experimental evidence linking prestin conformational changes to function and report the discovery of voltage-dependent self-association. Voltage-dependent interactions provide a fluorescence signature for prestin activity and a molecular basis for the mechanism of electromotility. Finally, we have developed a biotinylated prestin reporter construct that allows extracellular binding of prestin, identification of the membrane localized fraction, and potentially provides a platform for forced oligomerization.

ACKNOWLEDGEMENTS

Without the assistance of others the work contained in this thesis would not have been possible. I would like to thank my graduate advisor, Dr. Robert Raphael for his endless enthusiasm for both science and the development of talent among young scientists.

I am also extremely grateful to each of my thesis committee members: Dr. Rebekah Drezek, Dr. Michael Gustin, and Dr. Frederick Pereira. Thanks to each of you for the valuable scientific advice you've provided as well as an occasional recommendation letter. I was very fortunate to have assembled a group of investigators with diverse interests and areas of expertise, but a common supportive nature.

In particular I would like to acknowledge the contributions of Dr. Frederick Pereira. Fred, any time I've needed help you've been there for me during this fulfilling, but sometime trying, training process. I cannot even begin to list all that I've learned from you. Your mentoring has made me a better scientist and I hope future research endeavors put us in collaboration once again.

The auditory research community in Houston has also been highly supportive and critical to the successful completion of my research project. I was very fortunate to have worked with many leaders in the field: Dr. William Brownell, Dr. Ruth Anne Eatock (now at Harvard Medical School), Dr. Brenda Farrell, Dr. John Oghalai, and Dr. Lavanya Rajagopalan. I am forever grateful for the assistance you provided during my struggles with the always challenging patch clamp technique. I would also like to thank key

personnel of the Pereira Laboratory: Haiying Liu, Dr. Lavanya Rajagopalan, and Dr. Celina Montemayor, for assistance with biochemistry and site-directed mutagenesis, friendship, and support. I'm grateful to my colleagues at Rice: Dr. Joff Silberg, Shirley Liu, Peter Nguyen, Crystal Stanworth, and Peng Zhai, for additional assistance with molecular biology and helpful project discussions.

I would also like to acknowledge past and present members of the Raphael Laboratory. Each and every person contributed positively to the past six years of my life. In particular I would like to thank Dr. Louise Organ, Dr. Jenni Greeson, Dr. Imran Quraishi, Dr. Yong Zhou, and (soon to be Dr.) Ramsey Kamar. In addition to this list I would like to acknowledge the contribution of Dr. Brandon Bucklen, who was not in our laboratory, but assisted with computer programming. I admire each of you as scientist and engineer, but must admit that this is greatly overshadowed by how much I value your friendships.

As is true in all stages of life, it's the friendships that make each day rewarding. I've made many great lifelong friends at Rice, and although I cannot list everyone who has inspired me, please know that I couldn't have achieved this goal without you.

To Crystal, thank you for believing in me, thank you for listening, and thank you for making me laugh. You are truly a bright light in my life, and I hope in upcoming years I get the opportunity to return the favor many times over.

Last, but not least, I would like to thank my family for the love and support that they provide each and every day. Mom, Dad, and Kevin, thanks for never letting me fall short of reaching my goals.

TABLE OF CONTENTS

LIST OF FIGURES

LIST OF TABLES

CHAPTER 1

INTRODUCTION

1.1 Research motivation and significance

Von Bâekâesy was awarded the Nobel Prize in 1961 for his discovery of tonotopic mapping within the cochlea, in which low frequency stimulation causes resonant basilar membrane vibration near the apex, whereas high frequencies cause selective vibration near the cochlear base (Von Bâekâesy 1960). This distributed passive response is the result of varying mechanical properties, in which the basilar membrane increases width and decreases stiffness toward the apex of the cochlea (Pickles 1988). The cochlea was later found to provide active amplification of basilar membrane motion (Rhode and Robles 1974), but it was not until the discovery of outer hair cell (OHC) motility (Brownell et al. 1985) that the cellular basis of the cochlear amplifier could begin to be understood.

OHCs undergo length changes of up to 5% in response to altered transmembrane potential, elongating under hyperpolarization and contracting under depolarization (Kachar et al. 1986; Ashmore 1987). Recently, this motility has been attributed to the motor protein prestin, using subtraction hybridization PCR (Zheng et al. 2000). The mechanism for prestin activity remains elusive, and amazingly, activity is independent of ATP, calcium, and the microtubule or actin systems (Kachar et al. 1986; Holley and Ashmore 1988; Kalinec et al. 1992) The motor is thought to undergo voltage-dependent structural rearrangements on the order of $0.4-8 \text{ nm}^2$ (Iwasa 1993; Santos-Sacchi 1993;

Gale and Ashmore 1994; Adachi and Iwasa 1999) that correspond to a net axial force of 5 nN in OHCs (Iwasa and Adachi 1997).

Prestin is a fascinating protein, clearly warranting detailed study. Prestin provides efficient conversion between mechanical and electrical energy (20 fC/nN) that exceeds the best man-made piezoelectric material (Dong et al. 2002). Our key findings contribute to the current understanding of prestin function. This thesis work was motivated by and fulfilled the following specific aims:

SA1: Characterize the effects of mutation of prestin cysteine residues on prestin function and oligomerization

SA2: Experimentally demonstrate prestin conformational change using fluorescence resonance energy transfer

SA3: Design a new reporter system for exogenously expressed prestin that allows labeling of the membrane localized protein

The first specific aim required site-directed mutagenesis, sequence verification, plasmid purification, and assessment of protein trafficking and membrane localization, prior to investigation of the aim. Construct development was the first molecular biology undertaking carried out by our research group. To evaluate function we used the whole-cell patch clamp method, which was the first implementation of this technique in our laboratory. As such all protocols were developed *de novo* in support of the project goals.

The second specific aim combined patch clamp procedures with our laboratory's existing expertise in florescence resonance energy transfer (FRET) methods. To couple

the two methods additional procedures were developed and implemented. This included adapting patch clamp equipment to create a shallow approach angle to accommodate confocal microscope optics, establishing methods for continuously monitoring cell membrane resistance, and synchronizing membrane scanning with adjustment of transmembrane voltage; this was all pioneering work.

The third specific aim was the most extensive cloning endeavor undertaken by our laboratory to date. We were motivated to design this reporter based on the results of the other two aims. The reporter allows clear identification of the membrane-localized fraction, and delineation from trafficking protein and protein retained in the endoplasmic reticulum – golgi apparatus system. It also provides a platform for forcing prestin interaction, allowing further study of the functional utility of higher order oligomers. In this thesis we develop the new reporter system, demonstrate proper localization, and show evidence of prestin activity.

1.2   Relation to previous work

Sulfhydryl reagents, which bind the thiol group of cysteine residues, have been shown to alter OHC motility (Kalinec and Kachar 1993) and prestin-associated charge movement when applied extracellularly (Santos-Sacchi and Wu 2004), indicating that cysteine residues reside in functionally important locations within prestin or prestin-associated proteins. Prestin is also known to form higher order oligomers (Matsuda et al. 2004; Navaratnam et al. 2005; Greeson et al. 2006; Zheng et al. 2006; Rajagopalan et al. 2007; Sturm et al. 2007; Detro-Dassen et al. 2008), but it is unknown if cysteine residues

contribute to these assemblies through intermolecular disulfide bonding, as some data suggests (Zheng et al. 2006). We provide the first mutational study that characterizes prestin oligomerization and function upon replacement of individual cysteine residues. Existing model of electromotility, either area change (Iwasa 1994; Iwasa 2000) or membrane bending (Raphael et al. 2000), incorporate prestin conformational change within the mechanism for cellular motility. Prestin-associated charge movement is likely the manifestation of prestin conformational change, however direct experimental confirmation is lacking. We provide the first direct observation of prestin conformational change by monitoring changes in prestin self-association at various imposed transmembrane potentials. Finally, many groups have suggested that the 8-11 nm particles observed in the freeze fractures of the lateral membrane of OHC (Gulley and Reese 1977; Forge 1991; Kalinec et al. 1992), are prestin tetramers (Zheng et al. 2006; Mio et al. 2008). To evaluate a potential functional role for prestin oligomerization we have developed a new tool that will allow forced association through cross-linking.

1.3   Thesis structure and organization

Chapter 2 provides relevant background information for the studies undertaken in this thesis. This chapter reviews auditory physiology, important results from studies of outer hair cell electromotility and prestin function, and provides a review of patch clamp technique, the method used for measuring capacitance and assessing prestin function. Chapter 3 addresses SA1 and is a traditional electrophysiological study of prestin function. Following a well-established paradigm, mutated forms of prestin are assessed

in a heterologous expression system, and prestin function characterized through its ability to move charge in the membrane. Chapter 4 satisfies SA2 and presents the results of a sophisticated experimental technique coupling quantitative fluorescence microscopy and electrophysiology. The local electrical environment of prestin is precisely controlled using patch clamp while prestin self-interaction is measured. Chapter 5 combines molecular biology and protein engineering to develop of a new research tool for studying prestin. In closing, the major contributions of the research are summarized (Chapter 6) and detailed plans for future studies, expanding on each major area of the thesis, are provided (Chapter 7).

CHAPTER 2

BACKGROUND

2.1   Auditory pathway

The process of hearing involves reception of sound pressure waves and delivery of this stimulus to the sensory organ of the inner ear. The system is highly sensitive and operates over an extensive range of frequencies. Human hearing is able to detect sound pressures as low as 20 micropascals (Gelfand 1981; Ashmore 2008) over a frequency range covering three orders of magnitudes, from 20 to 20,000 Hz (Geisler 1998).

The gross anatomy of the auditory system is diagrammed in Figure 2.1. Sound waves enter the outer ear and travel inward though the auditory canal toward the tympanic membrane. Vibration of this membrane sets the three articulated ossicles of the middle ear into motion (Fig. 2.1). The ossicles, or middle ear bones, transmit sound-induced vibrations to the cochlea, a coiled structure that resembles a snail shell and houses sensory epithelium called the organ of Corti. Membrane motion within the cochlea is detected by neuroepithelial cells known as hair cells that reside within the organ of Corti. Hair cells possess a tuft of stereocilia that protrudes from their apical end and is specialized for mechanoelectrical transduction. These cells detect membrane motion and stimulate the auditory nerve to allow perception of sound by the brain.
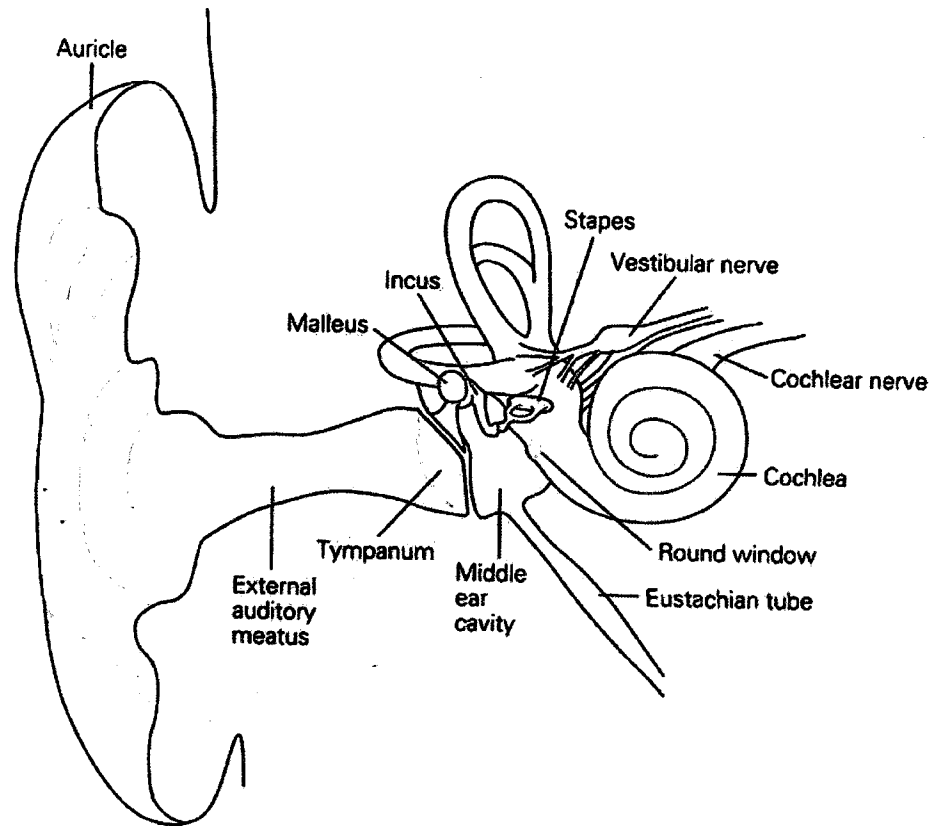
FIGURE 2.1 Gross anatomy of the auditory system. Sound waves travel down the auditory canal, to the middle ear where they are transduced into a fluid pressure wave that propagates through the spiral turns of the cochlea. Transduction is carried out by the inner ear bones: the malleus, incus, and stapes which resemble a hammer, anvil, and stirrup, respectively. Within the cochlea specialized hair cells transduce membrane motion, induced by the fluid pressure wave, into electrical signals that are relayed to the brain via the auditory nerve. Figure from (Kandel et al. 2000).

2.2   Cochlear physiology

In humans the cochlea is 34 mm long (Ashmore 2008) and spirals two and three-quarter turns to the apex. In cross-section the coils are revealed to contain three fluid filled compartments (Fig. 2.2). The scala vestibuli and scala tympani are continuous compartments that are linked at the helicotrema, or apex of the cochlea. Motion of the footplate of the stapes at the oval window creates a pressure wave in the scala vestibuli that is readily transmitted across Reissner's membrane, a thin two cell layer boundary, into the scala media. As the traveling fluid pressure wave propagates toward the apex of the cochlea it simultaneously induces vibration of the basilar membrane (BM). The stiffness and width of this membrane varies along the length of the cochlea, and BM oscillation is maximized at the location where the membrane's characteristic resonant frequency matches that of the incoming pressure wave (Pickles 1988). Sensory hair cells, located in the organ of Corti, are anchored to the BM by supporting cells (Fig. 2.3). The organ of Corti contains a single row of inner hair cells (IHCs) and 3-4 rows of outer hair cells (OHCs). Both classes of cells have stereocilia whose deflection is dependent on BM motion. Deflection of hair cell stereocilia causes opening of mechanically gated ion channels. This process, known as mechanotransduction, is further described in the following section, and is ultimately responsible for the electrical signaling that encodes sound.
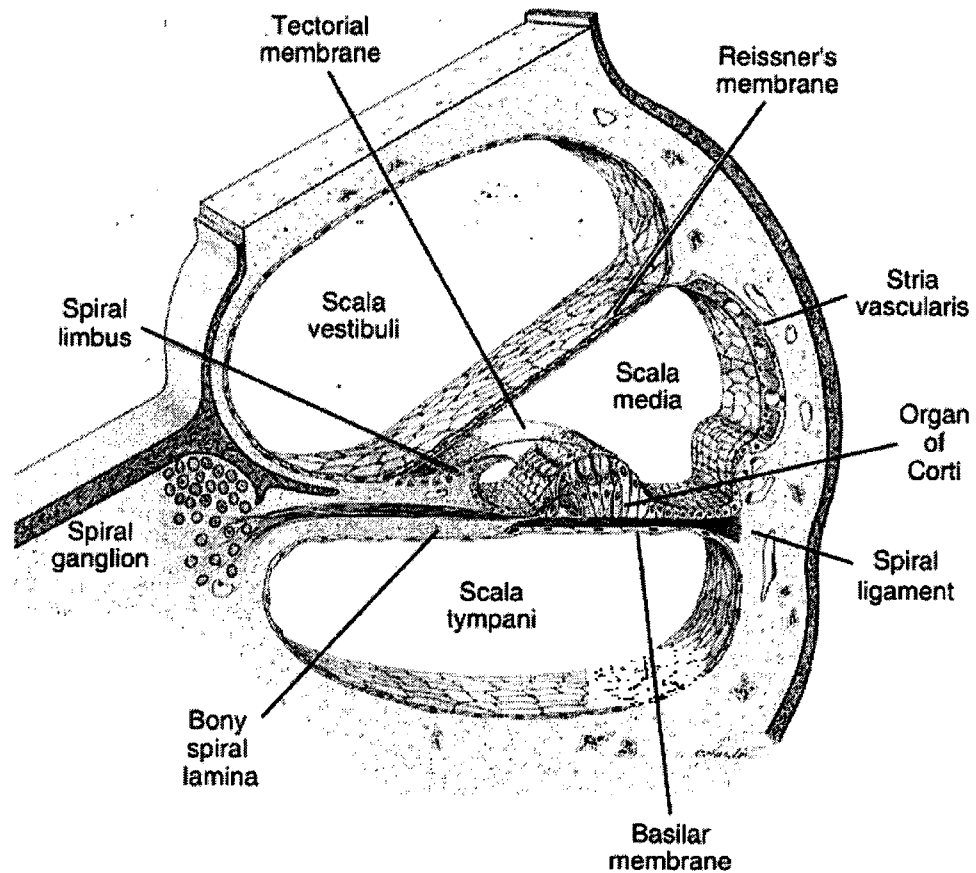
FIGURE 2.2 Cross-section of a cochlear turn. A cross-section of a turn reveals that the coils of the cochlea are composed of three compartments, the scala vestibuli, media, and tympani. Pressure wave are input into the scala vestibuli and transferred across Reissner's membrane into the scala media. These waves cause motion of the basilar membrane that is detected by hair cells within the organ of Corti. Figure from (Geisler 1998)
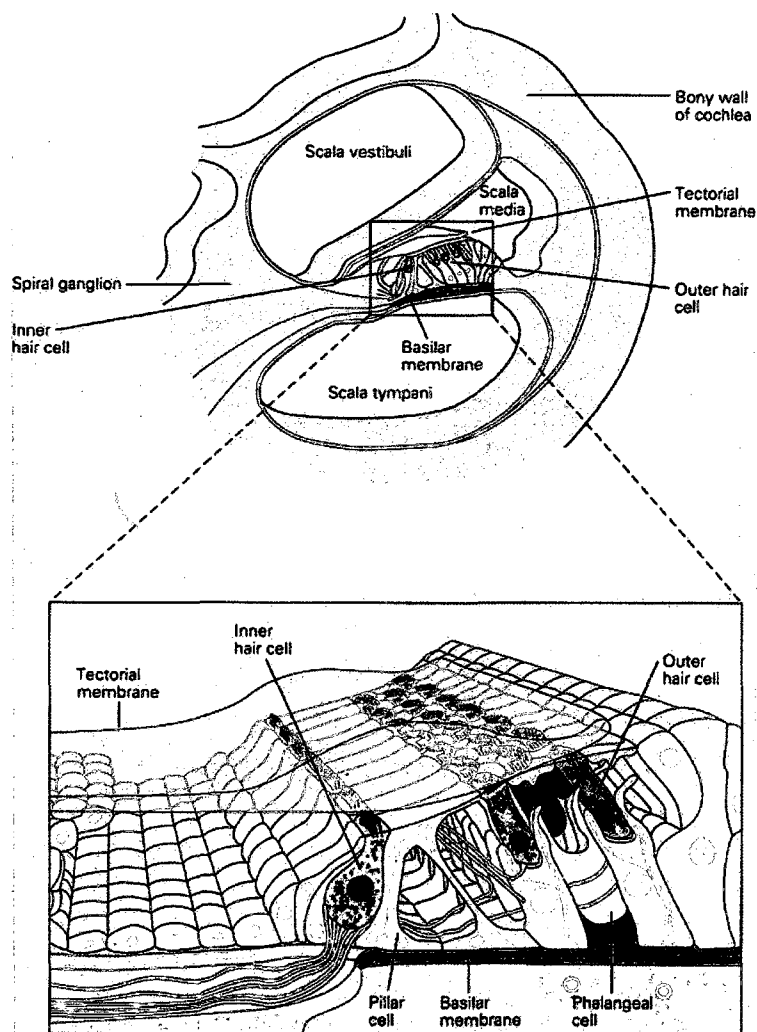
FIGURE 2.3 Cellular organization of the organ of Corti. Sensory hair cells, including a single row of inner hair cells (IHCs) and 3-4 rows of outer hair cells (OHCs), are attached to the basilar membrane by a variety of supporting cells. Specifically, OHCs are connected to the basilar membrane though supporting cells called Deiter (or Phalangeal) cells (Geisler 1998). The apical portion of OHCs is secured by a connective tissue called the reticular lamina (RL) and the stereocilia tips are inserted into a gelatinous substrate called the tectorial membrane (TM). IHC stereocilia are in close opposition, but not inserted into the TM. Figure from (Kandel et al. 2000).

Unique ionic environments in specific compartments of the cochlea provide the concentration gradients necessary for mechanotransduction. The scala vestibuli and tympani contain perilymph, which has a high Na^+ composition, similar to cerebral spinal fluid. Perilymph bathes the basolateral walls of the hair cells. The apical region of the hair cell faces a high K^+ fluid called endolymph, which is generated and maintained in the scala media by active transport mechanisms. The endolymph is at a high positive potential, whereas the other compartments are at or near the potential of the surrounding bone (Pickles 1988). This difference in potential, referred to as the endocochlear potential, has been measured as +80 mV relative to the perilymph (Salt et al. 1987). The tissue adjacent to the scala media named the stria vascularis contains marginal cells that are responsible for the endolymph composition.

2.3   Hair cells and mechanoelectrical transduction

Hair cells are specialized receptor cells present in both the vestibular system and the cochlea. At the apical end of the cell stereocilia of 0.1 to 0.3 μm diameter protrude from a rigid and flat cuticular plate (Pickles 1988). The stereocilia are stiff projections composed of tightly packed hexagonal arrays of actin bound by fimbrin (Geisler 1998). At the insertion point into the cuticular plate, the diameter of each stereocilium is reduced, creating a pivot point that allows deflection when the fibers are subjected to lateral forces (Pickles 1988).

Cochlear hair cells have 50 to 100 stereocilia that are arranged in a staircase pattern with each successive row containing taller stereocilia than the previous. They move as a unit since adjacent stereocilia are connected by protein linkages (Geisler 1998). Lateral links form horizontal connections among the rows and between stereocilia in individual rows. Tip links, a fine filament made of cadherin 23 (Sotomayor et al. 2005), connect the top of shorter stereocilium with the lateral wall of stereocilium in the taller neighboring row. The tip link acts as a gating spring for an unidentified mechanosensitive cation channel, which is located within the stereocilia lateral wall.

At rest the tip link is under low levels of tension and the stretch-sensitive cation channel conducts about 10% of the time (Geisler 1998; Kandel et al. 2000). A small, but steady flux of cations, primarily K^+ since this is the predominant species in the endolymphatic fluid, enters through these channels when the hair bundle is in the neutral position. Deflection of the bundle toward the largest stereocilium increases the tension in the tip link and consequently opens the mechanosensitive ion channel. This greatly increases the inward flux of cations (K^+ and Ca^{2+}) from the endolymph and depolarizes the hair cell. Rotation of the stereocilia in the opposite direction, toward the shorter neighbors, minimizes the tension in the gating spring, and has the net effect of hyperpolarizing the hair cell (Fig. 2.4).
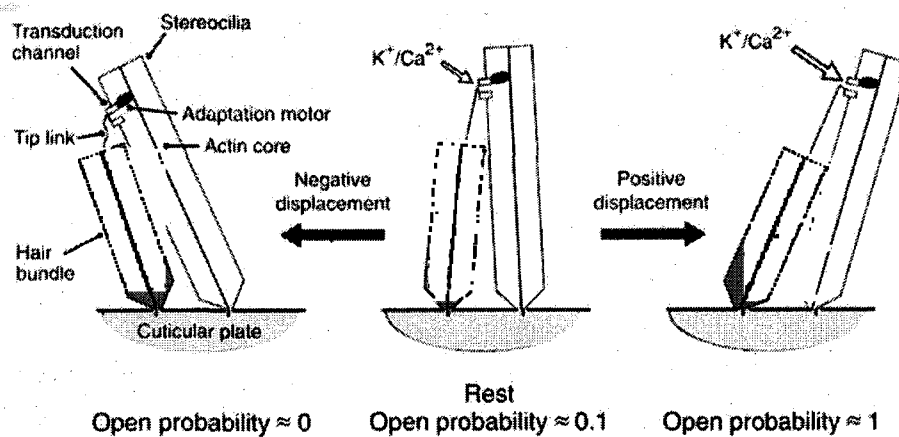
FIGURE 2.4 Gating of the mechanotransduction channel via the tip link. Changing the tension of the tip link changes the conductance probabilities of the non-specific cation channel. Figure from (Geisler 1998)

The microstructure of the organ of Corti enables hair cells to detect BM motion via stereocilia displacement and mechanotransduction. The cuticular plates of the OHCs are secured by a connective tissue called the reticular lamina (RL) and the stereocilia tips of OHC are inserted into a gelatinous substrate called the tectorial membrane (TM). Upward movement of the BM causes the RL to rock upwards and inwards, inducing rotation of the stereocilia toward the largest member and hair cell depolarization (Guyton and Hall 2000). Conversely, downward motion of the BM rocks the RL down and outwards, and induces hyperpolarization. IHC stereocilia are in close opposition, but not inserted to the TM. Fluid flow in the space between the TM and the RL causes inner hair cell (IHC) stereocilia displacement. The mechanical properties of the BM determine the location of maximum displacement for a particular frequency stimulus and therefore selective activation of hair cells. Varying BM mechanical properties along the length of the cochlea therefore accounts for the tonotopic organization of the cochlea, meaning that hair cells in the base selectively respond to high frequency sounds and those in the apex respond to low frequency stimulus.

The cochlea contains 3,500 IHCs and 12,000 OHCs that serve distinct functional purposes (Guyton and Hall 2000). IHCs receive up to 95% of the auditory nerve's afferent innervation and serve as the primary sensory cell of the cochlea (Jahn and Santos-Sacchi 1988). IHC stereocilia displacement results in release of neurotransmitter, and firing of afferent neurons. OHCs respond by undergoing whole cell length changes (Brownell et al. 1985), and this process, termed electromotility, is responsible for the

sensitivity and frequency selectivity of the cochlea. The details of electromotility are discussed in the following sections.

2.4   Outer hair cell electromotility

2.4.1   Cochlear amplifier

Detection of the cochlear microphonic (Wever and Bray 1930), an extracellular field potential recorded within and around the cochlea, provided an early piece of evidence hinting toward the existence of active amplification. Discovery of otoacoustic emissions (Kemp 1978) provided support for active cochlear processes, since sound could be detected emanating from a normally functioning inner ear. Loss of OHCs, by noise damage, or by chemical ablation, parallels a loss of tuning and a rise in the firing threshold of the auditory nerve, demonstrating the physiological importance of this class of cell (Ryan and Dallos 1975; Evans and Harrison 1976; Kiang et al. 1976; Dallos and Harris 1978). The OHC is cylindrically shaped and varies in length along the cochlea. The cells at the basal high-frequency location are short (~15 μm) compared to those at the low-frequency apex (>80 μm) (He et al. 2006; Ashmore 2008). The key feature of these cells is their ability to undergo axial length changes in response to altered transmembrane potential (Brownell et al. 1985), a process termed electromotility. The cells change length by 4-5% (Ashmore 1987), with hyperpolarization leading to elongation and depolarization causing contraction (Fig. 2.5). Currently, the consensus is that OHCs provide a frequency dependent boost to BM motion, which enhances the mechanical input to IHCs, thereby promoting enhanced tuning and amplification (He et al. 2006).
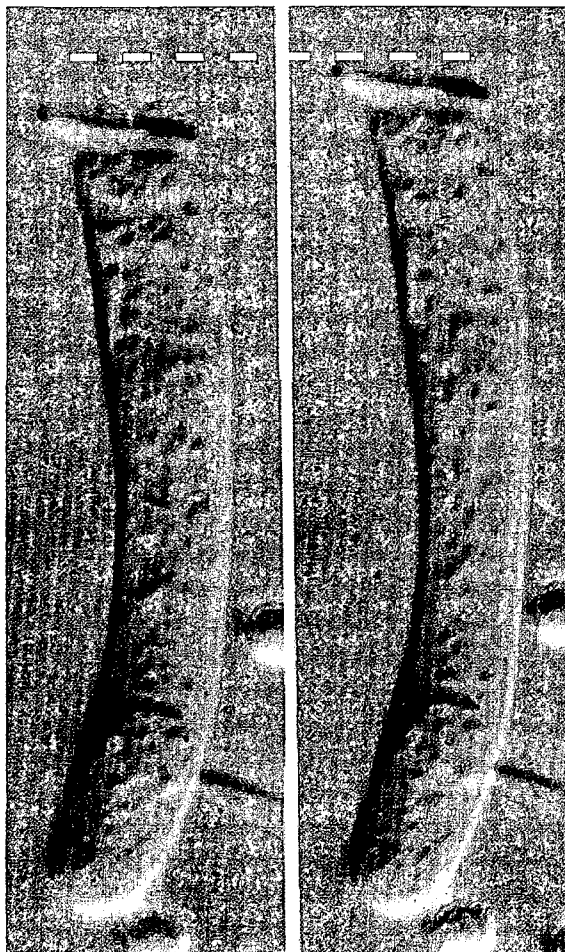
FIGURE 2.5 OHC electromotility. An OHC from the apical turn of the adult guinea pig cochlea is pictured. The cell is contracted when voltage clamped at +50 mV (left), whereas it becomes elongated when clamped at a command potential of -150 mV (right). Figure from (Holley and Ashmore 1988).

2.4.2 Nonlinear capacitance

Large displacement currents, analogous to the gating currents of ion channels (Sigg et al. 2003), accompany OHC electromotility (Ashmore 1990; Santos-Sacchi 1991). This current is the time rate of change of charge redistribution within the membrane in response to a changing electric field. Both OHC length change and measured charge movement show sigmoidal dependence on transmembrane voltage that saturates at extreme potentials (Fig. 2.6). Equivalently, the charge movement can be displayed as capacitance by taking the derivative with respect to voltage. The resulting bell-shaped curve is commonly referred to as nonlinear capacitance (NLC), since membranes without active components display only uniform, linear capacitance (~0.01 pF/μm^2). The tight coupling between OHC motility and NLC has established this measure as a reliable "electrical signature" of electromotility (Dallos and Fakler 2002; Santos-Sacchi 2003), and therefore a surrogate measure of OHC function. NLC measurements are obtained using patch clamp technique which is described in Section 2.6
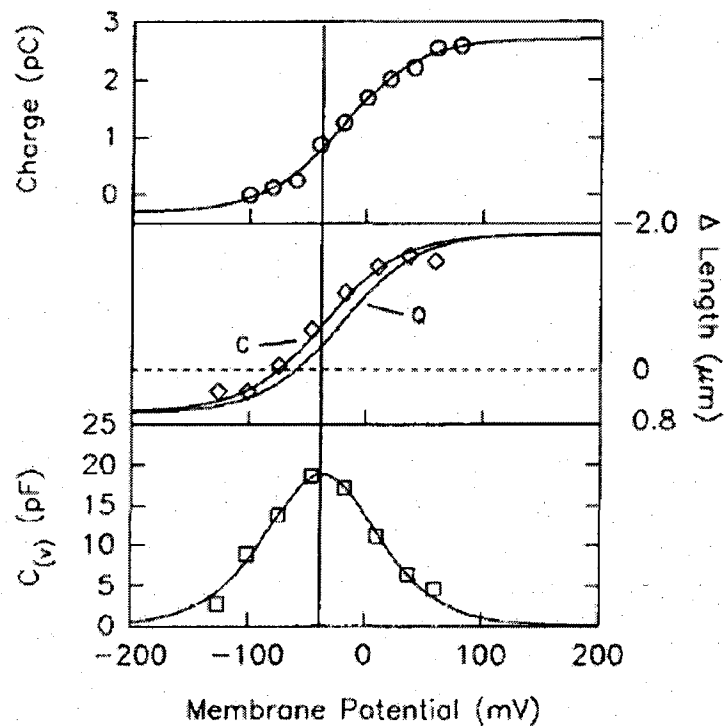
FIGURE 2.6 Voltage dependence of OHC charge movement, length change, and capacitance. Charge movement was determined by applying voltage steps and analyzing the resultant transient currents (circles). Capacitance was directly obtained by imposing a sinusoidal command voltage and measuring the current response (squares). Fits to both electrical measures closely approximate measured OHC length change (diamonds). Figure from (Santos-Sacchi 1991).

Charge movement and length change of the OHC motor are commonly modeled as a two-state transition and fit by a Boltzmann function. NLC is therefore fit by the derivative of the two-state Boltzmann function. Details of this procedure are specified in the experimental methods (Chapters 3-5), however the variable parameters of the fit include: Q_{max}, the maximum nonlinear charge movement provided by the motor; $V_{1/2}$, the voltage at which half-maximal charge transfer occurs, or equivalently, the voltage of peak nonlinear capacitance; and z, the valence of charge movement. Valence may represent a fractional elementary charge moved across the membrane, or the fraction of lipid bilayer traversed by a whole elementary charge. For OHCs from the low frequency region of the cochlea typical observed values include 2.5 pC, -40 mV, and 0.8, respectively (Santos-Sacchi 2003; Ashmore 2008). When prestin is expressed in heterologous systems Q_{max} is decreased by a factor of ten and $V_{1/2}$ hyperpolarized 20-30 mV, but z is nearly identical.

2.4.3   Characteristics of the motor

OHC electromotility occurs independent of ATP hydrolysis (Kachar et al. 1986; Holley and Ashmore 1988) and in the absence of intracellular calcium (Ashmore 1987). OHC motility persists even upon disruption of the actin or microtubule systems (Holley and Ashmore 1988). Taken together these data demonstrate that the OHC motor is not a conventional motor protein and distinctly different from myosin, kinesin, or dynein.

A variety of experimental evidence indicates that the motor is localized to the lateral membrane. Freeze fracture of the OHC lateral plasma membrane reveals a dense array of particles on the inner surface of the cytoplasmic leaflet (Gulley and Reese 1977).

These particles are 8-11 nm in diameter with an estimated packing density of $3000/\mu m^2$ (Kalinec et al. 1992) to $6000/\mu m^2$ (Forge 1991). OHC particle density exceeds that of IHCs ($\sim 2400/\mu m^2$) and non-motile, non-mammalian hair cells ($\sim 2100/\mu m^2$), and therefore might represent the OHC motor complex. Furthermore, OHC particle density is initially low and increases (Souter et al. 1995) during the onset of OHC motility (He et al. 1994). In microchamber experiments portions of the cell outside the chamber receive stimulation of opposite polarity to the externally exposed membrane. For example, a current passed down the chamber can hyperpolarize the membrane within the microchamber and simultaneously depolarize the external portion. By altering the extent of OHC insertion into the microchamber, motility was confirmed along the length of the lateral wall and the contribution of the motors was found to sum (Dallos et al. 1991). In a more quantitative approach, the motor was localized to the lateral wall through electrical amputation (Huang and Santos-Sacchi 1993). In this setup OHCs are partially contained within a microchamber and patch clamped at the free end. When identical voltage clamp stimulus are simultaneously delivered only the portion of the membrane outside the chamber is excited, and varying OHC insertion revealed NLC was restricted to the lateral wall. Clear evidence of a membrane based mechanism was demonstrated by maintenance of normal NLC despite removal of intracellular structures by internal digestion with trypsin (Huang and Santos-Sacchi 1994). This result was replicated with pronase (Takahashi and Santos-Sacchi 2001), a stronger protease that offers nearly complete digestion of native proteins to individual amino acids.

The motor is able to operate at frequencies relevant for hearing. Initial experiments using a microchamber were able to verify electromotile function up to 22

kHz (Dallos et al. 1991). Later, monitoring the deflection of an atomic force microscope tip demonstrated that the motor operates at speeds up to 79 kHz (Frank et al. 1999). Importantly, OHCs remain effective throughout the auditory frequency range. OHCs produce forces of ~0.1 nN/mV (Hallworth 1995; Iwasa and Adachi 1997) that are constant up to at least 50 kHz (Frank et al. 1999)

The most well-known pharmacological inhibitor of OHC electromotility is salicylate, the active metabolite of aspirin. This compound blocks NLC and motility (Shehata et al. 1991; Tunstall et al. 1995) and since it is amphipathic its effects are observed from either side of the membrane (Kakehata and Santos-Sacchi 1996). The data we provide in Chapter 4 provides new insight into the mode of salicylate inactivation, demonstrating the molecules ability to modulate prestin's conformational state. Sulfhydryl agents, which bind the thiol group (-SH) of cysteine residues, constitute another class of compound that affects OHC function. Organomercurials, the most penetrating sulfhydryl agents (van Iwaarden et al. 1992) strongly inhibit electromotility (Kalinec and Kachar 1993). Conversely, surface reactive compounds, unable to permeate the membrane, such as N-ethylmaleimide (NEM), dithiothreitol (DTT) and diamide do not affect motility.

2.4.4 *Models of electromotility*

Although a variety of phenomenological models have attempted to describe electromotility, two models, the area motor (Dallos et al. 1993; Iwasa 1994) and membrane bending (Raphael et al. 2000) models, currently receive the most attention.

According to the area motor model, hyperpolarization of the motor induces a conformational change to an elongated state, and the concerted action of many motor complexes mediates elongation of the OHC lateral wall. The fluctuation between states is suggested to provide 0.4-8 nm^2 area change in the plane of the membrane (Santos-Sacchi 2003). High motor density supports this theory, and the charge density and corresponding motor density within the OHC lateral wall have been estimated from NLC parameters to be near 8000 $e^-/\mu m^2$ and 10,000/μm^2, respectively (Huang and Santos-Sacchi 1993; Gale and Ashmore 1997).

The membrane bending model suggests that reorientation of membrane dipoles due to changing transmembrane potential alters the nanoscale curvature of the membrane. In this model, motor protein conformational change may initiate membrane curvature changes or occur as a secondary effect. The curvature changes are transmitted to the actin-spectrin cytoskeleton and result in OHC length change (Fig. 2.7). Membrane bending has been supported by experimental evidence showing the effect of salicylate and chlorpromazine, compounds which alter curvature, on the magnitude and voltage dependence of OHC motility and NLC (Brownell et al. 2001; Lue et al. 2001; Morimoto et al. 2002). The model also explains reduced OHC force generation upon disruption of spectrin by diamide (Adachi and Iwasa 1997). Amphipathic molecules have been shown to induce changes in membrane curvature (Greeson and Raphael 2009) and alter NLC (Fang and Iwasa 2007). Additionally, curvature changes have been predicted to result from voltage-dependent protein aggregation (Kim et al. 1998). Each of these factors, in addition to the fact that neither of the proposed models of electromotility has a firmly

established molecular basis, motivate our study of the effects of voltage stimulation on prestin-prestin interactions, which is described in Chapter 4.
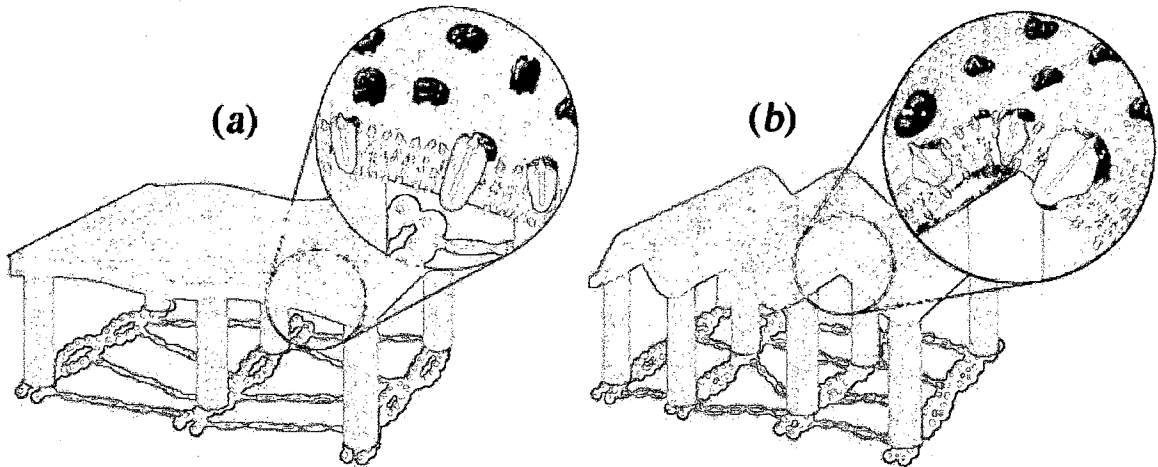
FIGURE 2.7 Membrane bending model of electromotility. In a changing electrical field, reorientation of membrane dipoles is suggested to alter the nanoscale curvature of the membrane. Since the actin-spectrin cytoskeleton, or cortical lattice, of the OHC is anchor to the plasma membrane by pillar proteins, membrane deformation causes (a) elongation of the cell under hyperpolarization, or (b) contraction upon depolarization. Figure from (Brownell et al. 2001)

2.5   The motor protein prestin

2.5.1   Identification and evidence of the OHC motor

The OHC motor protein was identified in 2000 through comparison of cDNA libraries between motile OHCs and non-motile IHCs (Zheng et al. 2000). The subtracted libraries revealed a protein that was able to produce the hallmarks of electromotility in a heterologous expression system.

The protein, named prestin, endowed TSA201 cells with NLC, and when aspirated into a microchamber showed voltage-induced cellular displacement of 0.2 μm (Zheng et al. 2000). Both NLC and motility were inhibited by salicylate application. Expression of the prestin gene (Zheng et al. 2000), the prestin protein (Belyantseva et al. 2000) and the emergence of electromotility (He et al. 1994) all coincide. Prestin location, identified through antibody labeling of OHCs (Belyantseva et al. 2000), is restricted to the OHC lateral membrane in agreement with the results of microchamber experiments and freeze fracture data, which both localized the motor complex to this region. 8-13 nm particles were observed through atomic force microscopy (AFM) imaging studies in prestin transfected CHO cells (Murakoshi et al. 2006), and this also supports the previous interpretation of the freeze fracture data. AFM measurements also revealed that HEK cells expressing prestin generate mechanical forces that were frequency independent up to at least 20 kHz (Ludwig et al. 2001).

A number of pieces of evidence gathered at the systems level also indicate prestin's involvement in the OHC motor complex. OHC from prestin knock-out mice

lack somatic motility, and those mice exhibit a 40-60 dB loss in hearing sensitivity (Liberman et al. 2002) and lack frequency sensitivity (Cheatham et al. 2004). Prestin deficient mice with a knock-in copy of non-functional prestin, the V499G/Y501H double amino acid replacement (Zheng et al. 2005), also show drastic hearing loss (Dallos et al. 2008). A missense mutation to the prestin gene has also been identified in a patient with non-syndromic hearing loss (Toth et al. 2007).

2.5.2   Structure

The *Prestin* gene encodes a protein of 744 amino acids with a predicted molecular weight of 81.4 kDa (Zheng et al. 2000; Matsuda et al. 2004). The crystal structure is currently unknown, but hydrophobicity analysis indicates that prestin is composed of up to 12 transmembrane domains (TMDs) long enough to span the membrane as either α-helices or β-sheets (Dallos and Fakler 2002). Both N- and C-termini have been shown to be cytoplasmic (Zheng et al. 2001). Reports demonstrating phosphorylation by cGMP-dependent kinase (Deak et al. 2005) and N-linked glycosylation (Matsuda et al. 2004; Iida et al. 2005) support a 12-pass model with re-entrant loops (Deak et al. 2005). In an alternate expression system glycosylation was not detected and therefore a 10-pass model has also been proposed (Navaratnam et al. 2005). Both topological models are presented and insight gained from our study of cysteine replacement mutants is detailed in Chapter 3.

Prestin is a member of a class of anion transporters called Solute Carrier Family 26 (SLC26). Prestin is unique to the family since each of the other members have established transport function (Mount and Romero 2004), and closely related family

members, pendrin (SLC26A4) and PAT1 (SLC26A6), do not exhibit NLC (Zheng et al. 2000; Oliver et al. 2001; Zheng et al. 2001). SLC26 proteins share several conserved features including a hydrophobic core, a sulfate transport motif (STM) and a C-terminal sulfate transporter and anti-sigma (STAS) domain. In prestin, helices near the STM are tightly packed and critical for NLC function (Rajagopalan et al. 2006). The role of the prestin STAS domain is unknown, but STAS has been shown to be important for plasma membrane localization, regulation of protein-protein interaction, and sulfate transport activity in other systems (Shibagaki and Grossman 2004; Rouached et al. 2005; Shibagaki and Grossman 2006).

2.5.3   Voltage sensing

Prestin shares the greatest sequence homology with PAT1, however PAT1 does not exhibit NLC. In an attempt to understand prestin voltage sensing, charged residues from the prestin hydrophobic core, which were not conserved with PAT1, were substituted by neutral amino acids, either individually or in groups (Oliver et al. 2001). The replacements did not abolish NLC, and therefore it was concluded that prestin voltage sensing is not an intrinsic property. Membrane patches from prestin transfected cells in varying patch clamp configurations (Section 2.6.1, Fig. 2.10) and ionic environments demonstrated that prestin function requires intracellular Cl⁻ (Oliver et al. 2001). Intracellular Cl⁻ depletion reduces charge density and shifts $V_{1/2}$ to depolarized potentials (Fakler and Oliver 2003; Rybalchenko and Santos-Sacchi 2003; Santos-Sacchi et al. 2006) suggesting two mechanisms of voltage sensing. Cl⁻ ion(s) bind prestin and are either directly involved in charge translocation (Dallos et al. 2006), or cause an allosteric change that allows outward movement of a positive gating charge in response

to depolarized transmembrane potential (Rybalchenko and Santos-Sacchi 2003; Rybalchenko and Santos-Sacchi 2008). Under both scenarios membrane hyperpolarization places prestin in an elongated conformational state and depolarization causes contraction (Fig. 2.8).

Salicylate competitively binds prestin with 300 times the affinity of Cl^-, but provides comparatively small charge movement (Oliver et al. 2001). This effectively blocks electromotility and likely explains the mechanism for hearing loss induced by aspirin overdose.

Short state
(depolarized)

Long state
(hyperpolarized)

cell membrane

prestin molecule

Cl$^-$ binding site

Cl$^-$
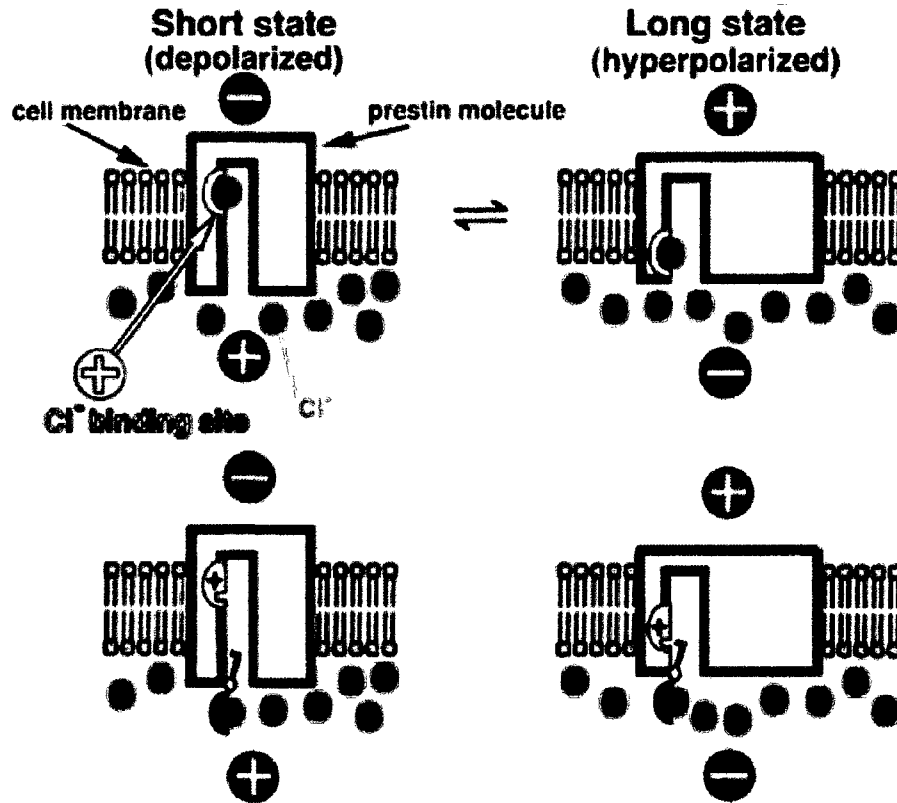
FIGURE 2.8 Two models of chloride-dependent prestin activity. *Top*: Since an intrinsic voltage sensor has not been discovered and intracellular anions were found to be essential for prestin activity, a model was proposed in which Cl$^-$ functions as an extrinsic voltage sensor (Oliver et al. 2001). Cl$^-$ is assumed to associate with a positively charged binding site and the combination is translocated in response to changes in transmembrane potential. Movement of this gating charge has been suggested to correspond with the contracted and elongated conformational states of prestin. *Bottom*: Alternately, Cl$^-$ has been suggested bind, allosterically modify prestin, and unlock movement of a positive gating charge which modulates prestin conformation (Rybalchenko and Santos-Sacchi 2003; Rybalchenko and Santos-Sacchi 2008). Figure from (Dallos et al. 2006).

2.5.4 Prestin interactions

Prestin forms higher order oligomers and these interactions have been measured biochemically using Western blot (Matsuda et al. 2004; Zheng et al. 2006; Rajagopalan et al. 2007; Sturm et al. 2007; Detro-Dassen et al. 2008), optically through fluorescence resonance energy transfer (FRET) in heterologous expression systems (Navaratnam et al. 2005; Greeson et al. 2006), and verified *in vivo* through yeast two-hybrid assay (Zheng et al. 2006). Monomer, dimer, trimer, and tetramer populations are typically observed, but it is unknown if the various oligomeric states serve a functional role. It has been suggested that prestin dimers are composed of disulfide-bonded monomers and the prestin tetramers are assembled by hydrophobic interaction of dimers (Zheng et al. 2006). The prestin tetramer has been suggested as the molecular identity of the OHC lateral wall protein particles detected by freeze fracture (Zheng et al. 2006; Mio et al. 2008). The 3-dimensional reconstruction of a structure believed to be a prestin tetramer is shown in Figure 2.9. Currently, this is the only high resolution image showing what is considered by many as the fundamental element of electromotility.
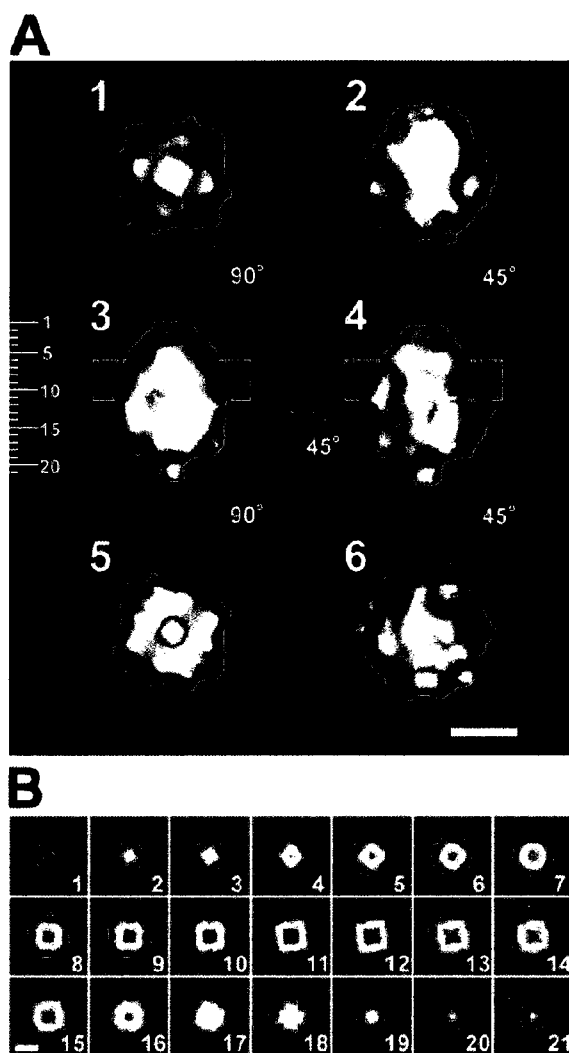
FIGURE 2.9 3D reconstruction from TEM images of prestin oligomers. **(A)** The bullet shaped structure, shown at 2 nm resolution, is 115 Å in height and 77 Å at the widest span. Based on size this image is suggested to be a prestin tetramer. The membrane is represented by a 30 Å band and shows that prestin has a large cytoplasmic domain (panel 3 and 4). Other orientations are shown based upon the rotations displayed. Scale bar 50 Å and ruler in nm. **(B)** The structure is shown in cross-sections at 5.5 Å intervals in a plane parallel to the membrane (1-extracellular, 21-cytoplasmic). Just below the plasma membrane a low-density core is observed (panels 11 and 12). Same scale bar as in (A). Figure from (Mio et al. 2008).

The origin of the prestin self-interactions is not known, but the intracellular termini are both likely candidates. The ability of purified prestin C-termini to form complexes of dimers and tetramers (Pasqualetto et al. 2008) highlights the potential involvement of STAS in prestin self-interactions. Involvement of the N-terminus is suggested by the observation that a 20 amino acid truncation simultaneously reduced FRET and inhibited function (Navaratnam et al. 2005). The latter effect is interesting since it implies prestin function might require prestin-prestin interactions. The results provided in Chapter 4 show that this is likely the case, but in addition to oligomerization being required, our data suggest that modulation of prestin self-interactions is mechanistically related to prestin charge transfer.

In addition to prestin self-interactions, prestin likely associates with important accessory proteins in the OHC. Recently, a yeast two-hybrid screen revealed that several electron transport proteins, a variety of transmembrane proteins, and seven yet to be characterized gene products interact with prestin (Zheng et al. 2009).

2.6 Patch clamp technique

2.6.1 Modes of operation

In 1945 Alan Hodgkin and Andrew Huxley used voltage clamp to capture the first intracellular recording of a nerve action potential from a giant squid axon (Hodgkin and Huxley 1945). With refinements to the technique Erwin Neher and Bert Sakmann were

later able to record currents from single ion channels, proving their involvement in fundamental cell processes and action potential conduction (Neher and Sakmann 1976). In 1991 the two were awarded the Nobel Prize for this ground breaking discovery. The modern form of the technique, the patch clamp (Neher et al. 1978; Hamill et al. 1981), provides various methods for studying populations of membrane components (ion channels, integral membrane proteins, etc.), or the constituents of regional patches of membrane, either on the cell or in isolation. In addition, isolated patches can be studied in either orientation, with the cytoplasmic or exoplasmic faces exposed to the bath (Fig. 2.10). We use the whole-cell configuration to obtain NLC measurements as an assay of prestin function.

2.6.2 Representative electrical circuit

A patch clamped cell in whole-cell mode can be represented as a simple three component electrical circuit (Fig. 2.11). In the diagram, capacitive (C_m) and resistive (R_m) properties of the membrane are represented and placed in series with the resistance imposed by patch pipette access, termed series resistance (R_s). The series resistance (R_s) is the sum of the open-bath patch pipette resistance and additional resistance introduced due to adherent membrane within the patch pipette tip.

The resultant resistance for R_m and R_s placed in parallel R_p (not physically represented by shown circuit) and series R_t are shown as Equations 2.1 and 2.2, since they are useful in simplifying subsequent expressions.

$$R_p = \frac{R_m R_s}{R_m + R_s}$$

$$R_t = R_m + R_s$$

Low resistance seal (50MΩ)

Suction

GigaOhm seal
CELL ATTACHED (ON-CELL) MODE

Pulse of suction
or voltage

Pull

Pull

WHOLE CELL
MODE

OUTSIDE-OUT
PATCH

INSIDE-OUT
PATCH
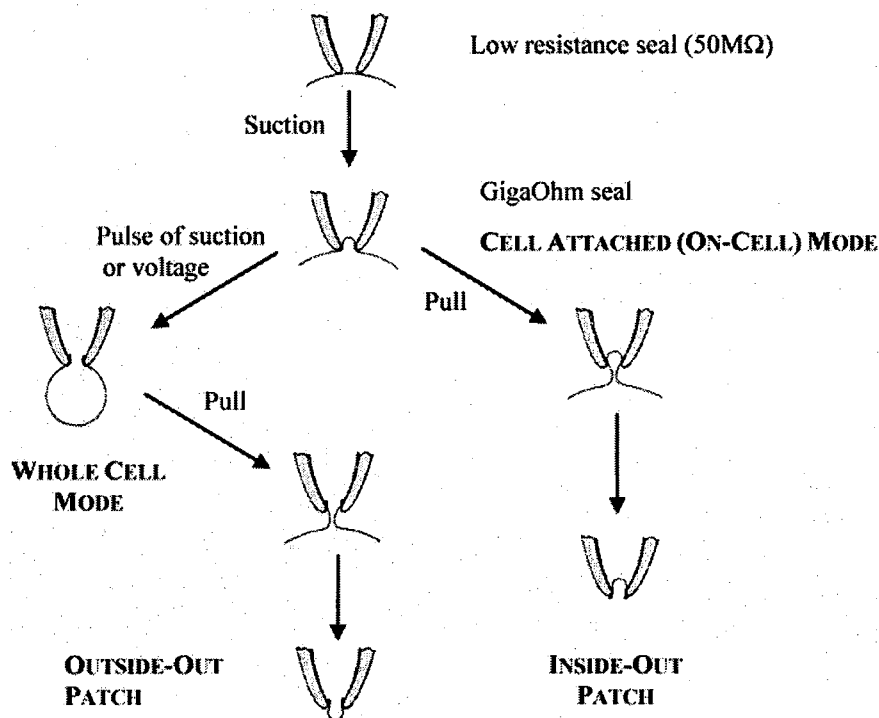
FIGURE 2.10 Methods to obtain the four common patch clamp modes. Impacting the cell and applying slight suction increases seal integrity in on-cell mode. From this configuration whole-cell mode can be obtained by applying a short negative pressure pulse or an inside-out patch of membrane extracted by withdrawing the pipette (the cell must be firmly attached to the substrate). The inside-out patch exposes the cytoplasmic surface to the external bath solution. The opposite conformation can be obtained by withdrawing the pipette after obtaining whole-cell mode. Figure adapted from (Hamill et al. 1981).
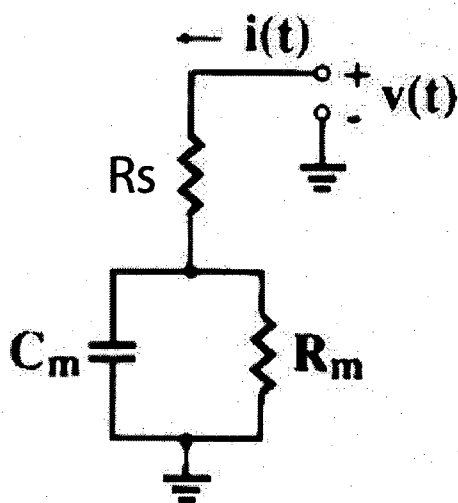
FIGURE 2.11 Equivalent electrical circuit for whole-cell configuration. The simple three component circuit is comprised of a series resistance R_s, which arises from the open-bath resistance of the pipette that is further increased due to adherent membrane to the pipette tip, and cell membrane capacitance (C_m) and resistance (R_m). Figure adapted from (Gillis 1995).

2.6.3 Patch clamping procedure

Specific methods are provided in each experimental chapter (Chapters 3-5), but the general procedure for whole-cell patch clamping is briefly summarized below. The patch pipette is lowered into the bath solution under positive pressure to prevent debris from contaminating the pipette tip. Through application of 5mv/5ms square wave pulses, current measurements are taken to determine open-bath pipette resistance. Next, offset potentials between the reference electrode and the pipette are canceled such that the DC pipette currents are close to zero. The cell is impacted, neutral pressure restored, and moderate aspiration applied to obtain a gigaohm on-cell seal with the membrane. Square wave pulses now show fast capacitive spikes on the current trace (0.5-5 μs time constants); these are caused by charging of the pipette and are corrected (subtracted) using the internal circuitry of the amplifier (C_{fast} compensation). Negative pressure is used to rupture the cell membrane and gain access to the cell interior, and square wave pulses now cause slow capacitive spikes (time constant on order of 100 μs) representing charging of the cell membrane. Following cancellation of slow capacitive transients (C_{slow} compensation), the currents recorded reflect net current flow within and across the cell membrane. Determination of prestin function requires characterization of whole-cell capacitance as a function of transmembrane voltage. We obtain this information by applying a sinusoidal command voltage and monitoring the current response. Details of the stimulus protocol are included in the methods section for each experiment (Chapters 3-5) and the mathematical basis for the Lindau-Neher method is explained in the Appendix.

2.7 Motivation for research plan

In chapter 3 we investigate the hypothesis that disulfide bonds are responsible for prestin oligomeric assemblies (Zheng et al. 2006) and determine if prevention of disulfide bonding shows functional effects. Experiments have attempted to obtain this type of information using chemical treatments (Santos-Sacchi and Wu 2004), but various reducing agents failed to affect oligomers observed using gel electrophoresis and Western blot (Zheng et al. 2006), so it is unclear that the treatments reached the intended cysteine targets. We provide unambiguous results using a mutational strategy, making amino acid replacements that closely match cysteine in size (serine) or hydrophobic character (valine). The mutational strategy has previously been used to investigate glycosylation (Matsuda et al. 2004), phosphorylation (Deak et al. 2005), and charged residues within prestin (Oliver et al. 2001; Bai et al. 2006). Our results also provide interesting information pertaining to currently proposed topological models (Deak et al. 2005; Navaratnam et al. 2005) and the idea of a low density core (see Fig. 2.9) (Mio et al. 2008).

In chapter 4 we investigate the voltage dependence of prestin-prestin interactions. Prestin self-interactions have previously been established (see Section 2.5.4), characterized near the cell's resting potential (Navaratnam et al. 2005; Greeson et al. 2006), and suggested to be necessary for prestin function (Navaratnam et al. 2005). Our data supports the idea that oligomerization might be required for prestin activity (Navaratnam et al. 2005), but the voltage dependence we report further suggests that

changes in self-association might be necessary to the mechanism of nonlinear charge movement. We also present interesting results pertaining to salicylate inactivation. Salicylate is thought to compete with Cl^- binding with prestin (see Fig. 2.8) (Oliver et al. 2001; Rybalchenko and Santos-Sacchi 2003; Rybalchenko and Santos-Sacchi 2008). Our data support this claim, but additionally suggest that the compound might allosterically modulate prestin conformation to cause inactivation.

Since prestin interactions appear to be functionally important, we designed a reporter construct that can provide a system for forced oligomerization. This new reporter system is characterized in Chapter 5. This construct, also addresses a common concern which arises in mutational studies of prestin – namely that loss of function can result from loss of prestin activity, decreased trafficking (due to retention in the endoplasmic reticulum and golgi systems), or a combination of the two. The reporter system we describe allows selective labeling of the membrane bound fraction, which will help in differentiating between various situations that reduce prestin-associated charge movement.

CHAPTER 3

CYSTEINE REPLACEMENT IN PRESTIN SHOWS THAT DISULFIDE BONDS ARE NOT REQUIRED FOR PRESTIN-ASSOCIATED CHARGE MOVEMENT

3.1 Motivation for cysteine replacement

A large displacement current, analogous to the gating current in ion channels, has been established as a reliable electrical signature for electromotility (Ashmore 1990; Santos-Sacchi 1991), but to date, little is known about the structure or mechanism of action of prestin. Proposed topologies have been suggested based on hydrophobicity analysis of prestin and the family of anion transporters to which it belongs. The family, named solute carrier family 26 (SLC26), likely span the membrane 10 to 14 times (Moseley et al. 1999; Saier et al. 1999; Mount and Romero 2004). Prestin (SLC26A5) has been shown to have intracellular N- and C-termini (Zheng et al. 2001), and therefore an even number of transmembrane domains. Ten and 12-pass models of prestin secondary structure have been proposed (Fig. 3.1, Table 3.1) based on data suggesting phosphorylation (Deak et al. 2005) and conflicting reports of N-linked glycosylation (Matsuda et al. 2004; Navaratnam et al. 2005).
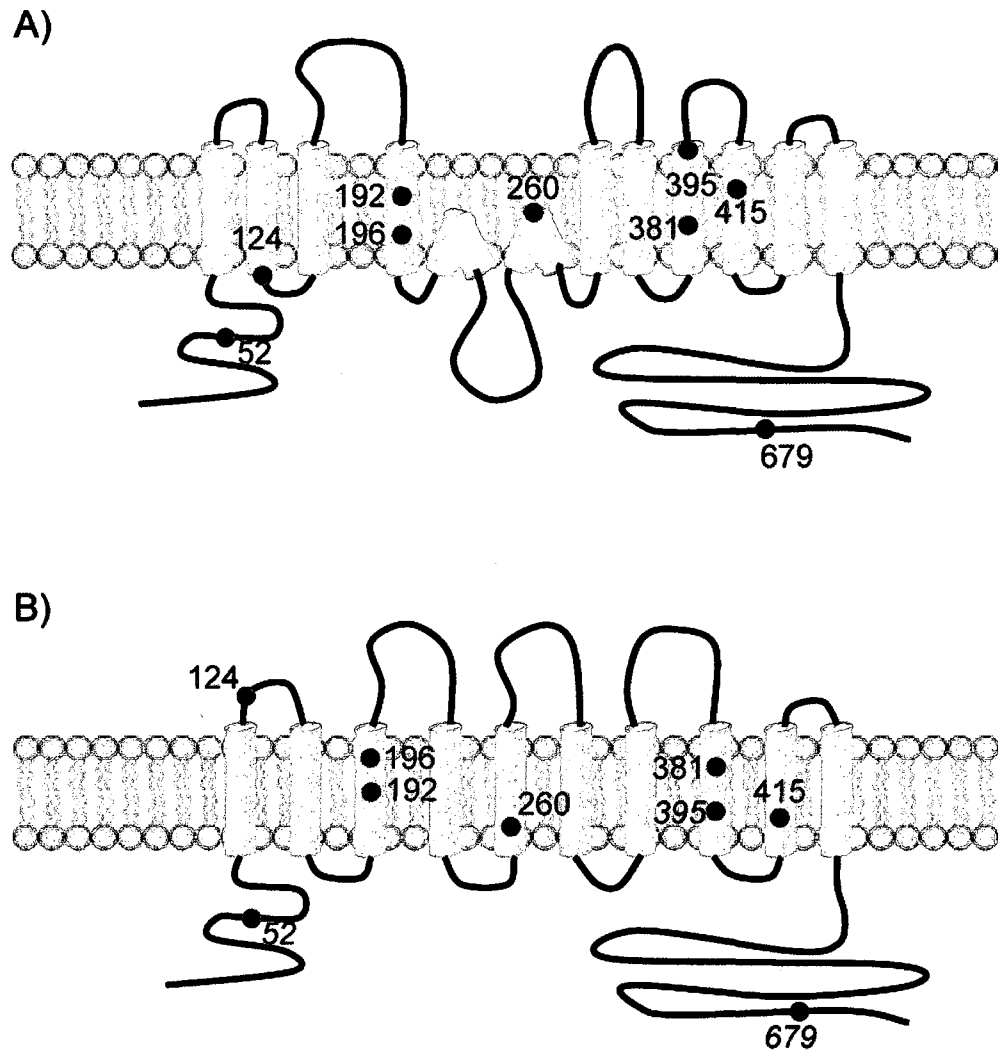
FIGURE 3.1 Proposed prestin topologies. **(A and B)** 10- and 12-pass models of prestin secondary structure have been proposed based on data suggesting phosphorylation (Deak et al. 2005) and conflicting reports of N-linked glycosylation (Matsuda et al. 2004; Navaratnam et al. 2005). Residue numbers for cysteine locations are shown and all but 52, 395, and 679 are unique to prestin in comparison to PAT1 (SLC26A6) (McGuire et al. 2006).

TABLE 3.1 Alpha-helix boundaries in commonly accepted prestin topologies: Re-entrant 12-pass (Zheng et al. 2001; Matsuda et al. 2004; Deak et al. 2005), 10-pass (Navaratnam et al. 2005), Evolutionary Trace defined (Rajagopalan et al. 2006) models.

	Prestin residue number		
TMD	Re-entrant loop	10-pass	Evolutionary Trace
1	80-100	94-122	83-105
2	103-123	128-156	111-129
3	132-152	179-199	132-148
4	184-204	212-232	178-206
5	212-232	258-278	209-232
6	254-274	282-306	261-276
7	287-307	336-364	288-307
8	335-355	374-398	342-363
9	375-395	410-432	375-398
10	415-432	476-499	412-432
11	442-462		438-453
12	480-500		468-484

Interestingly, a majority of prestin cysteine residues are contained within or near transmembrane domains, and six of nine are not shared with the family member having highest prestin homology, PAT1 (SLC26A6) (McGuire et al. 2006). PAT1 lacks the electrical signature of prestin function, nonlinear capacitance (NLC) (Waldegger et al. 2001), and comparison to this protein was originally used in an attempt to understand prestin voltage sensing (Oliver et al. 2001).

Prestin forms higher order oligomers and these interactions have been measured biochemically using Western blot (Matsuda et al. 2004; Zheng et al. 2006; Rajagopalan et al. 2007; Sturm et al. 2007; Detro-Dassen et al. 2008), optically through fluorescence resonance energy transfer (FRET) (Navaratnam et al. 2005; Greeson et al. 2006), and verified *in vivo* through yeast two-hybrid assay (Zheng et al. 2006). It has been suggested that prestin dimers are composed of disulfide-bonded monomers (Zheng et al. 2006), however, no groups have previously used mutagenesis to investigate whether cysteines are playing a role in oligomerization. It is unclear if oligomerization plays a functional role, but published data suggest that the cysteines reside in locations important to electromotility since sulfhydryl reagents, which bind cysteine residues and sterically hinder conformational change, alter the cellular level response and NLC of OHCs. Among these reagents the most severe inhibition of electromotility (Kalinec and Kachar 1993) and the greatest alteration to NLC (Santos-Sacchi and Wu 2004) are caused by organomercurials, the most penetrating sulfhydryl agents. This indicates that one or more reactive thiol groups are present in a functionally important and relatively protected region of prestin, but no data describe which cysteine residue(s) are responsible.

To address these gaps in the prestin literature we have investigated the effects of amino acid replacement of cysteine, with either serine or valine, upon prestin oligomerization and function as determined by NLC (McGuire et al. 2007; McGuire et al. 2008). Serine is a close match to cysteine in size, whereas valine is a close match to cysteine in hydrophobicity. Mutations often perturb prestin function, and it is often difficult to establish the precise cause. In this chapter we use Western blot to differentiate between loss of function mutations and those with impaired membrane trafficking.

We show that cysteine 196 and 415 are critical for function, and conclude that if disulfide bonding is present in prestin it does not have a functional role that can be detected via NLC. Our data also suggest that cysteine 260 and 381 are likely exposed to a hydrophilic local environment. Such exposure might suggest that these residues line an aqueous pore (likely occluded), and this idea has been suggested by TEM imaging of oligomeric prestin structures (Mio et al. 2008).

3.2 Materials and methods

3.2.1 Construct design

Gerbil prestin (AF230376) was amplified from cDNA (forward/reverse primers: 5'ggaattccaccatggatcatgccgaag3'/5'cgggatcccgtgcctcgggtgtggtgg3') digested (EcoRI and BamHI), and inserted into the multiple cloning site (MCS) of the pEGFP-N1 (Clontech, Palo Alto, CA) to create a C-terminal fusion protein. A point mutation was made to the GFP (A206K) to prevent non-specific interaction of the fusion proteins (Tsien 1998;

Zacharias 2002). The mutation denoted A206K is actually located at residue 207 of the Clontech vector due to an insertion that enhances mammalian translation efficiency. Prestin-GFP cDNA served as a template and PCR primers were used to produce the mutant constructs required in our study (serine and valine replacements, see Table 3.2). Each mutant construct (coded as 'wild type residue'-'prestin residue location'-'mutant residue' in the text; ex. C52S) was sequence verified (3130XL Genetic Analyzer; Applied Bio-systems, Foster City, CA) to ensure that prestin, the linker region, and GFP did not contain any unintended polymerization errors (Baylor Sequencing Core, Houston, TX).

3.2.2 Plasmid expression and cell culture

HEK293 cells were grown in T75 flasks and 6-well plates containing DMEM supplemented with 10% BCS (Invitrogen, Carlsbad, CA), 1% penicillin-streptomycin, 14.3 mM HEPES, and 16.1 mM $NaHCO_3$. Only cells below passage 20 were used for any of our studies and this is below conservative limits established for electrophysiological studies (20-30 passages) (Thomas and Smart 2005). Cells were transfected with wild type (WT) or mutant prestin-GFP plasmids using 2µg DNA and 3 µL Fugene 6 transfection reagent (Roche, Indianapolis, IN) according to the manufacturer's directions. For electrophysiology and imaging studies, cells were trypsinized and replated onto #1.5 coverslips or MatTek dishes (MatTek Corp., Ashland, MA) 8-12 hours after transfection and then evaluated 24-48 hours post-transfection. In select experiments cholesterol depletion was accomplished through application of 10 mM Methyl-β-cyclodextrin suspended in DMEM (mβCD; C4555, Sigma-Aldrich, St. Louis,

MO) to the cells for 15 or 30 minutes (at 37°C) prior to patch clamp evaluation. For

Western blot experiments protein was collected 24 or 48 hours post-transfection.

TABLE 3.2 Prestin mutants with replacement of various cysteine residues

Prestin mutation	Primer set (5' to 3'; mutation highlighted)
C52S	gcaggcgttcacaagcactcccaaaaagataagaaac gtttcttatcttttttgggagtgcttgtgaacgcctgc
C124S	ttttatcctgttatcatgtactcttctttgggacctccagaca tgtctggaggtcccaaagaaagagtacatgataacaggataaaa
C192S	ctctcaggaatcattcagtttagdctaggtgtgtgcag ctgcacacacctaggctaaactgaatgattcctgagag
C192V	gaatcattcagttrgtcctaggtgtgtgcaggtttgga tccaaacctgcacacacctaggacaaactgaatgattc
C196S	taggtgtgagcaggtttggatttgtggc gccacaaatccaaacctgctcacaccta
C196V	taggtgtggtcaggtttggatttgtggc gccacaaatccaaacctgaccacaccta
C192.196S	ggaatcattcagtttagcctaggtgtgagcaggtttggatttg caaatccaaacctgctcacacctaggctaaactgaatgattcc
C260S	ttaaaaacctcaacgtgtcttccctaggcgtcggc gccgacgcctagggaagacacgttgaggtttttaa
C381S	ctttggggataagcaactccatcggatcttaccag ctggtaagatccgatggagttgcttatccccaaag
C395S	ccttctccatttccagctccttgtctcgcagccttgtt aacaaggctgcgagacaaggagctggaaatggagaagg
C395V	ccttctccatttccgtctccttgtctcgcagccttgtt aacaaggctgcgagacaaggagacggaaatggagaagg
C415S	ctcgcaggtagcttggcctcgctgatgattctg cagaatcatcagcgaggccaagctacctgcgag
C415V	ctcgcaggtgtcttggcctcgctgatgattctg cagaatcatcagcgaggccaagacacctgcgag
C679S	atttatgtgtacttagcaggaagcagcccacaagtcgtgaatgac gtcattcacgacttgtgggctgcttcctgctaagtacacataaat

3.2.3 Electrophysiology

2-4 MΩ micropipettes were formed from Kimax-51 capillary tubes (1.5/0.8 mm OD/ID) on a P-97 puller (Sutter, Novato, CA). The patch pipettes and extracellular bath both contained common blocking solutions (Pipette: 130 mM CsCl, 2 mM $MgCl_2$, 10 mM EGTA, 10 mM HEPES; Extracellular: 99 mM NaCl, 20 mM TEA-Cl, 2 mM $CoCl_2$, 1.47 mM $MgCl_2$, 1 mM $CaCl_2$, 10 mM HEPES) to minimize ionic conductance (Deak et al. 2005). All solutions were titrated to pH 7.3 and dextrose added to obtain 300 ± 3 mOsm (Osmette A; Precision Systems, Natick, MA). Coverslips seeded at low cell density formed the base of a patch clamp chamber in which the cells were bathed in extracellular solution and an agar bridge provided electrical continuity with the reference bath containing pipette solution. $Ag^+/AgCl$ electrodes were used to record current flow. Only healthy, single cells showing suitable GFP fluorescence were attempted. During the experiment micropipette placement was controlled using a Burleigh PCS-6200 Micromanipulator (EXFO Life Sciences, Rochester, NY), and pipette pressure monitored (PM01R digital pressure meter; WPI, Sarasota, FL). Amplifier and electrode offsets were compensated in open-bath and on-cell seals in excess of 1 GΩ were obtained. Pipette capacitance was compensated before rupturing the membrane to establish whole-cell mode. All cells retained for analysis exhibited series resistance less than 10 MΩ, and membrane resistance in excess of 1 GΩ.

Membrane capacitance (C_m) and membrane resistance (R_m) were determined by applying a sinusoidal command voltage at a superimposed DC offset and then

determining the real and imaginary components of the admittance, the complex current response scaled by the command voltage (Lindau and Neher 1988). We use a software-based phase-sensitive detector implemented in PatchMaster software (HEKA, Mahone Bay, NS) to acquire this information. Specifically, we apply an 800 Hz, 10 mV sinewave and measure the current response as DC holding potential is stepped from -140 to +140 mV (or -160 to +160 mV for some mutants with altered NLC) in 2 mV increments (HEKA EPC 10 Plus Amplifier with 18-bit DAC). At each DC potential four complete sinusoidal voltage cycles occur and discrete capacitance values are calculated from the latter three.

Multiple capacitance versus voltage (DC holding potential) traces are acquired for each cell and each of the individual recordings is fit to the first derivative of the two-state Boltzmann function (Eqn. 3.1) using MATLAB (MathWorks, Natick, MA).

$$C_m = \frac{Q_{max}\left(\dfrac{ze}{kT}\right)}{\exp\left[\left(\dfrac{ze}{kT}\right)\left(V - V_{1/2}\right)\right]\left(1 + \exp\left[-\left(V - V_{1/2}\right)\left(\dfrac{ze}{kT}\right)\right]\right)^2} + C_{lin} \qquad \text{Eqn. 3.1}$$

Q_{max} is the maximum nonlinear charge movement provided by prestin. $V_{1/2}$ is the voltage at which half-maximal charge transfer occurs, or equivalently, the peak of the capacitance versus holding potential curve. z is the valence of charge movement by prestin. Boltzmann's constant k, absolute temperature T, and the charge carried by an electron e, are all constant values. The first term of the fit represents the nonlinear component,

caused by prestin-related charge movement, while the second term is linear capacitance (C_{lin}) derived from the dielectric properties of the membrane and is proportional to cell size. Since variation in cell size causes differences in the maximal charge transfer (Q_{max}), the charge movement is normalized to C_{lin}, and computed on a cell-by-cell basis. This quantity, designated as charge density, has units of fC/pF (Oliver and Fakler 1999). Mean fit parameters are determined for each cell and pooled for each experimental group. We tested WT prestin and various prestin mutants with single amino acid replacements. For comparison of $V_{1/2}$ or z between various experimental groups (Figs. 3.4, 3.6, and 3.9) representative NLC curves are reconstructed from averaged Q_{max}, $V_{1/2}$ and z for each group, and each result is normalized to maximal nonlinear capacitance ($Q_{max}ze/4kT$). Normalized curves are not appropriate for comparing charge densities (Figs. 3.3, 3.10, and 3.11), so in this case representative NLC curves are reconstructed from mean $V_{1/2}$, z, and Q_{max}/C_{lin} assuming 17.6 pF linear capacitance (mean C_{lin} of WT prestin cells).

3.2.4   Western blot

At 24 or 48 hours post-transfection, HEKs were harvested and resuspended in lysis buffer (10 mM Tris, 1 mM EDTA, 1X Protease inhibitor cocktail, 0.5 mM PMSF) to collect total protein. Lipid was removed following the procedure of Wessel and Flugge (Wessel and Flugge 1984). Protein was resuspended in 1X sample buffer (62.5 mM Tris, 10% glycerol (v/v), 2% SDS (w/v), 0.7 M βME) and total protein determined by Bradford assay to ensure equal loading. After incubation at 95 °C for 5 minutes samples were separated by electrophoresis in 4-15% polyacrylamide gradient SDS (0.1% w/v) gels in standard running buffer (25 mM Tris, 192 mM glycine, 0.1% SDS). Blots were transferred to nitrocellulose overnight (transblotting buffer: 25 mM Tris, 192 mM

glycine, 20% methanol v/v). Western blots were labeled with 1:1000 dilution of mouse anti-GFP (B2 Ab) or goat anti-prestin (N-20 Ab) primary antibodies (Santa Cruz Biotechnology, Santa Cruz, CA) and 1:5000 dilution of peroxidase labeled horse anti-goat or horse anti-mouse IgG secondary antibodies (Vector laboratories, Burlingame, CA), respectively. ECL Western blotting detection reagents (GE Healthcare Bio-Sciences Corp, Piscataway, NJ) and autoradiography films (Kodak) were used to visualize prestin-GFP banding patterns. Blots were stripped (62.6 mM Tris, 0.2% SDS (w/v), 100 mM βME) and reprobed for β-actin (Abcam, Cambridge, MA) to verify equal total protein loading.

Quantification of Western blot bands intensities was performed on an Odyssey gel imaging system (LI-COR, Lincoln, NE). Membrane fractions of total protein, collected 48 hours post-transfection, were separated on 4-12% gradient SDS polyacrylamide gels. Blots were labeled with goat anti-prestin (N-20 Ab), rabbit anti-APP (amyloid precursor protein to track equal loading), and two infrared secondary dyes (LI-COR). Goat anti-rabbit IRDye 680 was excited by 685 nm diode laser light and the signal captured at 720 nm (APP channel). Donkey anti-goat IRDye 800CW was excited by 785 nm diode laser light and the signal captured at 820 nm (prestin channel). PageRuler molecular weight standards (Fermentas life science, Glen Burnie, MD) are also detected fluorescently. Scans were performed at 169 μm resolution and 3.6 orders of magnitude intensity values recorded to effectively prevent signal saturation. Odyssey 3.0 software was used to measure pixel volume in order to quantify the amount of protein in a select region of the gel. Pixel volume (counts mm^2) is the sum of the intensity values for all pixels in a defined region of the gel multiplied by the area of the defined region.

3.2.5 Confocal imaging

Localization of the prestin-GFP fusions to the membrane was verified using confocal microscopy. To selectively label the cell membrane transfected HEKs were incubated with 25 μM di-8-ANEPPS (Invitrogen, Carlsbad, CA) for 20 minutes at room temperature. Cells were washed with PBS and imaging was performed on an LSM 510 microscope (Zeiss, Thornwood, New York) using a 63X, 1.4NA objective. Both GFP and di-8 were excited with a 488 nm Argon laser. Using dichroics and bandpass filters, the GFP and Di-8 fluorescence signals were isolated in separate channels ranging 500-530 nm and 650-710 nm, respectively. The pinhole for each channel was set to 2.66 Airy units.

3.3   Experimental results

3.3.1 Mutant prestin constructs traffic to the cell membrane

We examined 8 prestin mutants with single amino acid replacement of cysteine with serine, one double mutant with two cysteines mutated to serines, and 4 mutants in which valine replaced a single cysteine (see Table 3.2). Each prestin-GFP construct was transfected into HEK cells and living cells were imaged 24-48 hours post-transfection. The membranes of the HEKs were clearly delineated using the membrane intercalating dye, di-8-ANEPPS. Confocal images verified that each of our cysteine replacement mutants successfully reached the cell membrane, based upon coincidence of di-8 and GFP fluorescence, the former distributed within the external leaflet of the lipid bilayer and the latter fused to the prestin molecule. Figure 3.2a shows brightfield, GFP, di-8, and

overlay images (clockwise from lower left) for C124S prestin. Thresholding was used to remove pixels with fluorescent intensity values in the lower 20% (approximately) for di-8 or GFP and the remaining colocalized signal (pixels with non-zero fluorescent values in each channel) is shown in Figure 3.2b. It appears that C124S prestin is trafficking normally to the membrane since the colocalized signal is restricted to the region of the membrane (Fig. 3.2b) and GFP signal is not distributed uniformly within the cytoplasm (Fig. 3.2a). Misfolded proteins would not show localization (Rotman-Pikielny et al. 2002). This image is representative of the results uncovered for each mutant, but further analysis focuses on more quantitative measures of membrane incorporation such as charge density.

3.3.2 Functional implications of cysteine replacement with serine

To determine if cysteine residues are necessary for prestin function mutations were introduced into the plasmid DNA to encode amino acid replacement with serine. We screened the single amino acid replacement mutants C52S, C124S, C260S, C381S, C395S, C415S, C679S, and the double replacement C192.196S to locate transmembrane domains (TMDs) in prestin that were sensitive to the substitution. Whole-cell patch clamping of these mutants in HEK cells revealed alterations in the NLC that can be segregated into three distinct classes: 1) a shift of the $V_{1/2}$ to depolarizing potentials, 2) tightening of the NLC curve, reflective of increased valence of charge movement, and 3) decreased area under the NLC curve, representing reduced charge movement. These results are summarized in Figures 3.3-3.6.
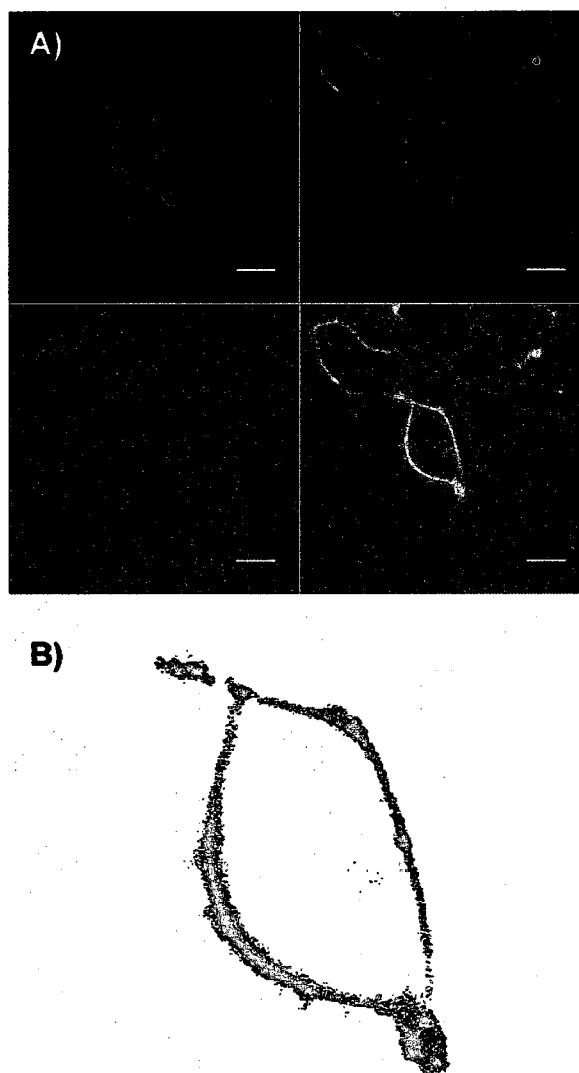
FIGURE 3.2 Cysteine replacement mutants membrane localize. **(A)** Brightfield, GFP, di-8, and overlay images (clockwise from lower left) for C124S prestin show that the protein traffics to and occupies the cell membrane. The fluorescence of the prestin-GFP fusion protein coincides with that of di-8-ANEPPS, a lipid-like probe that partitions into the cell membrane. Scale bar 10 μm. **(B)** After thresholding to remove low intensity pixels, an overlay of the remaining colocalized signal is clearly restricted to the region of the membrane. 75% of pixels with GFP fluorescence also have di-8 signal, and these are displayed in (B).

Substitution of cysteine in TMD 4 (C192.196S) and TMD 10 (C415S) impaired prestin function. C192.196S (7.37 ± 0.81 fC/pF) and C415S (7.07 ± 1.33 fC/pF) prestin both had significantly reduced charge density compared to wild type (WT) controls (18.27 ± 1.89 fC/pF) (mean ± SE; p< 0.01), but both had $V_{1/2}$ and z consistent with WT prestin (Fig. 3.3a). Charge densities for the remaining mutants appear normal and are approximately 15 fC/pF (Fig. 3.3b).

Substitution of either cysteine in TMD 9 altered the operating setpoint for prestin charge movement, by shifting $V_{1/2}$. C381S (-57.2 ± 3.2 mV) and C395S (-6.1 ± 2.0 mV) prestin both had significantly depolarized $V_{1/2}$ compared to WT controls (-78.6 ± 3.6 mV) (mean ± SE; p < 0.01), shifted by approximately 21 and 73 mV, respectively (Fig. 3.4a). The altered $V_{1/2}$ was not accompanied by any other functional abnormality since charge density and z were consistent with WT protein. The measured $V_{1/2}$ for each prestin mutant is reported in Figure 3.4b.
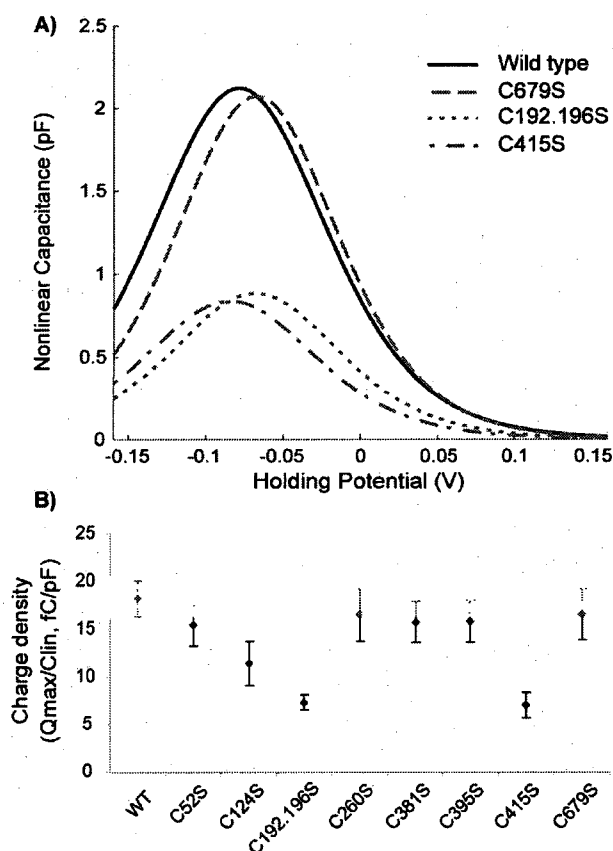
FIGURE 3.3 Cysteines of TMD 4 and 10 are required for full charge movement. **(A)** NLC curves constructed from mean $V_{1/2}$, z, and charge density (see methods). C192.196S and C415S prestin show reduced area under the curve indicating reduced charge movement compared to WT prestin. $V_{1/2}$ and z for these mutants are consistent with WT measures (see Figs 3.4 and 3.6). Mutants with normal charge movement capabilities show similar area under the curve compared to WT prestin; C679S is shown as an example. **(B)** Most serine substitutions provided normal charge movement of approximately 15 fC/pF, however, C192.196S and C415S prestin exhibited significantly reduced levels compared to WT controls ($p < 0.01$). *WT* 18.27 ± 1.89 (n=21), *C52S* 15.46 ± 2.15 (n=11), *C124S* 11.46 ± 2.28 (n=8), *C192.196S* 7.37 ± 0.81 (n=7), *C260S* 16.54 ± 2.75 (n= 12), *C381S* 15.79 ± 2.14, *C395S* 15.86 ± 2.19 (n=10), *C415S* 7.07 ± 1.33 (n=12), *C679S* 16.59 ± 2.69 (n=10). All values in fC/pF (mean ± SE).
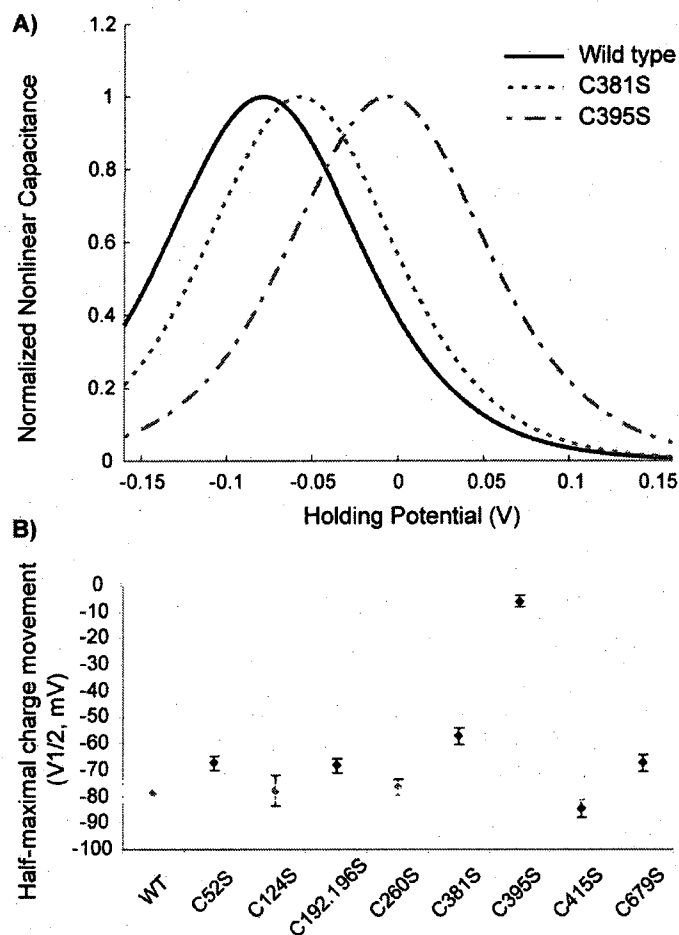
FIGURE 3.4 Cysteines of TMD 9 affect $V_{1/2}$ of NLC. **(A)** NLC curves constructed from mean $V_{1/2}$, z, and Q_{max} are normalized to the peak capacitance of each group. C381S and C395S prestin show depolarized $V_{1/2}$ compared to WT prestin (p < 0.01), but charge density and z are consistent with WT measures (see Figs 3 and 5). **(B)** $V_{1/2}$ for all groups: *WT* -78.6 ± 3.6 (n=21), *C52S* -67.3 ± 2.5 (n=11), *C124S* -77.8 ± 5.6 (n=8), *C192.196S* -68.3 ± 2.8 (n=7), *C260S* -76.5 ± 3.1 (n= 12), *C381S* -57.2 ± 3.2, *C395S* -6.06 ± 2.0 (n=10), *C415S* -84.6 ± 3.4 (n=12), *C679S* -67.4 ± 3.0 (n=10). All values in mV (mean ± SE).

$V_{1/2}$ is known to be sensitive to membrane cholesterol concentration (Rajagopalan et al. 2007). Since the shift observed in the C395S mutant was of similar magnitude to that observed following cholesterol depletion of HEKs expressing WT prestin (~74 mV upon 30 minute incubation with mβCD at 37°C (Rajagopalan et al. 2007)) we tested C395S prestin cholesterol sensitivity. Despite already being shifted 73 mV from wild type prestin, C395S prestin NLC was further depolarized 69 and 111 mV upon 15 or 30 minute depletion (respectively) with mβCD (Fig. 3.5). Retained cholesterol sensitivity indicates that the C395S $V_{1/2}$ shift from WT prestin, and the WT $V_{1/2}$ shift upon cholesterol depletion, do not share a common mechanism.

Fitting NLC data to the derivative of the Boltzmann function assumes that prestin undergoes a transition between two states, commonly interpreted as a conformational change of the protein. One cysteine mutation, located in TMD 6 altered the mechanics this transition, indicated by a change in the valence of charge movement (Fig. 3.6a). C260S (0.80 ± 0.01) increased the abruptness of the prestin state transition, elevating z 19% above the wild type value (0.67 ± 0.07) (mean ± SE; p< 0.01). The measured z for each prestin mutant is reported in Figure 3.6b.
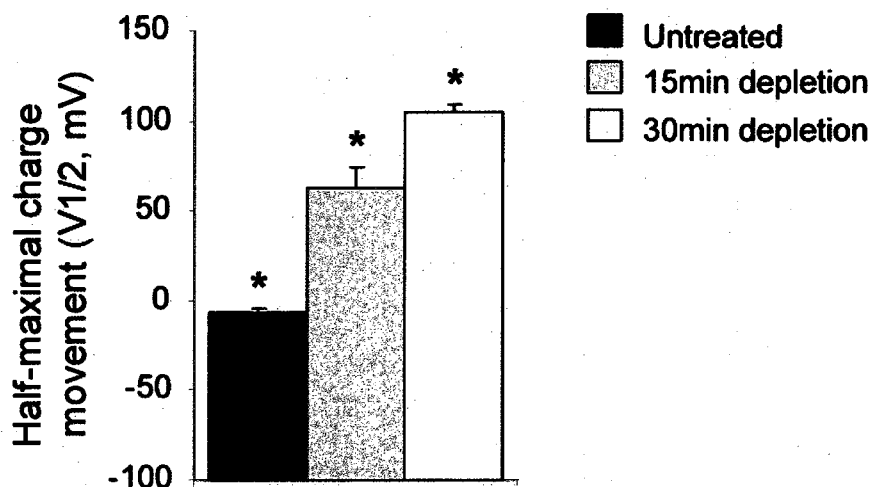
FIGURE 3.5 C395S mutant retains sensitivity to membrane cholesterol composition. Untreated C395S prestin has $V_{1/2}$ of -6.06 ± 2.0 mV (n=15) which is 73 mV more depolarized than WT prestin. Depletion of HEK membrane cholesterol by 10 mM mβCD application for 15 or 30 minutes causes further depolarization of $V_{1/2}$ to +63.0 ± 11.4 mV (n=5) and +105.0 ± 3.8 mV (n=4), respectively. The 69 mV (15 minute depletion) and 111 mV (30 minute depletion) shifts are statistically significant from $V_{1/2}$ of untreated C395S and each other (p < 0.05). All $V_{1/2}$ reported as mean ± SE.
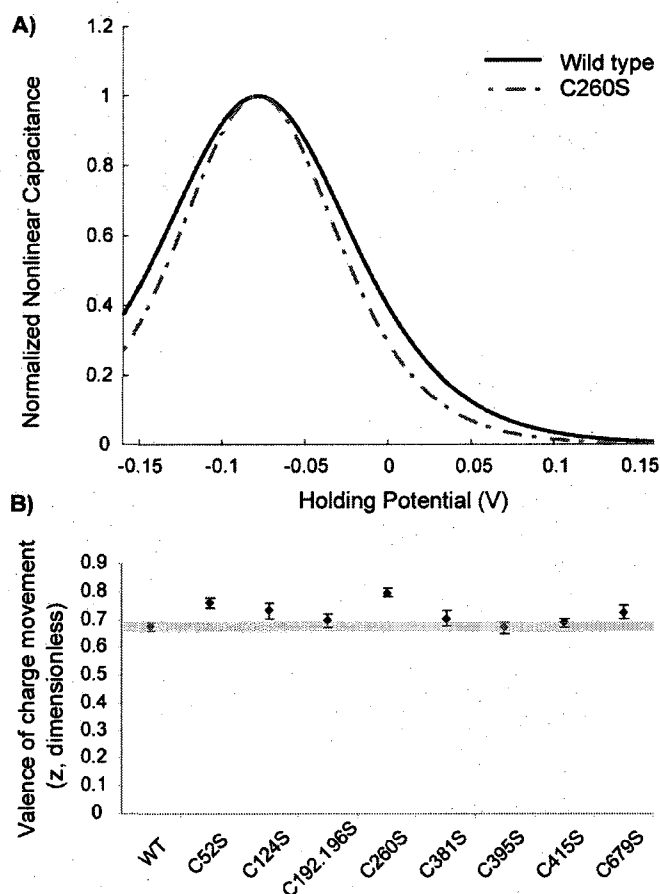
FIGURE 3.6 Cysteine substitution in TMD 6 alters the mechanics of charge movement. **(A)** NLC curves constructed from mean $V_{1/2}$, z, and Q_{max} are normalized to the peak capacitance of each group. Since $V_{1/2}$ was consistent with WT prestin (see Fig 4), C260S NLC was translated and aligned with the wild type to illustrate the effects of increased valence of charge movement. C260S had significantly higher valence than WT prestin ($p < 0.01$) which corresponds to a narrowed voltage range over which the prestin state transition occurs. Charge density did not differ from WT control (see Fig 3) **(B)** z for all groups: *WT* 0.67 ± 0.01 (n=21), *C52S* 0.76 ± 0.02 (n=11), *C124S* 0.73 ± 0.03 (n=8), *C192.196S* 0.70 ± 0.02 (n=7), *C260S* 0.80 ± 0.01 (n= 12), *C381S* 0.70 ± 0.03, *C395S* 0.67 ± 0.02 (n=10), *C415S* 0.69 ± 0.02 (n=12), *C679S* 0.72 ± 0.02 (n=10). All values are dimensionless (mean ± SE).

3.3.3 Serine replacement mutants show altered oligomeric profiles

Each serine replacement mutant was analyzed by SDS-PAGE Western blot. Prestin and GFP have predicted MWs of 81.4 kDa and 26.9 kDa (respectively), making the total size of the fusion ~110 kDa for the un-glycosylated monomer. When expressed in HEK cells, prestin glycosylation typically adds approximately 20 kDa and this corresponds to the band we observe at ~130 kDa. Depending on the extent of glycosylation in higher order states the dimer, trimer, and tetramer are expected between 220-260, 330-370, and 440-480 kDa, respectively. A 4-15% gradient polyacrylamide gel allowed visualization of oligomers up to trimer (Fig. 3.7, bands labeled M, G, D, T). By 24 hours post-transfection, mutants with functional alteration of $V_{1/2}$ or z showed each of the four bands detected in the WT prestin-GFP fusion. Mutants with reduced charge density (C192.196S and C415S) showed reduced levels of total monomer with large reduction in the intensity of the glycosylated monomer band, which was virtually non-existent at 24 hours. The glycosylated monomer band of C192.196S remained low while C415S partially recovered (qualitatively) by 48 hours post-transfection (Fig. 3.7, lanes 3 and 5).

FIGURE 3.7 Cysteine mutants with reduced charge density show altered oligomeric profiles. Serine replacement mutants (Figs 3.3, 3.4, and 3.6) were analyzed by SDS-PAGE in a 4-15% gradient gel (blot probed by mouse anti-GFP). Equal total protein loading is demonstrated by re-probing for actin. Mutants showing $V_{1/2}$ shift or z increase showed normal oligomeric populations within the resolving capacity of the gel (un-glycosylated monomer **M**, glycosylated monomer **G**, dimer **D**, trimer **T**). Charge density mutants, C192.196S and C415S, showed qualitatively reduced glycosylated monomer levels at both 24 and 48hrs post-transfection. Lanes: **1**-C52S, **2**-C124S, **3**-C192.196S, **4**-C395S, **5**-C415S, **6**-C381S, **7**-C260S, **8**-C679S, **9**-WT, **10**-Untransfected HEK.

The intensities of the glycosylated monomer band were quantified using an infrared gel imaging system. Each of the serine mutants from Figure 3.7 were re-evaluated and conditions were optimized for evaluation of this band: 1) Protein was collected 48 hours post-transfection, due to apparent recovery of C415S, and 2) The gel was probed by an anti-prestin antibody, which does not react with higher order oligomers, but provides superior monomer signal compared to the anti-GFP antibody. Additionally, single serine replacement mutants (C192S and C196S) were included to better understand the nature of the TMD 4 charge density mutant (C192.196S); these constructs are fully characterized later in Figure 3.10. Un-glycosylated monomer (~110 kDa) and glycosylated monomer (~130 kDa) bands were detected for WT prestin-GFP and each mutant construct (Fig. 3.8a). The intensity of the glycosylated monomer band, measured as a pixel volume (counts mm^2), was normalized to the pixel volume of amyloid precursor protein (APP), a commonly expressed integral membrane protein, to correct for slight differences in total protein loading. The normalized band intensity, or amount of glycosylated monomer, for each group is plotted in order of decreasing charge density (Fig. 3.8b). The last four mutants (C192.196S, C415S, C196S, and C192S) have significantly reduced charge density from WT ($p<0.05$) and the two with normal levels of glycosylation (C415S and C196S) are likely normally folded. Mutants with charge densities that are not significantly different from WT (C679S, C260S, C395S, C381S, C52S, C124S) all show normal or elevated levels of glycosylated monomer.

A)
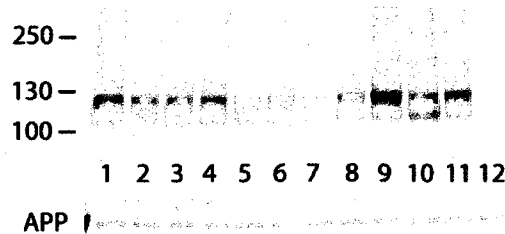
B)
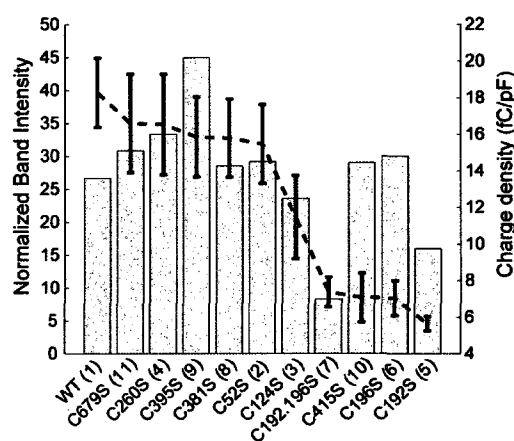
FIGURE 3.8 Quantification of monomer band intensities. **(A)** The glycosylated monomer bands of serine replacement mutants were quantified using a gel imaging system and infrared fluorescent secondary probes. Protein was acquired 48 hours post-transfection and separated by SDS-PAGE in a 4-12% gradient gel (blot probed by goat anti-prestin and rabbit anti-APP). Equal total protein loading is demonstrated by APP. Lanes: **1**-WT, **2**-C52S, **3**-C124S, **4**-C260S, **5**-C192S, **6**-C196S, **7**-C192.196S, **8**-C381S, **9**-C395S, **10**-C415S, **11**-C679S, **12**-Untransfected HEK. **(B)** The intensity of the glycosylated monomer band normalized to the intensity of APP (gray bars) and mean charge density (dotted line with SE bars) is plotted for each lane of (A). The plot is organized in order of decreasing charge density with lane numbers of (A) shown in parentheses. C192.196S, C415S, C196S and C192S all show significantly reduced charge density compared to wild type ($p < 0.05$).

3.3.4 Valine substitution partially restores function disrupted by serine substitution

At locations where substitution of cysteine with serine significantly altered function valine replacement was made and function re-characterized using whole-cell patch clamp and NLC. Specifically, we studied sites that showed altered $V_{1/2}$ or charge density due to the likelihood of physiological significance of these parameters. C395S prestin was depolarized 73 mV from WT prestin, however when valine was used as a cysteine replacement altered $V_{1/2}$ was no longer detected (Fig. 3.9).

The origin of charge density loss upon serine substitution within TMD 4 (C192.196S) was probed with two single replacement mutants (C192S and C196S) and individual valine substitutions (C192V and C196V). Substitution of either cysteine by serine had the same effect as the double mutant, significantly reducing charge density by about 11.6 fC/pF or 63% from WT controls (Fig. 3.10b). Valine replacement at either the 192 or 196 location restored charge density to levels indistinguishable from WT prestin. $V_{1/2}$ and z of C196V showed slight alteration from values obtain from WT, but WT $V_{1/2}$ and z were observed in each of the other mutants (Fig. 3.10a).
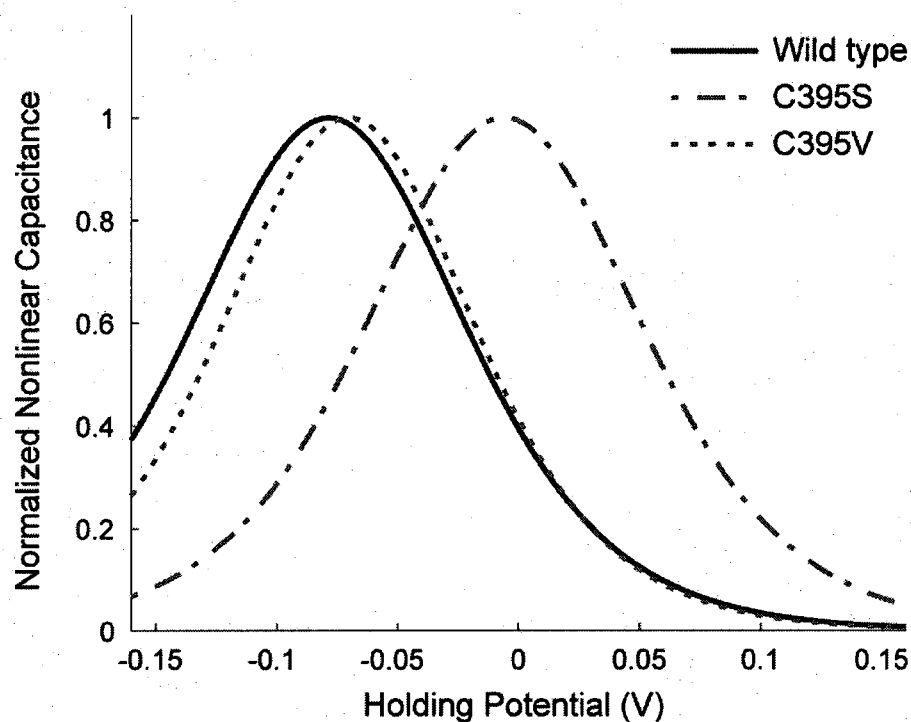
FIGURE 3.9 Valine removes the shift induced by serine replacement at residue 395. NLC curves constructed from mean $V_{1/2}$, z, and Q_{max} are normalized to the peak capacitance of each group. C395S prestin had significantly depolarized $V_{1/2}$ compared to WT prestin ($p < 0.01$), but otherwise normal z and charge density (Q_{max}/C_{lin}). C395V exhibited z and $V_{1/2}$ that were consistent with WT prestin, but had reduced charge density ($p<0.05$). C395V (n=15): $V_{1/2}$ -70.4 ± 2.6 mV, z 0.73 ± 0.02, Q_{max}/C_{lin} 6.50 ± 0.73 fC/pF (mean ± SE).
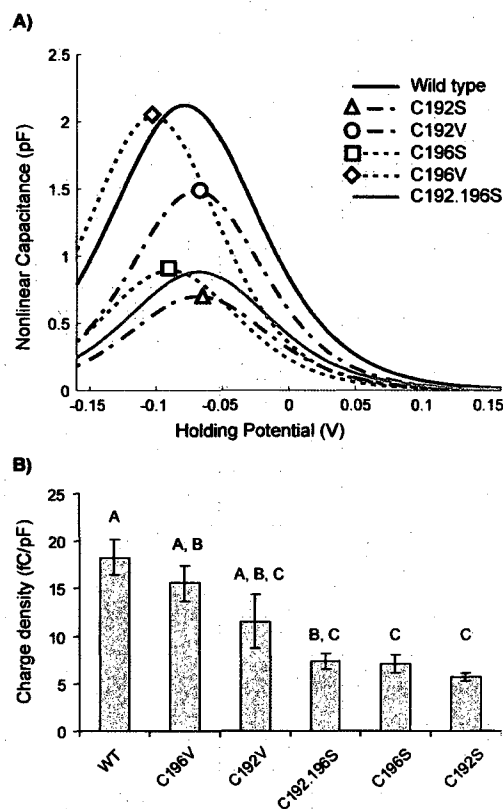
FIGURE 3.10 Valine substitution is well-tolerated in the hydrophobic core of TMD 4. **(A)** NLC curves constructed from mean $V_{1/2}$, z, and charge density (see methods). All curves show $V_{1/2}$ and z consistent with WT prestin, except for C196V which was significantly different for both ($p<0.05$). $V_{1/2}$ (mV) and z (dimensionless) for all groups (mean ± SE): **WT** -78.6 ± 3.6 mV and 0.67 ± 0.01 (n=21), **C192S** -68.4 ± 1.8 mV and 0.72 ± 0.01 (n=16), **C192V** -69.8 ± 1.8 mV and 0.75 ± 0.02 (n=10), **C196S** -89.5 ± 2.0 mV and 0.74 ± 0.03 (n=15), **C196V** -102.2 ± 1.8 mV and 0.76 ± 0.02 (n=14), **C192.196S** -68.3 ± 2.8 mV and 0.70 ± 0.02 (n=7). **(B)** Any substitution of cysteine by serine in TMD 4 reduced charge density ($p<0.05$) whereas valine was well-tolerated and not shown to differ from WT prestin. Bars that do not share a common letter are significantly different ($p<0.05$). **WT** 18.27 ± 1.89 (n=21), **C196V** 15.57 ± 1.88 (n=14), **C192V** 11.48 ± 2.83 (n=10), **C192.196S** 7.37 ± 0.81 (n=7), **C196S** 7.05 ± 0.95 (n=15), **C192S** 5.65 ± 0.40 (n=16). All values in fC/pF (mean ± SE).

Similar tolerance of valine substitution was discovered in TMD 10. At residue location 415, serine drastically reduced charge density and valine restored WT levels (Fig. 3.11). C415V NLC is hyperpolarized 6mV compared to WT prestin ($p < 0.05$), but shares consistent z with WT.

3.3.5 Valine replacement provides expected glycosylation band intensities.

The intensities of the glycosylated monomer bands were quantified for each of the serine and valine replacement mutants that were functionally characterized in Figures 3.9-3.11. Un-glycosylated monomer (~110 kDa) and glycosylated monomer (~130 kDa) bands were detected for WT prestin-GFP and each mutant construct (Fig. 3.12a). The normalized band intensity, or amount of glycosylated monomer, for each group is plotted in order of decreasing charge density (Fig. 3.12b). The last five mutants (C192.196S, C415S, C196S, C395V, and C192S) have significantly reduced charge density from WT ($p<0.05$) and the three with normal levels of glycosylation (C415S, C196S, and C395V) are likely normally folded. Figure 3.12 confirms the previous results (Fig. 3.8) for C192.196S, C415S, C196S, and C192S. Also in agreement with previous results, mutants with charge densities that are not significantly different from WT all show normal or elevated levels of glycosylated monomer, with C395S consistently producing abnormally high levels of glycosylated monomer (Figs. 3.8 and 3.12). Interestingly, valine substitutions that restored charge density compared with serine replacement (C196V, C415V, C192V) also showed normal levels of glycosylated monomer.
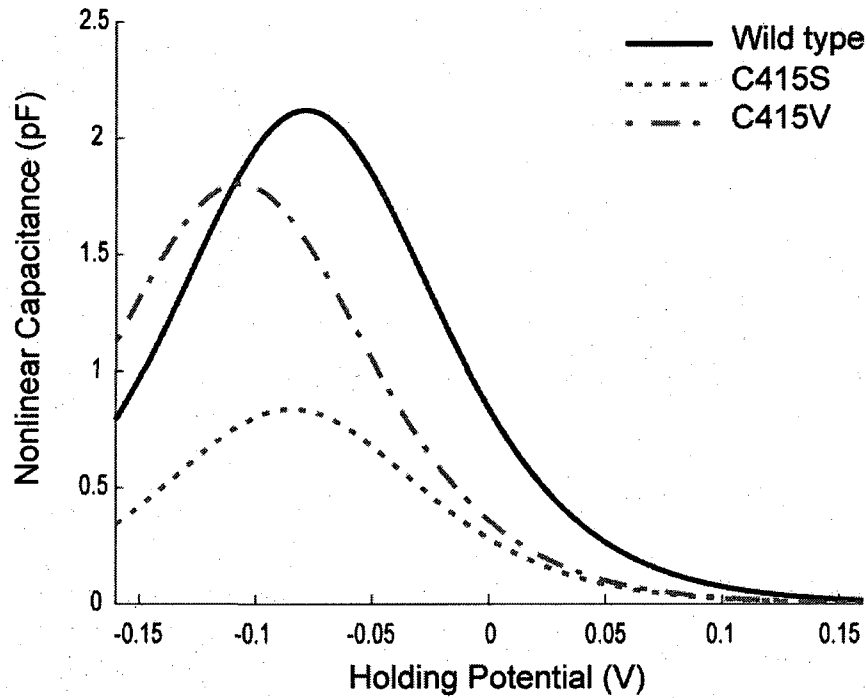
FIGURE 3.11 Valine substitution in TMD 10 provides normal charge density. NLC curves constructed from mean $V_{1/2}$, z, and charge density (see methods). C415S showed reduced charge density (p<0.01), but normal $V_{1/2}$ and z, compared to WT prestin. The charge density (Q_{max}/C_{lin}) was restored, $V_{1/2}$ hyperpolarized (p < 0.05), and z remained normal compared to wild type when valine was substituted instead of serine. C415V (n=15): $V_{1/2}$ -107.2 ± 2.7 mV, z 0.68 ± 0.01, Q_{max}/C_{lin} 15.23 ± 2.43 fC/pF (mean ± SE).

—

A)
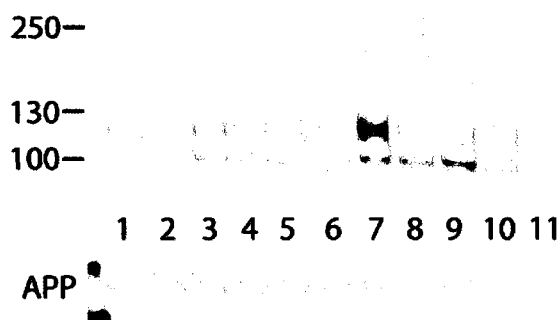
B)
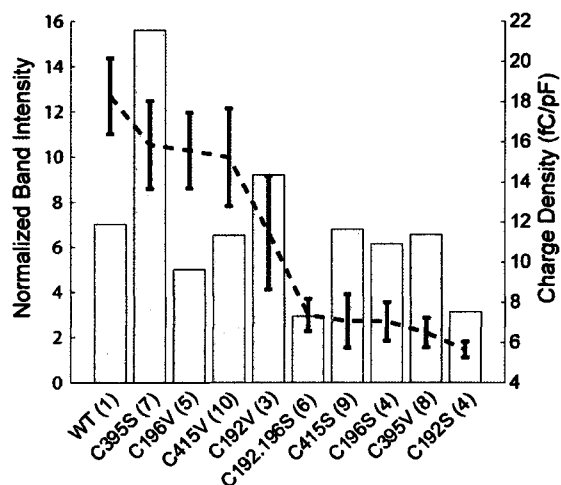
FIGURE 3.12 Comparison of monomer band intensities between serine and valine replacement mutants. **(A)** The glycosylated monomer bands were evaluated as described in Figure 3.8. Lanes: **1**-WT, **2**-C192S, **3**-C192V, **4**-C196S, **5**-C196V, **6**-C192.196S, **7**-C395S, **8**-C395V, **9**-C415S, **10**-C415V, **11**-Untransfected HEK. **(B)** Normalized glycosylated monomer band intensity is plotted in order of decreasing charge density with lane numbers of (A) shown in parentheses. C192.196S, C415S, C196S, C395V and C192S all show significantly reduced charge density compared to wild type ($p < 0.05$).

3.3.6 *Charge density varies with prestin membrane concentration*

To compare detected NLC to the amount of protein in the membrane, quantitative western blot data for each mutant group (serine and valine replacements, Figs. 3.8 and 3.12) was plotted as a function of charge density (Fig. 3.13). The pixel volumes of the glycosylated monomer bands were normalized to that of WT prestin and in cases of replicate measures (C395S, C192.196S, C415S, C196S, C192S) the mean band intensity was used. Regression analysis showed that membrane prestin concentration was directly proportional to measured charge movement ($R^2 = 0.68$). Mutations that caused loss of function (C415S, C395V, and C196S) or exhibited abnormally high membrane concentration (C395S) were not used in the regression (open squares).
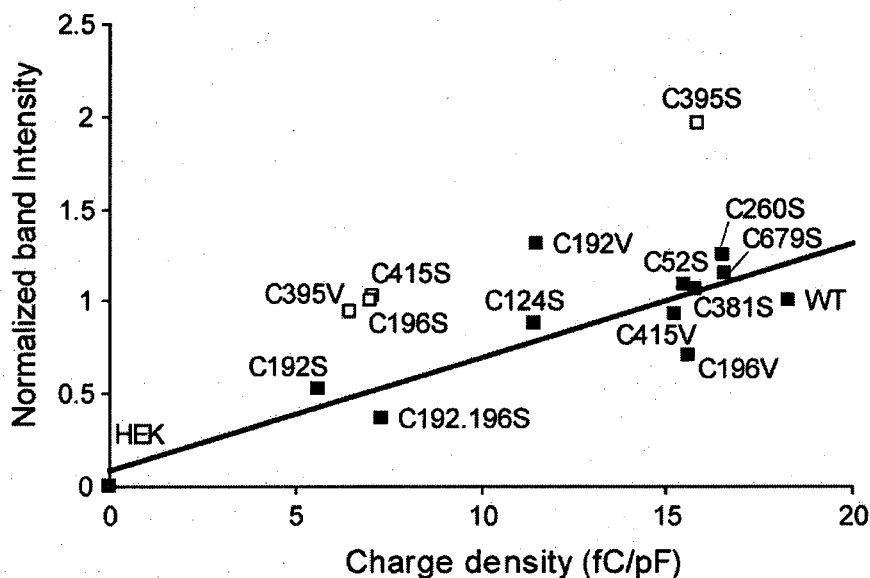
FIGURE 3.13 Charge density varies linearly with prestin membrane concentration. The glycosylated monomer band intensities from Figures 3.8 and 3.12 (normalized for equal protein loading) were plotted as a function of mean measured charge density. All values were normalized to the band intensity of WT prestin and in cases of replicate measures (C395S, C192.196S, C415S, C196S, C192S) the mean band intensity was used. Loss of function charge density mutants (C415S, C395V, and C196S) and mutants with abnormally high band intensity (C395S) were omitted (open squares), and linear regression of the remaining groups (closed squared) provided $y = 0.0611x + 0.091$ ($R^2 = 0.68$).

3.4   Discussion

3.4.1   Functional consequences of cysteine substitution by serine

To determine if cysteine residues are necessary for prestin function mutations were introduced that encode amino acid replacement with serine. Serine was chosen since it was an isosteric replacement, differing from cysteine by a single atom in the side chain. The difference between the apparent molar volumes of cysteine and serine is only 16% (Zamyatnin 1972). Our analysis revealed several residues that were important for prestin function as assayed by NLC. Specifically, we observed three types of alterations in the NLC: 1) shifted $V_{1/2}$, which changes the voltage range over which charge movement occurs, 2) tightening of the NLC curve, reflective of increased valence of charge movement, and 3) decreased area under the NLC curve, representing reduced charge movement. It is not surprising that each substitution site that resulted in alteration of NLC was contained within the hydrophobic core of prestin, since the transmembrane domains are highly conserved in comparison to other solute carrier protein family members (Okoruwa et al. 2008).

Cysteine residues in transmembrane domains 4 and 10 (Fig. 3.1a) all were important for charge transfer. Substitution by serine was not well-tolerated and greatly impaired function (Fig. 3.3). Replacement at residue 192, 196, or at both locations was equally destructive, providing 63% inhibition (Fig. 3.10). Comparable inhibited function resulted from C415S substitution in TMD 10 (Fig. 3.3). Since uncoupling of NLC and motility has not yet been reported for OHCs, the charge density mutants might have the

greatest physiological relevance in comparison to other forms of functional change ($V_{1/2}$ and z). A potential link between charge density and physiological function is supported by evidence that force generation in prestin transfected HEK cells is enhanced by prestin exhibiting normal charge movement capabilities, but unaffected by a non-functional mutant form (Zhang et al. 2007). The decreased charge density exhibited by C192S, C196S, C192.196S, and C415S can be reasonably explained through impaired prestin function, or decreased surface expression due to impaired trafficking. We used a combination of confocal imaging, Western blot, and NLC measurement to differentiate between these possible explanations (detailed in Section 3.4.2).

The discovery of loss of function mutations embedded within prestin transmembrane domains is fairly unique. Few mutations within the hydrophobic core, with the exception of those selected by evolutionary trace analysis (Rajagopalan et al. 2006), have been reported that both membrane localize and disrupt prestin charge movement. Most mutations have been shown to only alter $V_{1/2}$ (without altered charge density), or lose NLC due to an inability to insert into the plasma membrane (Dallos et al. 2006). For example, mutation of non-conserved charged amino acids (Oliver et al. 2001), the glycosylation site (Matsuda et al. 2004), or phosphorylation site (Deak et al. 2005), predominately affect $V_{1/2}$. Loss of function has been reported for a double point mutation outside the TMDs (Y499G/Y501H) (Zheng et al. 2005), or truncation of the N- or C-termini (Navaratnam et al. 2005; Zheng et al. 2006), but proper targeting has been questioned in the case of C-terminal deletions or domain swaps (Zheng et al. 2005).

3.4.2 *Membrane localization and estimation of trafficking efficiency*

Confocal imaging provides indisputable confirmation that prestin (and various mutated forms) reaches the membrane, through the coincidence of fluorescence from membrane restricted dyes and the GFP fusion (representative image, Fig. 3.2). This information is of limited value however since it does not indicate the concentration of prestin in the membrane, only the presence of protein. Quantitative fluorescent microscopy is challenging due to differences in cell-to-cell expression levels, and high throughput screens such as flow cytometry require surface reactive antibodies to identify the membrane fraction. Due to these challenges we interpret charge density as a quantitative measure of the amount of prestin in the membrane, and in cases of reduced charge density rely on Western blot data to infer whether the decrease was due to loss of function (mutation) or reduced surface expression. Most of the serine replacement mutants showed normal banding patterns (un-glycosylated and glycosylated monomer, dimer, and trimer; see results section) even in cases of altered $V_{1/2}$ or z from WT prestin (Fig. 3.7). If disulfide bonding links monomers, then hydrophobic forces were sufficient to maintain dimer formation. Reduced charge density mutants, however, showed qualitatively reduced levels of total monomer and glycosylated monomer (G) that persisted 48hrs post-transfection. Since disappearance of G band could be indicative of misfolding we quantitatively assessed band intensity for each serine replacement mutant. Of the four serine replacement mutants with significantly reduced charge density from WT prestin, two show normal G band intensity, C415S and C196S (Fig. 3.8). While C192.196S and C192S might have reduced function as the result of misfolding and reduced trafficking, we conclude that charge density reduction in the cases of C415S and

C196S are direct results of mutation since loss of de-glycosylation by itself is not known to impair function (Matsuda et al. 2004).

3.4.3 Possible explanations for loss of function

Cysteines at amino acid 196 and 415 of prestin appear to be crucial to motor activity. Western blot analysis with varying reducing treatments has shown that prestin dimers might consist of disulfide bond linked monomers (Zheng et al. 2006), and if this assembly is functionally important cysteine 196 and/or 415 might be involved. Disulfide bond mediated dimerization has been well documented in membrane proteins, such as seven-pass G-protein-coupled receptors (GPCRs) (Romano et al. 1996; Bai et al. 1998; Goldsmith et al. 1999; Zeng and Wess 1999; De Jesus et al. 2006), often with distinct functional significance (Bai et al. 1999; Rios et al. 2001; Romano et al. 2001). It is also quite likely that disulfide bonds could serve a more traditional role in prestin and act to reinforce favored protein conformation and increase stability (Alberts 2002). Rhodopsin is a classic example of a functionally important intramolecular disulfide bond, since it is required for proper folding and forms a binding pocket for the retinal chromophore (Tanuj Sapra et al. 2006).

Alternately, cysteine residues 196 and 415 of prestin may serve as palmitoylation sites. Palmitoylation is the post-translational addition of the lipid palmitate (16-carbon saturated fatty acid) to cysteine residues via a thioester covalent bond. This reversible process increases the hydrophobicity of proteins and can influence protein trafficking, localization, protein-protein interaction, and function (Basu 2004). GPCRs are commonly palmitoylated on cysteine residues located in close proximity to

transmembrane domains (Resh 1999; Basu 2004), with amino acids near the exoplasmic leaflet being particularly important (Resh 1999; Simons and Toomre 2000). Palmitoylation is thought to target proteins to lipid rafts, subdomains of the plasma membrane that are enriched in sphingolipids and cholesterol (Edidin 2003). These highly ordered phases of the membrane sequester and concentrate individual receptors and play an important role in signal transduction (Simons and Toomre 2000). Wild type prestin is known to populate lipid rafts (Sturm et al. 2007). Furthermore, palmitate turnover occurs on the order of hours, and could provide a mechanism to regulate membrane sorting or protein association (Bijlmakers and Marsh 2003). Interestingly, some dually acylated proteins (Src family tyrosine kinases) appear to localize in membrane microdomains known as caveolae (Anderson 1993; Parton and Simons 1995; Resh 1999), 50-70 nm microinvaginations of the plasma membrane, and membrane curvature has been suggested to play a central role in OHC electromotility (Raphael et al. 2000).

Finally, serine replacement at residue 196 or 415 may have disrupted the purported Cl^- binding pocket of prestin. In chloride channels partial positive charges contributed by helix dipoles and side chain groups provide an energy well for anion conduction (Dutzler et al. 2002). In prestin, intracellular Cl^- is required for NLC and voltage sensing. Intracellular Cl^- depletion reduces charge density and shifts $V_{1/2}$ to depolarized potentials (Fakler and Oliver 2003; Rybalchenko and Santos-Sacchi 2003; Santos-Sacchi et al. 2006) implying that Cl^- ion(s) bind prestin and are either directly involved in charge translocation (Dallos et al. 2006) or cause an allosteric change that allows outward movement of a positive gating charge in response to depolarized transmembrane potential (Rybalchenko and Santos-Sacchi 2003). Since protein folding

is determined by complex interaction of amino acid physicochemical properties, our residue replacement may have altered tertiary structure and prevented Cl⁻ binding. Relevant amino acid properties include: physical size, hydropathic character, and hydrogen bonding capability. Reports of residue volume (Zamyatnin 1972; Goldsack and Chalifoux 1973; Bull and Breese 1974) and side chain volume (Krigbaum and Komoriya 1979) show Ser < Cys < Val (valine substitution is discussed later). Hydrophobicity follows the same rank order (Kyte and Doolittle 1982), with polar serine being hydrophilic and non-polar valine most strongly hydrophobic. Based on electronegativity of the side chain donor, serine provides stronger hydrogen bonds than cysteine, and valine does not hydrogen bond. Serine hydrogen bonds (5 kcal/mol) have been characterized as stabilizers of alpha helices (Senes et al. 2001).

3.4.4 Valine substitution eliminates some potential cysteine roles

Proof of functionally relevant disulfide bonding or palmitoylation would require equivalent charge density reduction with either serine or valine replacement. Instead, we saw restoration of function with C196V and C415V (Figs. 3.10 and 3.11). This does not preclude either process from occurring in prestin, but rather highlights that if these processes are present their loss is not detectable and hence not required for NLC. For example disulfide bonds may not directly affect prestin NLC measures, but could indirectly affect prestin function by altering residence time in the membrane. It is most likely that the reduced function of C196S and C415S is the result of disruption to the Cl⁻ binding pocket, because reduced charge density could not be explained by simple misfolding. This is potentially caused by introduction of incompatible physicochemical properties, such as significant differences in hydrophobicity, based on trends observed in

all tested mutants. The relationship between our mutants and current topological models are evaluated in a subsequent section.

Valine substitutions provide valuable data for the creation of a cysteine-less prestin construct. Such a construct could be used for cysteine scanning mutagenesis, a technique in which cysteines are re-introduced at various locations throughout the protein. The presence of a single cysteine would allow detailed topological study using thiol reactive probes and targeting of bulky sulfhydryl agents to various locations in prestin. The goal of the second procedure would be to identify locations within prestin (functional domains), sensitive to the treatment, whose motions might be important for nonlinear charge movement. Cysteine scanning mutagenesis is widely used in the study of transporters and ion channels in which membrane localized and fully functional cysteine-less constructs are available (van Iwaarden et al. 1992; Audia et al. 2006; Zhang et al. 2006). We have been working to develop an appropriate cysteine-less prestin-GFP fusion for the past couple years and found an all serine construct to be unsuitable (unpublished data). Our current findings suggest that serine substitution at residues 52, 124, 260, 381, 395, and 679, and valine substitution at 192, 196, and 415 might be feasible.

3.4.5   Other observed effects of cysteine substitution

Cysteine residues in TMD 9 were important for establishing the operating range of prestin function since substitution with serine drastically altered $V_{1/2}$ (Fig. 3.4). It has been suggested that reduction in membrane cholesterol levels during OHC development could tune prestin function by altering $V_{1/2}$ and consequently the charge moved during

receptor potential (Rajagopalan et al. 2007). Cholesterol affects both membrane material properties (Needham and Nunn 1990) and the extent of prestin self-association (Rajagopalan et al. 2007). Recently it was reported that a prestin mutation (K233Q, K235Q, and R236Q (Oliver et al. 2001)) causing a 65 mV hyperpolarizing shift in $V_{1/2}$ did not affect hearing of a knock-in strain of mice (Gao et al. 2007). However, the idea of cholesterol tuning remains plausible since the physiological consequence of a depolarizing shift (opposite polarity), such as that caused by C395S, is unknown.

Since the $V_{1/2}$ shift measured in the C395S mutant was of similar magnitude and polarity to the shift induced in cholesterol depleted HEK expressing WT prestin (Rajagopalan et al. 2007) we investigated if the two phenomena shared a common mechanism. C395S did not lose sensitivity to membrane cholesterol levels. In addition to the 73 mV C395S was depolarized compared to WT prestin (Fig. 3.4), depletion of membrane cholesterol established new, even further depolarized $V_{1/2}$ in a time-dependent manner (Fig. 3.5). We conclude that NLC shift resulting from cholesterol depletion is either the result of altered membrane material properties, or if cholesterol is interacting directly with prestin, the 395 site is not involved.

Interestingly, valine replacement at 395 restored normal $V_{1/2}$ (Fig. 3.9), but was a loss of function mutation since it significantly decreased charge density and exhibited normal glycosylated monomer levels (Fig. 3.12).

The physiological significance of charge movement valence is unknown. The valence of the Boltzmann function characterizes the voltage range over which prestin undergoes a hypothesized two-state transition. The transition is commonly thought of as

a prestin conformational change, so conceptually z can be thought of as a descriptor of the rate (tightness of voltage range) or abruptness of conformational change. C260S significantly altered the mechanics of the prestin two-state transition, elevating valence and reducing the voltage range over which charge transfer occurs (Fig. 3.6), while maintaining normal $V_{1/2}$ and charge density. Since C260S moved the same total charge as wild type prestin, the increase in valence can also be interpreted as a more complete translocation of charge. For example WT prestin ($z = 0.67 \pm 0.01$) moves the charge carried by an electron 67% across the membrane, and this is increased to nearly complete translocation in C260S (80%, see Fig. 3.6). It would be interesting to see if any structural differences are apparent in oligomers of C260S at 2 nm resolution, in particular if the dimensions of the low density core are altered (Mio et al. 2008).

3.4.6   Charge density varies with prestin membrane concentration

Our mutations altered both prestin membrane concentration and charge density. After eliminating mutants in which amino acid replacement caused loss of function (C415S, C196S, and C395V) we observed linearity between the concentration in the membrane and whole-cell prestin activity (Fig. 3.13). This is an important control since it proves that point mutagenesis is not intrinsically disruptive to prestin function. The slight variation in charge density among constructs that are not statistically different than WT prestin (C124S and all with greater charge density) is readily explained due to slight variations in surface expression. An inducible promoter system would be required to systematically map the linearity within the low charge density region. Interestingly, C395S produced nearly twice as much glycosylated monomer as WT prestin without any increase in measured charge density. This indicates that pools of nonfunctional prestin

reside in the membrane in addition to an active fraction that accounts for prestin-associated charge movement.

3.4.7 Relation to proposed topological models

Our cysteine mutations can be rationalized in terms of the existing topological models and even make predictions regarding local residue environments. Since physical size is closely matched between cysteine and serine, hydropathic character seems to be the crucial property affecting whether cysteine replacement is tolerated. Based on hydrophobicity (Kyte and Doolittle 1982) valine is expected to substitute well for buried residues (Bordo and Argos 1991) within the hydrophobic helices, and serine would be suitable near interfaces and other water exposed regions. Cysteines at locations 192 and 196 are predicted to reside within the hydrophobic core by each of the suggested topological models (Fig. 3.1, Table 3.1) and therefore it is not surprising that serine replacement inhibited function, evident by decreased charge movement, while valine replacement restored WT charge movement. Similar results are observed for cysteine substitution at 415, where two of the three models predict the site to be buried. The trend was reversed at site 395, with serine being tolerated and valine impairing charge movement. This suggests that the residue is interfacial, as suggested by the 12-pass re-entrant loop model, or if buried, as suggested by the other two models (12-pass evolutionary trace and 10-pass), the residue is likely exposed to an aqueous local environment. Based on this idea, C260S and C381S may provide information about the low density core of prestin oligomeric structures (Mio et al. 2008). If these residues are buried, their ability to tolerate serine replacement might imply that the residues line a water-filled occluded pore, an idea that is consistent with TEM data (Mio et al. 2008) and

suggested incomplete Cl$^-$ (Oliver et al. 2001) or charged residue (Rybalchenko and Santos-Sacchi 2003; Rybalchenko and Santos-Sacchi 2008) translocation in prestin.

3.5   Summary of results

We tested replacement of each of the 9 cysteine residues in prestin with serine and observed three types of alterations in the NLC: 1) shifted $V_{1/2}$, which changes the voltage range over which charge movement occurs, 2) tightening of the NLC curve, reflective of increased valence of charge movement, and 3) decreased area under the NLC curve, representing reduced charge movement.   While each alteration impacts an aspect of function, decreased charge density might be the most physiologically relevant since decoupling of charge movement and electromotility has not been reported.   In general, decreased charge density can be explained through impaired prestin function, or decreased surface expression due to impaired trafficking.   Of the five mutations that produced significantly reduced charge density (C192S, C196S, C192.196S, C395V, and C415S) three showed normal levels of glycosylated monomer (C196S, C395V, and C415S), indicating that these constructs were likely normally folded and the mutation accounted for diminished function.   Analysis of the functional mutants revealed that charge density was linearly related to the concentration of prestin in the membrane. Valine substitutions were made at each location where serine impaired charge density (192, 196, and 415) and in each case function was restored indicating that if disulfide bonding or palmitoylation are involved in prestin, they do not serve a functional role that can be detected via NLC.   Interestingly, both cysteine 196 and 415 are unique to prestin

in comparison to its most closely related SLC26 family member PAT1 (McGuire et al. 2006), which does not exhibit NLC (Waldegger et al. 2001). These sites might be important structural determinants of the Cl^- binding pocket. Overall our analysis suggests that cysteines 52, 124, 260, 381, 395, and 679 reside in water-exposed hydrophilic locations based on maintenance of normal charge density upon serine substitution; cysteines 192, 196, and 415 are buried in the hydrophobic core since these locations did not tolerate serine, but instead produced normal charge movement with valine. Combining serine and valine substitutions might allow development of a functional, membrane-localized, cysteine-less prestin mutant, for more detailed study of prestin topology and further characterization of functionally relevant domains.

CHAPTER 4

VOLTAGE-DEPENDENT PRESTIN SELF-INTERACTIONS DEMONSTRATE CONFORMATIONAL CHANGE OF THE PRESTIN MOTOR[1]

4.1   Motivation for monitoring prestin self-interactions

The unique ability of outer hair cells (OHCs) to change their length in response to changes in transmembrane potential, a process termed electromotility, requires the activity of the transmembrane motor protein prestin (Zheng et al. 2000). The ability of prestin to move charge within the cell membrane has commonly been used as a surrogate measure of OHC motility and accepted as a signature of electromotility (Ashmore 1990; Santos-Sacchi 1991). This intramembranous charge movement is displayed as a nonlinear capacitance (NLC) in OHCs (Santos-Sacchi 1991; Huang and Santos-Sacchi 1993; Tunstall et al. 1995) and in mammalian cells exogenously expressing prestin (Zheng et al. 2000; Chambard and Ashmore 2003; Deak et al. 2005; Iida et al. 2005; Rajagopalan et al. 2006; Rajagopalan et al. 2007). NLC is interpreted as a description of the occupancy probability of the two conformational states of prestin. Specifically, prestin is modeled to adopt an expanded conformation for hyperpolarized potentials and a contracted conformation at depolarized potentials (Dallos et al. 1993; Iwasa 1994; Oliver et al. 2001). This molecular description, links nonlinear charge movement to prestin conformational change as the underlying mechanism of OHC motility. However, direct

---

[1] Data in this chapter was collected in collaboration with Ramsey I. Kamar

measures of voltage-dependent structural changes in prestin are necessary to verify this connection.

We investigated whether changes in the transmembrane electric field induce molecular motion by measuring fluorescence resonance energy transfer (FRET) between C-terminally tagged prestin proteins. Our data demonstrate that prestin-prestin FRET decreases upon membrane depolarization over an operating range of voltages relevant to electromotility. Furthermore, the changes in prestin FRET occur over a similar voltage range as prestin-associated charge movement (NLC) suggesting that both measures are tightly coupled by a voltage-dependent conformational change in prestin. These results are the first direct evidence of voltage-induced motion in prestin and demonstrate a fluorescence signature associated with prestin-dependent motility.

4.2   Materials and methods

4.2.1   Plasmid design

The gerbil prestin gene (accession number AF230376) was inserted into the multiple cloning site (MCS) of the pECFP-N1 and pEYFP-N1 vectors (Clontech, Mountain View, CA) to create C-terminal fusion proteins (denoted prestin-CFP and prestin-YFP) (Greeson et al. 2006). A positive FRET control was created by amplifying CFP   from   pECFP-N1   (forward/   reverse   primers: 5'-acacggtaccaatggtgagcaagggcgaggagc-3'/5'-caccaccggtcccttgtacagctcgtccatgccgaga-3') and inserting into the KpnI and AgeI site of the remaining MCS of the prestin-YFP

fusion. This resulted in a prestin-CFP-YFP fusion with a short five amino acid sequence (GPVAT) separating the fluorescent proteins.

4.2.2 Prestin expression and cell culture

HEK293 Cells were grown in 6-well plates containing DMEM supplemented with 10% BCS (Invitrogen, Carlsbad, CA), 1% penicillin-streptomycin, 14.3 mM HEPES, and 16.1 mM NaHCO$_3$. Cells below passage 25 were transfected with both prestin-CFP and prestin-YFP using 2 µg of each plasmid DNA and 3 µL/plasmid Fugene 6 transfection reagent (Roche, Indianapolis, IN) according to the manufacturer's directions. For the positive FRET control a single plasmid, prestin-CFP-YFP, was transfected. Eight hours after transfection cells were trypsinized and replated onto #1.5 coverslips and then imaged 24-36 hours post-transfection in extracellular patch solution at room temperature. PBS was used to acquire FRET measurements in unpatched cells and is noted in the relevant figures.

4.2.3 FRET microscopy

Fluorescence resonance energy transfer (FRET) has been used to detect the interactions of proteins within living cells (Tsien 1998) due to its sensitivity to displacements between molecules in the 1-10 nm range (Lakowicz 1999). The FRET efficiency (E) is related to the separation between fluorophores (r) and their Förster radius (R_o), or the radius at which the pair produces 50% of the maximal FRET (Eqn. 4.1).

$$E = 1/(1 + (r/R_o)^6)$$
Eqn. 4.1

FRET measurements were performed on the Zeiss LSM 510 scanning confocal microscope using "multitrack" between donor (CFP) and acceptor (YFP) channels to allow fast switching between photomultiplier tubes (PMTs), laser wavelengths, and settings for each channel every scan. This prevented donor emission from entering the acceptor channel. Donor and acceptor XFPs were excited with 458 and 514 nm light, respectively, both from an Ar^+ laser. Fluorescence was collected with a 63X, 1.4NA microscope objective. Using a secondary dichroic and separate bandpass filters for each channel, CFP fluorescence was collected in a band that effectively spanned 480-520 nm and YFP fluorescence was collected in a band spanning 545-590 nm. A pinhole placed in front of the PMT detector, in a conjugate plane to the focal plane of the objective, was set to 2 Airy units.

Only cells with clear membrane localized prestin-CFP and prestin-YFP fluorescence were patch clamped (see Section 4.2.5). After a stable whole-cell patch was established, regions of interest (ROIs) were selected as depicted in Figure 4.1. Briefly, an approximately 10.5 µm square region, labeled region 1, was placed on a segment of membrane with sufficient and uniform fluorescence. Three circular regions, each with diameters of approximately 2.9 µm (labeled region 2, 3, and 4) were contained within region 1. Region 2, the YFP bleach region, and region 3, the control region, were centered on the cell membrane. Region 4 was placed outside the cell, to monitor the background signal in the CFP channel. At the onset of the FRET measurement 40

imaging scans (580 ms/scan) were taken of region 1 to allow the CFP fluorescence level to stabilize. After these scans, the acceptors in region 2 were bleached at high laser power (~9 seconds) to de-quench the donors in that region only. The transmembrane potential was clamped at the desired test voltage at during the 30th scan of region 1, 10 frames (~6 seconds) prior to the bleach. Finally, 10 additional imaging scans of region 1 were acquired post bleach.

4.2.4 FRET analysis

The FRET efficiency (E) was determined by measuring the donor fluorescence before (F_{da}) and after (F_d) photobleaching the acceptors using Equation 4.2 (Lakowicz 1999):

$$E = 1 - (F_{da} - BG)/(F_d - BG)$$
Eqn. 4.2

F_{da} and F_d are the fluorescence of the donor in the presence (subscript da) and absence (subscript d) of the acceptor and BG is the average background signal in the donor channel of region 4 over the entire experiment.
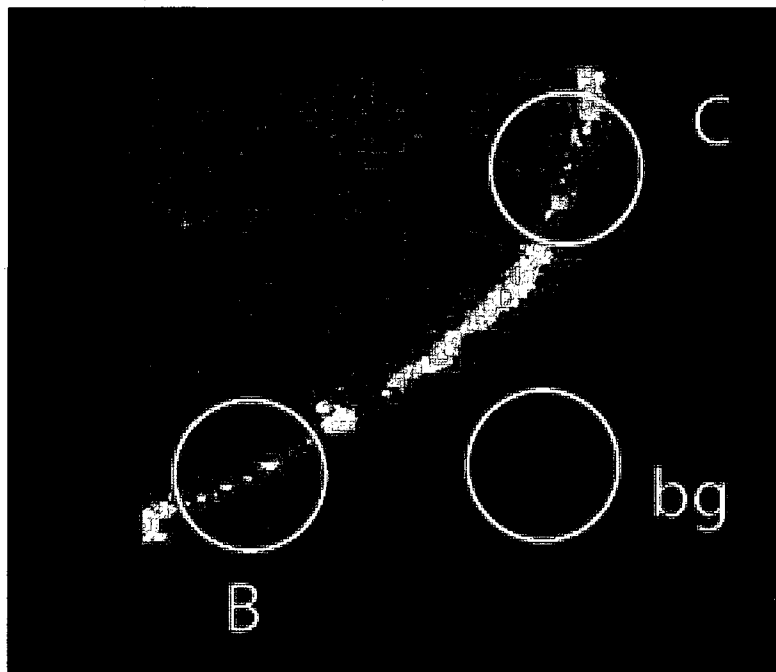
FIGURE 4.1 Region of interest placement for FRET measurement. The fluorescent image shows a region of HEK cell membrane with well-localized prestin-CFP and prestin-YFP. The YFP and CFP channels are shown in overlay. The image shows the bleach (B), control (C), and background (bg) regions of interest (ROIs). Yellow false color represents YFP fluorescence, which has been photobleached in the bleach region, and blue false color represents CFP fluorescence.

Efficiencies were calculated for both the bleach and the control regions. In principle FRET efficiency should be zero in the control region since the donors have not been de-quenched. In practice however, we measure a background control efficiency of about 3%. Imaging causes mild photobleaching and the non-zero control efficiency might be explained by diffusion of donors, from outside region 1, into the control region during the 9 second period that the acceptor is being bleached, or by donors that regain their fluorescence immediately prior to F_d determination (Garcia-Parajo et al. 2000). We correct for these unavoidable, systematic errors by subtracting the control efficiency from the efficiency measured in the bleach region on a cell-by-cell basis and we report this difference as the experimentally determined FRET. Only cells that had control efficiency between -5 and +10% where retained for analysis and the mean FRET is reported for each voltage tested. The FRET versus voltage data was fit to a Boltzmann function shown in Equation 4.3.

$$E(V) = A_2 + (A_1 - A_2)/(1 + e^{(V-V_0)/\alpha})$$ Eqn. 4.3

A_1 and A_2 are the hyperpolarized and depolarized asymptotes, respectively; V_o is the potential at half-maximal FRET; and α is a parameter describing the width of the FRET versus voltage relationship.

4.2.5 Electrophysiology

2-4 MΩ micropipettes were formed from Kimax-51 capillary tubes (1.5/0.8 mm OD/ID) on a P-97 puller (Sutter, Novato, CA). The patch pipettes and extracellular bath both contained common blocking solutions (Pipette: 130 mM CsCl, 2 mM $MgCl_2$, 10 mM EGTA, 10 mM HEPES; Extracellular: 99 mM NaCl, 20 mM TEA-Cl, 2 mM $CoCl_2$, 1.47 mM $MgCl_2$, 1 mM $CaCl_2$, 10 mM HEPES) to minimize ionic conductance (Deak et al. 2005). For experiments requiring prestin inhibition 10 mM salicylate was added to both solutions. All solutions were titrated to pH 7.3 and dextrose added to obtain 300 ± 3 mOsm (Osmette A; Precision Systems, Natick, MA). During the experiment micropipette placement was controlled using a Burleigh PCS-6200 Micromanipulator (EXFO Life Sciences, Rochester, NY), and pipette pressure monitored and neutralized before recording (PM01R digital pressure meter; WPI, Sarasota, FL). We only attempted to patch healthy, single cells showing suitable fluorescence. For all experiments gigaohm on-cell seals were obtained, normal NLC characteristics verified prior to FRET measurement, and membrane resistance monitored to ensure seal integrity during changes in the holding potential.

Membrane capacitance (C_m) and membrane resistance (R_m) were determined by applying a sinusoidal command voltage at a superimposed DC offset and then determining the real and imaginary components of the admittance, the complex current response scaled by the command voltage (Lindau and Neher 1988). We used a software-based phase-sensitive detector implemented in PatchMaster software (HEKA, Mahone Bay, NS) to acquire this information. Specifically, we applied an 800 Hz, 10 mV sinewave and measured the current response as DC holding potential was stepped from -

140 to +140 mV in 2 mV increments (HEKA EPC 10 Plus Amplifier with 18-bit DAC). At each DC potential four complete sinusoidal voltage cycles occur and discrete capacitance values are calculated from the latter three.

4.2.6 NLC analysis

Capacitance versus holding potential traces are fit to the first derivative of the two-state Boltzmann function (Eqn. 4.4) using MATLAB (MathWorks, Natick, MA). The first term of the fit represents the nonlinear component, caused by prestin-related charge movement, while the second term (C_{lin}) is linear capacitance derived from the dielectric properties of the membrane and is proportional to cell size. Since variation in cell size causes differences in the maximal charge transfer (Q_{max}), the charge movement is normalized to C_{lin}. This quantity, designated as charge density, has units of fC/pF (Oliver and Fakler 1999) and was reported along with the voltage at half-maximal charge movement ($V_{1/2}$) and valence (z). The fit also contains the following constants: e the elementary charge, k Boltzmann's constant, and T the absolute temperature (298 K).

$$C_m = \frac{Q_{max}\left(\frac{ze}{kT}\right)}{\exp\left[\left(\frac{ze}{kT}\right)(V - V_{1/2})\right]\left(1 + \exp\left[-(V - V_{1/2})\left(\frac{ze}{kT}\right)\right]\right)^2} + C_{lin} \qquad \text{Eqn. 4.4}$$

4.3   Experimental results

4.3.1   Voltage-dependent FRET decreases with depolarization

FRET was measured in live HEK cells co-expressing C-terminally tagged prestin FRET pairs while transmembrane voltage was controlled using the whole-cell patch clamp technique. NLC was acquired prior to each attempted FRET measurement (n = 240). The average values of $V_{1/2}$, z, and charge density (Q_{max}/C_{lin}) were -54.6 ± 0.9 mV, 0.728 ± 0.004, and 19.1 ± 0.53 fC/pF, respectively (mean ± SE). The FRET efficiency was characterized at imposed transmembrane voltages of -140, -90, -55, 0, +30, and +60 mV, which span the active range of prestin function (Zheng et al. 2000; Chambard and Ashmore 2003). In addition, we determined FRET in unpatched HEK cells measured in PBS to obtain measurements at the HEK cell resting potential (-50 ± 1.6 mV; see (Fliegert et al. 2007)).

The FRET efficiency is a function of transmembrane voltage and decreases upon depolarization, with the midpoint of the transition occurring near $V_{1/2}$ of NLC (Fig. 4.2, Table 4.1). The FRET efficiency measured at -140 mV (10.6 ± 2.0%) was significantly higher (p < 0.05) than that measured at +60 mV (3.2 ± 1.9%). Figure 4.3 shows the efficiencies in the bleach and control regions that were used to compute FRET at these two voltages. Our method did not allow us to explore potentials more hyperpolarized than -140 mV or more depolarized than +60 mV, since sustained current flow during the photobleaching phase of the measurement was accompanied by reduced membrane resistance and at times total seal loss. Our FRET analysis only includes cells which met

the following criteria during the course of the measurement: 1) the membrane did not move relative the ROIs, 2) membrane resistance remained constant and in excess of 1 $G\Omega$, and 3) normal NLC curves were obtained both before and after the FRET measurement. Approximately 40% of patched cells satisfied all of these criteria.
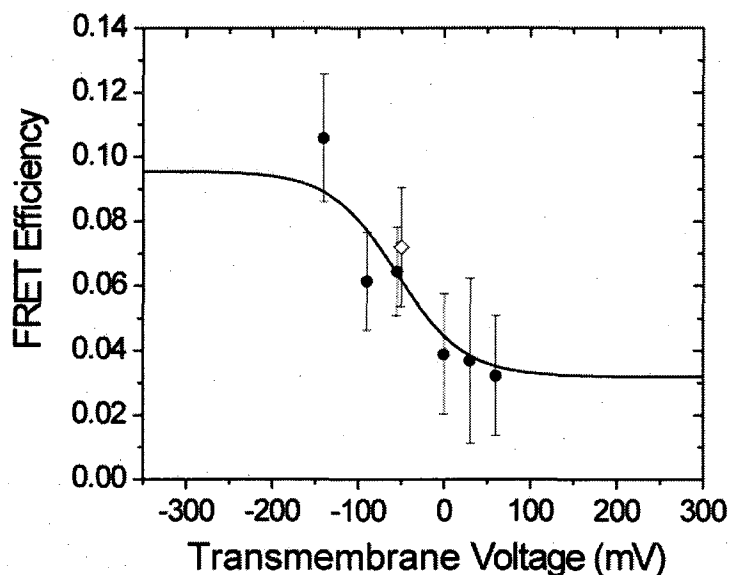
FIGURE 4.2 Prestin self-association decreases with depolarization. FRET was determined as the difference between efficiencies in the bleach and control region (see methods) and observed to decrease upon depolarization of transmembrane voltage. Solid circles represent groups of cells that were patch clamped and the open diamond represents unpatched cells measured at resting potential in PBS (-50 ± 1.6 mV from (Fliegert et al. 2007)). The number of cells measured for each potential, listed from left to right are: 7, 18, 16, 18, 22, 7 and 7. Error bars represent standard error using error propagation. The solid line is a fit of the FRET data to a Boltzmann function (Eqn. 4.3) and is weighted by the statistical error bars. The fit is constrained to have an asymptote of A_2 = 0.032, the FRET value of the depolarized tail (at +60 mV), and the center is constrained to V_o = -54.6 mV, the mean $V_{1/2}$ of the NLC data. Fit to the FRET data provides α = 39.03 mV and A_1 = 0.095 (discussion of the fit is provided in Section 4.3.2).

TABLE 4.1 FRET Efficiency values measured at various transmembrane potentials

Transmembrane voltage (mV)	FRET efficiency (%) Mean ± SE
-140	10.6 ± 2.0
-90	6.1 ± 1.5
-55	6.4 ± 1.4
-50*	7.2 ± 1.9
0	3.9 ± 1.9
30	3.7 ± 2.6
60	3.2 ± 1.9

* Reported resting potential of HEKs in PBS (Fliegert et al. 2007), all other voltages imposed by whole-cell patch clamp.
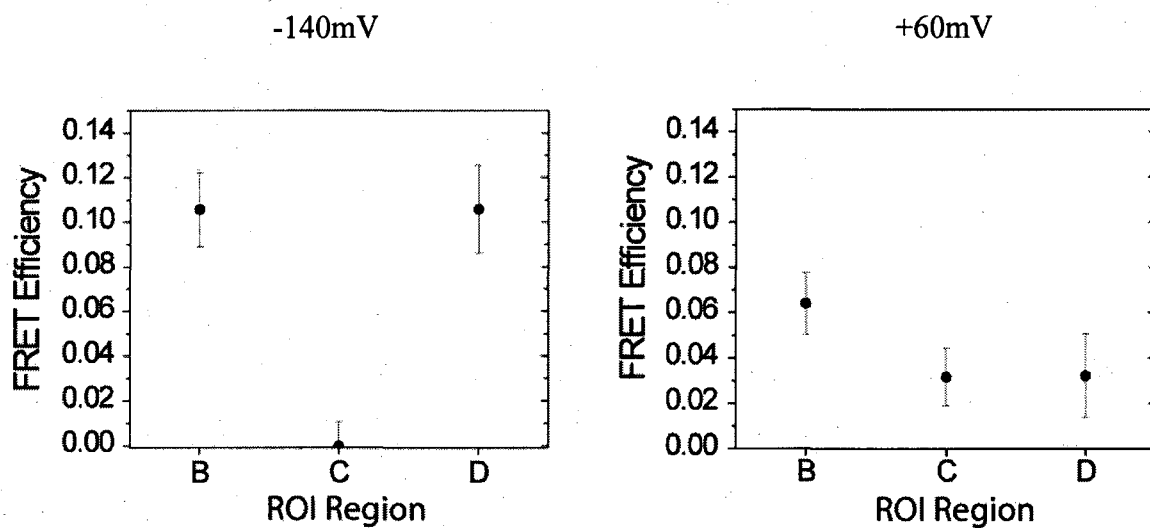
FIGURE 4.3 Variation in FRET efficiencies show statistical significance. Plots show bleach region efficiency (B), control region efficiency (C), and the difference ($D = B - C$), which is the reported FRET efficiency. The FRET at -140 mV (left) was significantly higher than at +60 mV (right), $p < 0.05$. For -140 mV (n = 7): B, C, and D were 10.6 ± 1.7, 0.0 ± 1.1, and 10.6 ± 2.0, respectively. For +60 mV (n = 7): B, C, and D were 6.4 ± 1.4, 3.2 ± 1.3, and 3.2 ± 1.9. All efficiencies (%) reported as mean ± SE.

4.3.2 Sigmoidal fit of the FRET data

We fit the FRET efficiency versus voltage data with a sigmoidal Boltzmann function (Eqn. 4.3), since a common theoretical model posits a two-state motor. Consistent with this fitting scheme, the midpoint of the FRET transition occurred near $V_{1/2}$ of the NLC data and the FRET data appeared to saturate at depolarized potentials (Fig. 4.2). Based on these observations the lower asymptote was constrained to the FRET value at +60 mV ($A_2 = 0.032$) and the midpoint constrained to $V_{1/2}$ of NLC ($V_o = -54.6$ mV). Fitting the Boltzmann function to the FRET data provides $\alpha = 39.03$ mV and $A_1 = 0.095$.

In Figure 4.4 we compare the derivative of the Boltzmann fit of the FRET data to the mean NLC curve. The mean NLC curve was reconstructed from average Boltzmann parameters (Q_{max}, $V_{1/2}$, and z) acquired from pre-FRET NLC curves (n = 240). The derivative of the Boltzmann fit to the FRET data takes the form shown in Equations 4.5 and 4.6. All parameters of Equation 4.5 and the constants of Equation 4.6 (e, k, and T) were previously defined (Eqns. 4.3 and 4.4, respectively). Further discussion of Equation 4.6 is provided below.

$$\frac{\partial E}{\partial V} = \frac{e^{-(V-V_o)/\alpha}}{(1+e^{-(V-V_o)/\alpha})^2} \qquad \text{Eqn. 4.5}$$

$$\frac{1}{\alpha} = \frac{z_{FRET}\, e}{kT} \qquad \text{Eqn. 4.6}$$
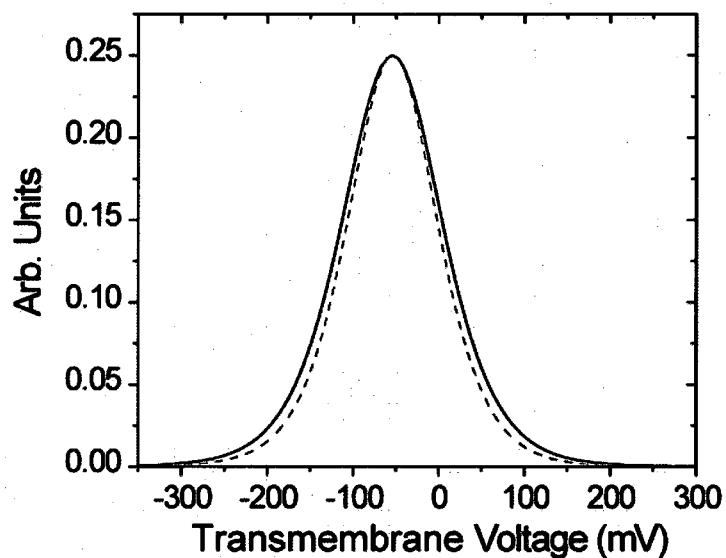
FIGURE 4.4 Comparison of fit to FRET data with mean measured NLC. The black solid curve is the derivative of the Boltzmann fit (Eqns. 4.5 and 4.6) to FRET data from Figure 4.2. The red dashed curve is average of fits (Eqn. 4.4) to measured NLC traces from 240 cells. Both curves are normalized to have a peak of 0.25 for display purposes. A parameterization of the widths differs by only 10% ($z_{FRET} = 0.655 \pm 0.340$ for the solid FRET curve, $z = 0.728 \pm 0.004$ for the dashed NLC curve).

The FRET and NLC fits were normalized to a unitless form, such that they both had a peak of 0.25, to allow direct comparison between the two. The independent fits show close agreement with each other. The width (a) of the function is inversely proportional to the dimensionless parameter z_{FRET} (Eqn. 4.6) which is analogous to the valence z of the NLC (Eqn. 4.4). We find that z_{FRET} differs from z by only 10%.

4.3.3 *Salicylate eliminates voltage-dependent FRET trend*

Cells co-expressing prestin-CFP and prestin-YFP were patch clamped in 10 mM salicylate (contained in both pipette and extracellular solutions) and FRET efficiency was measured at -90 and +60 mV (Fig. 4.5). As expected, cells showed a loss of NLC indicating a loss of prestin function (NLC data not displayed). The FRET efficiency at -90 mV (7.1 ± 1.3%) remains about the same as the untreated case (6.1 ± 1.5%), while the efficiency at +60 mV is significantly increased from 3.2 ± 1.9% to 9.6 ± 1.5% ($p < 0.05$). The latter effect indicates a departure from the previous trend, shown in Figure 4.2, where FRET decreased upon depolarization.
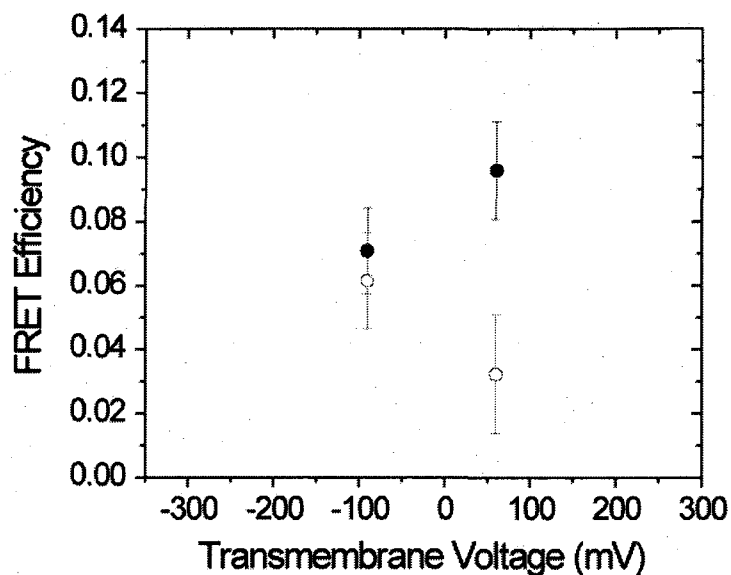
FIGURE 4.5 Effects of salicylate on voltage-dependent FRET. FRET efficiency was measured in cells co-expressing prestin-CFP and prestin-YFP at -90 mV (n = 16) and +60 mV (n = 13) with 10 mM salicylate application (solid circles). FRET in untreated cells (no salicylate) at -90 mV and +60 mV (from Fig. 4.2) are plotted for comparison (open circles). Application of 10 mM salicylate simultaneously eliminated NLC (data not shown) and FRET decrease-upon-depolarization. Salicylate did not affect the FRET measure at -90 mV which remained ~7% with or without the treatment. FRET at +60 mV, however, was significantly increased from 3.2 ± 1.9% to 9.6 ± 1.5% by salicylate application (p < 0.05). Values reported as mean ± SE.

4.3.4 FRET does not depend on prestin expression level

To test whether FRET efficiency is influenced by the amount of prestin expressed in the membrane, FRET was plotted versus charge density (Q_{max}/C_{lin}) for each holding potential tested. A representative plot of FRET versus charge density (for a holding potential of -90 mV) is displayed in Figure 4.6 and illustrates no correlation between the measures. Thus, the FRET efficiency does not show dependence upon charge density.

4.3.5 Validation of low FRET conditions

To test our ability to measure a true zero transfer efficiency, we performed a negative FRET control using unpatched cells expressing only donor molecules (prestin-CFP) in the membrane. We find no significant difference in FRET efficiencies between bleach and control regions (Figs. 4.7a and 4.7b) and therefore measure zero FRET. This result confirms that the low FRET efficiencies at 0, +30, and +60 mV in Figure 4.2 reflect true non-zero FRET measurements.
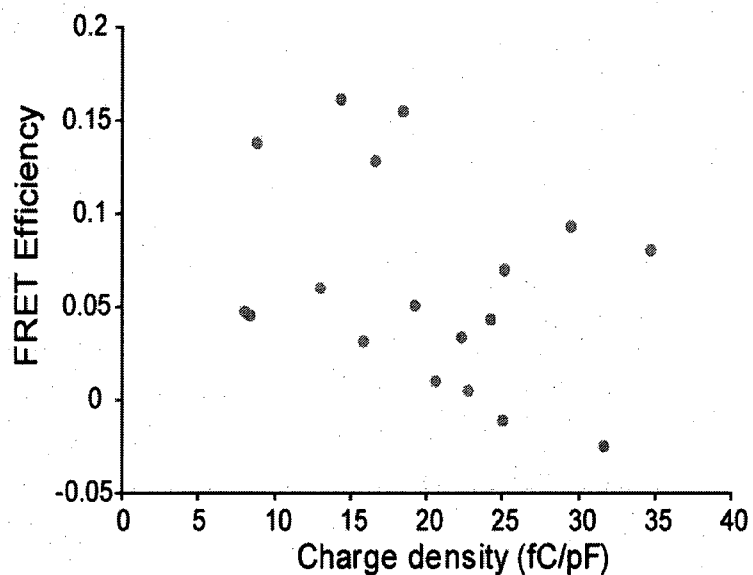
FIGURE 4.6 FRET measures do not depend upon prestin expression levels. Linear regression of data collected from cells clamped at -90 mV during the FRET measurement shows no correlation between the FRET efficiency and amount of prestin in the membrane, determined by charge density measurement. The null hypothesis that the slope differs from zero cannot be rejected (p = 0.19). All other voltage treatments showed similar results.
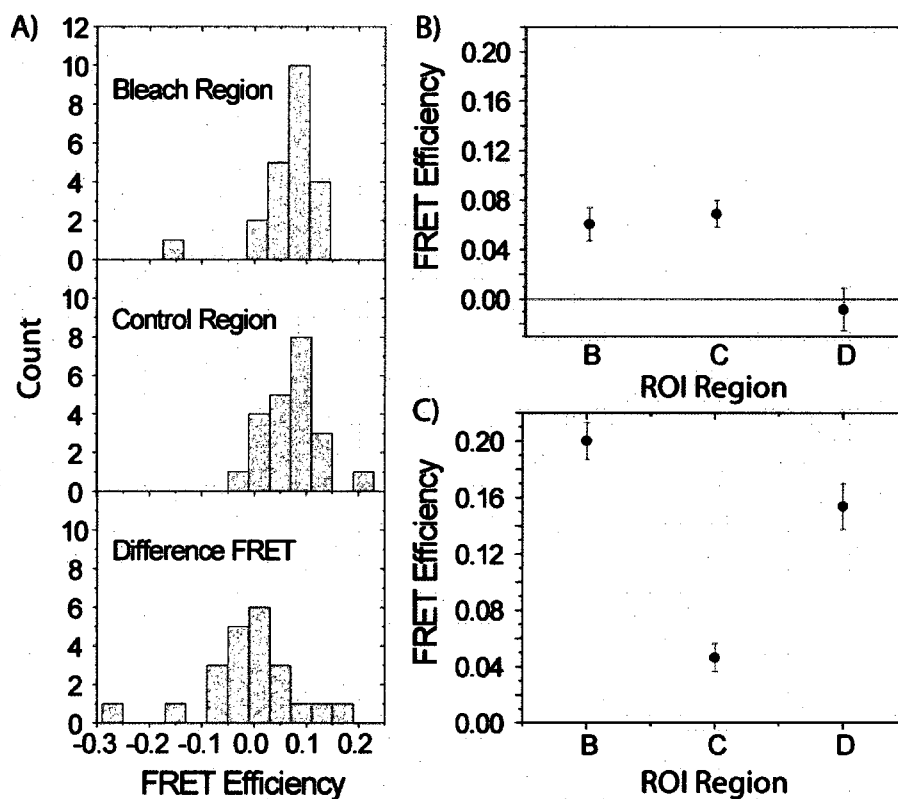
FIGURE 4.7 FRET controls provide expected results. The negative FRET control (cells expressing prestin-CFP only) displays zero measured transfer efficiency, and the positive FRET control (cells expressing prestin-CFP-YFP) shows a relatively high FRET efficiency. Both measurements were acquired from unpatched cells in PBS. (A) Histograms showing the measured efficiencies for the negative control (n = 22) display normal distributions for the bleach and control regions (top and middle panels, respectively), and the FRET efficiency which is determined from the difference between the bleach and control regions (bottom panel). (B) The plot showing the average of the three distributions in (A) shows zero FRET in the negative control. ROI B, C, and D, efficiencies (%): 6.1 ± 1.3, 6.9 ± 1.1, 0.0 ± 1.7, respectively (mean ± SE). (C) The plot showing the average efficiency in cells expressing the prestin-CFP-YFP positive control shows high FRET of 15.0 ± 1.6% (n = 15) and corresponds with a donor-acceptor distance of 6.71 ± 0.24 nm (using Eqn. 4.1; see Section 4.3.6 for a full description).

4.3.6   Assessing high FRET and estimating fluorophore separation

FRET was measured in unpatched cells expressing prestin-CFP-YFP to provide context for our voltage-dependent FRET measurements acquired from the cotransfection experiment (prestin-CFP and prestin-YFP).   The prestin-CFP-YFP construct was designed to provide: 1) an approximately fixed donor-acceptor distance, 2) relatively high FRET via close donor-acceptor separation, and 3) a sample in which all molecules undergo FRET by virtue of one-to-one pairing of CFP to YFP. We measured a large FRET efficiency (15.0 ± 1.6%, n = 15) compared to efficiencies measured from cells co-expressing prestin-CFP and prestin-YFP (Fig. 4.7c).

Although the separation and relative orientation of fluorophores in the prestin-CFP-YFP construct is not known, a rough estimate of the distance is made from structural information of the fluorescent proteins (XFPs) and the intervening amino acids. XFP barrel diameter is roughly 2.4 nm, the barrel length is roughly 4.2 nm (Ormo et al. 1996; Yang et al. 1996; Rekas et al. 2002), and the XFP termini adjacent to the linker residues are each 1-1.5 nm (estimated from Fig. 1 in (Rekas et al. 2002)). We estimate that the distance between chromophores of the XFPs is at most 9 nm, but likely smaller due to flexibility in the linker region. From the 15% efficiency we measure, we conclude that the average distance between the fluorophores is 6.71±0.24 nm (error calculated from statistical error in measured FRET and quoted error in R_o from (Tsien 1998)) using Equation 4.1 and R_o = 5nm (Tsien 1998). This distance is not unreasonable based on

known structural information, but most importantly, this result demonstrates that there are no serious systematic errors in our measurement of the FRET efficiency.

4.3.7 Distance representation of FRET data

Under certain conditions it is valid to estimate distances from the FRET efficiency measurements (discussed in Section 4.4.6). To provide this estimate of separation in prestin C-termini (Fig. 4.8), we solve Equation 4.1 for r/R_o in terms of E and replot the data from Figure 4.2. The data is fit to the same Boltzmann form as before (Eqn. 4.3), with the lower asymptote constrained to the minimum observed separation, the separation caused by -140 mV ($A_1 = 1.427$), and the midpoint constrained to $V_{1/2}$ of NLC ($V_o = -54.6$ mV). Fit to the data provides $\alpha = 37.55$ mV and $A_2 = 1.720$ and is superimposed on the plot (Fig. 4.8). From the width of the fit, we again obtain the characteristic voltage range of the data, and using an equation analogous to Equation 4.6 find that $z_{r/Ro} = 0.681 \pm 0.285$, which is different by less than 6.5% from z of the NLC. Going from the hyperpolarized to the depolarized asymptote, the fit to the data suggests that the voltage-induced conformational change causes the distance between the donors and acceptors to change from about $1.4R_o$ to $1.7R_o$, and this corresponds to a displacement of ~1.5 nm.
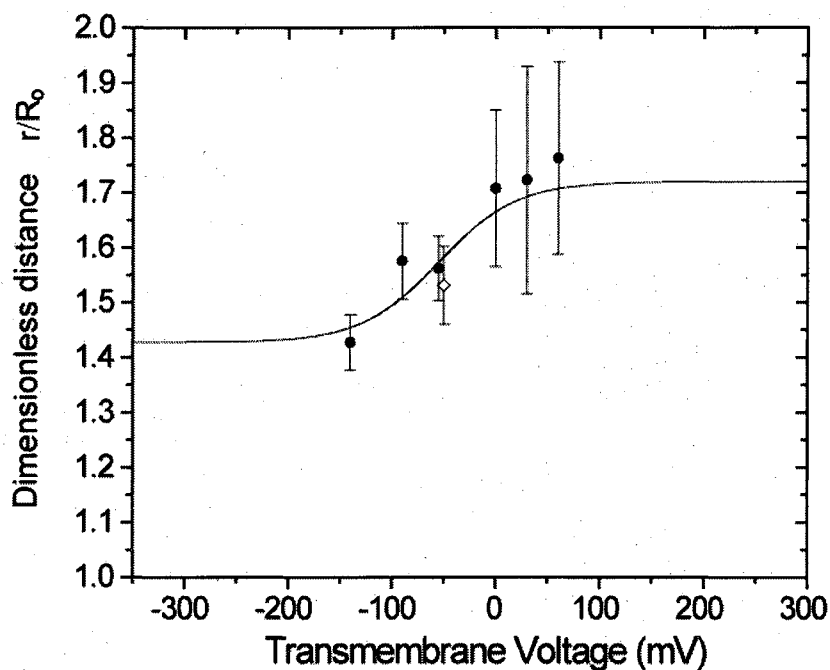
FIGURE 4.8 Voltage dependence of r/R_o, a dimensionless measure of FRET pair separation. Solid circles represent cells that are patch clamped and the open diamond represents cells measured at resting potential in PBS. Data was converted from the form displayed in Figure 4.2 with error bars calculated by propagating the error in E to r/R_o. Data is fit to a Boltzmann function that has the same form as the right hand side of Equation 4.3. The fit is constrained to have an asymptote of $A_I = 1.427$, the minimum separation obtained upon hyperpolarization, and the center is constrained to $V_o = -54.6$ mV, the mean $V_{1/2}$ of the NLC data.

4.4 Discussion

4.4.1 Confirmation of voltage-dependent conformational change in prestin

Although prestin is well-established as the membrane based molecular motor that drives electromotility (Zheng et al. 2000), presumably by undergoing a voltage-dependent conformational change, the details of prestin function at the nanoscale level are unknown. NLC in prestin expressing cells is generally interpreted as charge movement due to voltage-dependent conformational changes in prestin, which move charged moieties within the lipid bilayer (Oliver et al. 2001; Muallem and Ashmore 2006; Rybalchenko and Santos-Sacchi 2008). Reports of electromechanical motion in prestin transfected cells (Zheng et al. 2000; Ludwig et al. 2001; Zhang et al. 2007) and loss of motility in prestin deficient OHC systems (Liberman et al. 2002; Zheng et al. 2005) provide evidence that prestin exerts direct mechanical forces on the cell membrane and indirect support that electromotility is driven by a conformational change in prestin. However, no previous experiment has provided direct evidence of a conformational change or any other structural change of prestin in response to voltage stimulation.

Demonstrating that prestin does in fact undergo a voltage-dependent structural change is requisite for assessing the validity of common models for electromotility (Dallos et al. 1993; Iwasa 1994; Raphael et al. 2000). The common model of prestin activity is a two-state area motor model in which individual functional motor units change area between an extended and a compact state and their concerted activity causes whole cell length change (Dallos et al. 1993; Iwasa 1994; Oliver et al. 2001).

Alternately, a possible role for changes in membrane curvature has been suggested, and this phenomenon is potentially mediated by changes in conformation or oligomerization (Raphael et al. 2000; Spector et al. 2006).

Our observation of voltage-dependent FRET provides proof of voltage-dependent conformational changes within prestin. Since the C-terminus of prestin is contained within the cytoplasm and unable to sense changes in the electric field, altered C-terminal interactions are most likely caused by structural changes in the prestin hydrophobic core. Conformational changes of the prestin transmembrane domains alter the separation and/or orientation of the XFPs, which we detect as altered FRET efficiency. The voltage-dependent change in FRET efficiency occurred near the $V_{1/2}$ of NLC (Fig. 4.2) and spanned the same voltage range ($z \sim z_{FRET}$, see Fig. 4.4), showing that a change in prestin-prestin interactions occurred concurrently with charge movement in the bilayer. The voltage dependence of the FRET transition was abolished in the presence of salicylate, an inhibitor that reduces prestin-related charge movement (Fig. 4.5). Therefore, we conclude that the changes in FRET, which we observe in response to altered transmembrane potential, reflect conformational changes in prestin and constitute a "fluorescence signature" for prestin-dependent motility.

4.4.2 Salicylate affects prestin conformation

Salicylate is known to inhibit NLC and electromotility in cells expressing prestin (Kakehata and Santos-Sacchi 1996). We have shown that application of 10 mM salicylate to prestin transfected cells disrupts the FRET efficiency versus transmembrane voltage trend seen in Figure 4.2. This supports a link between prestin activity and

voltage dependent FRET, but additionally may provide insight into the mechanism of salicylate inhibition. The FRET results suggest that salicylate may allosterically bind to prestin causing a conformational change in the molecule that changes the character of the motor. Specifically, salicylate may inhibit prestin function by inducing a non-functional conformation characterized by increased C-terminal interactions at depolarized transmembrane potentials (Fig. 4.5). This interpretation is supported by fluorescence polarization microscopy studies that suggest a direct interaction of salicylate with prestin (Greeson and Raphael 2009).

4.4.3   A possible functional role for prestin oligomerization

The observation of 8-11 nm particles in the OHC membrane and prestin transfected cells (Gulley and Reese 1977; Kalinec et al. 1992; Murakoshi et al. 2006) has been used to argue that prestin exists natively as a multimer. Several groups have demonstrated that prestin forms oligomers (Zheng et al. 2006; Rajagopalan et al. 2007; Sturm et al. 2007; Detro-Dassen et al. 2008; Mio et al. 2008; Pasqualetto et al. 2008), and typically monomer, dimer, trimer, and tetramer populations are observed. Prestin self-interactions have been quantified using FRET (Navaratnam et al. 2005; Greeson et al. 2006; Wu et al. 2007), however there are no previous reports of voltage-dependent interactions.

Based on the results of the positive and negative FRET controls (Fig 4.7), and our demonstration that FRET is not influenced by the amount of prestin in the membrane (Fig 4.6), we conclude that the FRET we measure results from specific prestin-prestin interactions. It has been shown that the N-terminus of prestin might play a role in prestin

oligomerization and truncation of more than 20 amino acids from this terminus resulted in concurrent loss of self-association and NLC (Navaratnam et al. 2005). The implication was that oligomerization might be required for prestin activity. Our data supports this idea, and further suggests that oligomerization might not only be needed for function, but might also be intimately involved in the mechanism of nonlinear charge movement.

4.4.4   Saturation of FRET data at extremes of holding potential

Our data demonstrate a decrease in prestin-prestin FRET over a transmembrane potential range from -140 mV to +60 mV. We were unable to measure FRET outside this range because excessive current flow led to reduced membrane resistance, likely resulting from electropermeabilization (Akinlaja and Sachs 1998; Navarrete and Santos-Sacchi 2006). In the range we examined, we observed what appeared to be the onset of saturation due to three successive measures with low and equivalent FRET efficiency (0, +30, and +60 mV in Fig. 4.2). New experimental techniques are needed to verify behavior at extreme hyperpolarized voltages, but based on tight coupling to NLC (Fig 4.4), and the relationship between NLC and motility, we expect saturating behavior.

4.4.5   Possible sources of FRET voltage dependence

Based upon the observation that the FRET efficiency is a monotonically decreasing function of transmembrane potential (Fig. 4.2), we propose some molecular level interpretations of the voltage-dependent FRET. The dependence could arise from either: 1) a voltage-triggered shift in the oligomeric state distribution, 2) a change in conformation within intact oligomers from an unchanging distribution, or 3) a

combination of the two. We refer to each of these scenarios in the following sections of the discussion.

If the voltage dependent change in FRET is the result of a change in oligomeric state of prestin (scenario 1), this would imply that depolarization causes the distribution to shift toward lower oligomeric states (ex. dimer to monomer). This could be caused by a conformational change that creates steric hindrance at interaction sites to other prestin molecules and leads to a decrease in the population of a particular higher order state. If however the distribution of oligomeric states remains constant with transmembrane voltage, then this implies that conformational changes occur within intact oligomeric assemblies and results in increased C-terminal tag separation upon depolarization (scenario 2). Our data rule out the possibility that depolarization shifts the oligomeric distribution towards higher order states or initiates a conformational change in which the C-terminally located FRET pairs get closer together, because these scenarios would necessarily lead to an increase in FRET efficiency.

4.4.6 Relating FRET efficiency to physical quantities

When considering models of electromotility it is more relevant to discuss parameters that directly describe the state of the motor (as a function of membrane potential) rather than the FRET efficiency. Specifically, we are interested in relating the FRET efficiency to either a distance between fluorescent tags within a motor complex or the fraction of prestin molecules adopting a particular state. Direct conversion of FRET efficiency to either quantity is only accurate under the following conditions: 1) for any voltage there is a single donor-acceptor distance throughout the sample, and 2) 100% of

the donors are undergoing FRET (i.e. no donors unpaired from acceptors). Both conditions are presumably ensured by the positive FRET control (prestin-CFP-YFP, Fig. 4.7c), but in the case of cotransfection neither criteria are likely fully satisfied; as such, our conversions of the FRET data to relevant physical quantities are only approximations.

4.4.7 Two-state motor model picture

In the case of the commonly adopted two-state thermodynamic description of prestin, the area motor model (Dallos et al. 1993; Iwasa 1994), the relevant quantity is the fraction of molecules within a particular conformational state. Both of our suggested explanations for the FRET voltage dependence (scenario 1 and 2) are consistent with the area motor model, since the transition between states could represent a transition between two functionally relevant oligomeric states, or two discrete conformational states within an intact oligomer.

The desired quantity, the fraction of motors in a particular state, is directly proportional to the measured FRET efficiency, so we were able to fit a Boltzmann function (Eqn. 4.3) directly to the FRET versus transmembrane potential data to model the motor state transition (Fig. 4.2). From the fit we extracted a dimensionless parameter z_{FRET}, which is mathematically analogous to the NLC valence (z) and closely agrees with the experimentally measured value of z (Fig. 4.4). This is the first correlation of NLC to an optical measure that is directly sensitive to prestin movement on the molecular level, and supports the hypothesis that both charge movement and motility reflect a voltage-dependent conformational change in prestin.

4.4.8 Continuous motor model picture

In the case that the motor changes its conformational state in a continuous fashion, as is suggested by the membrane bending model (Raphael et al. 2000; Scherer and Gummer 2005), the fluorescent tag separation is the physical quantity of interest. Continuous models are compatible with a conformational change within an intact oligomer (scenario 2), but do not provide the discrete states required to explain our voltage-dependent FRET through shifts in oligomerization (scenario 1).

We estimate voltage-dependent changes in the distance of the C-terminal tags using Equation 4.1 and replot the FRET efficiency data as a dimensionless length r/R_o in Figure 4.8. We find that the dimensionless parameter $z_{r/Ro}$, calculated from the width of a Boltzmann fit to the data, is in good agreement with the NLC valence z, again providing support for the assumption that prestin-associated charge movement reflects a conformational change in the prestin molecule.

Introduction of the prestin-tagged FRET pairs using cotransfection likely produces some samples with unpaired donors in the membrane, in which case our distance estimates overestimate actual FRET pair separation. To minimize the impact of this inconsistency, we report the voltage-dependent changes in separation. The calculated 1.5 nm change in distance between the FRET pairs is corroborated by estimates of the conformational displacement of prestin (Dallos et al. 1993; Dallos and Fakler 2002). Likewise, a 1.5 nm displacement could also easily be supported within the 8-11 nm structures observed from freeze fracture data (Gulley and Reese 1977; Kalinec et al. 1992), and the oligomeric prestin structures observed using AFM (Murakoshi et al.

2006) and TEM imaging (Mio et al. 2008). The conformational changes that result in the displacement of C-terminal tags are not inconsistent with published estimates of cross-sectional area changes ranging from 1 to 7 nm^2 (Iwasa 1993; Adachi and Iwasa 1999; Dong and Iwasa 2004). This range of cross-sectional area change of the OHC motor unit corresponds with an estimated 6.4 to 89.8 μm^2 total cellular area change based upon localization of the motor protein to 2139 μm^2 of the lateral wall (Huang and Santos-Sacchi 1993) and estimates of particle density ranging from 3000 to 6000/μm^2 (Forge 1991; Kalinec et al. 1992).

4.5   Summary of results

In this chapter we provide the first evidence of voltage-dependent prestin-prestin interactions. The decrease in C-terminal FRET with depolarization of transmembrane voltage could arise from either 1) a voltage-triggered shift in the oligomeric state distribution, or 2) a change in conformation within intact oligomers from an unchanging distribution. We also do not rule out the possibility that voltage-dependent FRET may result from a combination of these two events.

Our data can be interpreted by either a continuous membrane bending model or by a thermodynamically driven two-state area motor model. Distinguishing between the separate models is not possible, but in either case the apparent coupling between charge movement and the FRET voltage dependence suggests that prestin undergoes conformational changes in response to voltage in such a way that the interactions between prestin C-termini decrease with depolarization. Specifically, this was supported

by parameterization of the width (z_{FRET} or $z_{r/Ro}$) of the FRET-related transition (distance between XFP tags or the fraction of prestin molecules in a particular state) and observed consistency with the measured valence of nonlinear charge movement, z. Furthermore, we have supported the connection between voltage-dependent FRET and prestin function through the observation that salicylate both inhibits NLC and disrupts the voltage-dependent FRET trend, suggesting that both are a consequence of salicylate inhibiting conformational change of prestin.

Our report of voltage-dependent FRET is the first direct evidence that conformational changes in prestin occur in response to changes in transmembrane potential. These results provide strong support that a prestin conformational change is the underlying mechanism behind membrane-based electromotility, and suggest that changes in self-interaction might have fundamental involvement in the mechanism of nonlinear charge movement. Finally, our work establishes a "fluorescent signature" for prestin activity and provides support for the use of prestin as a fast FRET-based membrane voltage sensor.

CHAPTER 5

PROTEIN ENGINEERING OF THE PRESTIN MOLECULAR MOTOR

5.1 Genetic labeling for metabolic biotinylation

Biotin is a small coenzyme (vitamin H) synthesized by plants, bacteria, and some fungi (Shils and Shike 2006). It is bound to specific proteins via an amide linkage between the biotin carboxyl group and a unique lysine amino acid within an acceptor peptide sequence (Samols et al. 1988). Biotin is recognized and bound by two tetrameric proteins, avidin and streptavidin. The biotin-streptavidin interaction ($K_d = 10^{-13}$-10^{-14} M) is several order of magnitude greater than typical antibody-antigen interactions, making it one of the tightest and most stable (off-rate on the order of days) reactions known (Green 1990; Piran and Riordan 1990). Endogenous biotinylated proteins are very rare, with only four identified in mammals and no biotinylated surface proteins known in nature (Robinson et al. 1983; Chandler and Ballard 1988). The characteristics of the streptavidin-biotin interaction, and the lack of endogenous biotinylation makes it an important tool for protein purification and labeling strategies.

The most extensively studied endogenously biotinylated protein is the 1.3 subunit of *Propionibacterium shermanii* transcarboxylase (commonly called PSTCD) (Samols et al. 1988). The biotin acceptor peptide (BAP) sequence from PSTCD was fused to the C-terminus of various cytoplasmic enzymes and *in vivo* metabolic biotinylation demonstrated in bacterium and yeast (Cronan 1990). This technique was shown to biotinylate intracellular motifs in a C-terminally tagged 7-pass G-protein coupled

receptor (Lundstrom et al. 1995) and C-terminally tagged globular proteins with varying steric constraint and flexibility at the fusion terminus (Parrott and Barry 2000). Study of C-terminal tagging of secreted proteins (Parrott and Barry 2001) revealed that the mammalian biotin ligase, holocarboxylase synthetase (Chapman-Smith and Cronan 1999), is not contained in this pathway. Parrot and Barry expanded this technology and reported extracellular biotinylation of simple, single-pass integral membrane proteins (Parrott and Barry 2001). One of their constructs, BAP fused to the N-terminus of the platelet-derived growth factor receptor (PDGFR) transmembrane domain, was used to introduce streptavidin conjugated contrast agents to the surface of tumor cells and enhance magnetic resonance imaging (MRI) (Tannous et al. 2006).

5.2   Expansion of biotin acceptor peptide technology

In this chapter, we demonstrate the first use of BAP-PDGFR for extracellular biotinylation of multi-pass transmembrane proteins. We fused the BAP-PDGFR reporter to the N-terminus of prestin (Fig. 5.1). For illustrative purposes we show the 12-pass model of prestin topology which is supported by hydrophobicity analysis, proof of intracellular N- and C-termini (Zheng et al. 2001), data suggesting phosphorylation (Deak et al. 2005), and reports of N-linked glycosylation (Matsuda et al. 2004; Iida et al. 2005).
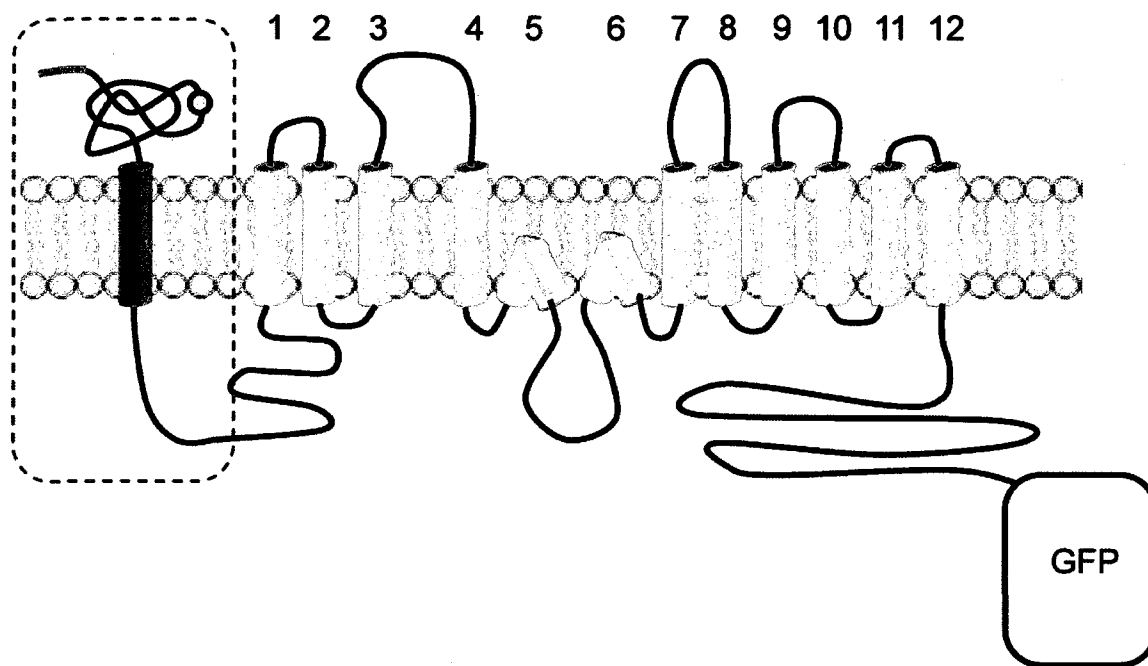
FIGURE 5.1 BAP-prestin-GFP fusion protein topology. A biotin acceptor peptide (BAP) has been fused to the exoplasmic face of the platelet-derived growth factor receptor (PDGFR) transmembrane domain and attached to a cytoplasmic linker. This engineered gene and the 12-pass motor protein prestin were cloned to the pEGFP-N1 plasmid (Clontech) to form a fusion protein with a convenient external binding motif. BAP can be cleaved from PDGFR by Factor Xa protease or prestin liberated by severing the cytoplasmic linker with enterokinase.

5.3   Materials and methods

5.3.1   Plasmid construction

The 736 bp BAP-PDGFR reporter gene was synthesized from a 24 primer set, composed primarily of 50 bp oligonucleotides (Table 5.1), designed using DNAWorks (Helix Systems, NIH) and the PCR-based synthesis methods of Hoover and Lubkowski (Hoover and Lubkowski 2002). The gene includes a 5' NheI restriction site, a murine Ig κ-chain leader sequence, a hemagglutinin A (HA) epitope tag, a biotin acceptor peptide (BAP), the transmembrane domain from platelet-derived growth factor receptor (PDGFR), a cytoplasmic linker region, and a 3' HindIII restriction site (Fig. 5.2). The BAP coding sequence was derived from base pairs 1-390 of the PinPoint Xa vector (Promega, Madison, WI). The leader sequence, which targets the fusion to the secretory pathway (Coloma et al. 1992), and the PDGFR transmembrane domain, which ensures exoplasmic display (Gronwald et al. 1988) of BAP, were isolated from base pairs 737-799 and 907-1053 (respectively) of the pDisplay vector (Invitrogen, Carlsbad, CA). All nucleotide segments were codon optimized from their original sources using a human codon frequency table (Hoover and Lubkowski 2002).

TABLE 5.1 Synthesis primers for N-terminal BAP-PDGFR reporter

Primer type/ number	Nucleotide sequence (5' to 3')
Fwd 1	AGACAGGCTAGCATGGAAACTGATACACTC
Rev 2	ACCCAAAGGAGAAGCACCCACAGGAGGAGTGTATCAGTTTCCATGCTAGC
Fwd 3	GGGTGCTTCTCCTTTGGGTACCGGGCAGTACCGGCGACTACCCTTACGAC
Rev 4	TCATTGCCGCCGCAGCGGCGTAGTCGGGCACGTCGTAAGGGTAGTCGCCG
Fwd 5	GCTGCGGCGGCAATGAAGCTGAAGGTGACCGTAAACGGCACGGCCTACGA
Rev 6	TTCTCGTGGCTTTTGTCCACATCGACGTCAACATCGTAGGCCGTGCCGTT
Fwd 7	TGTGGACAAAAGCCACGAGAACCCTATGGGCACAATTCTGTTCGGTGGCG
Rev 8	CAGCTGCAGGAGCAGGGGCACCACCTGTACCGCCACCGAACAGAATTGTG
Fwd 9	CCCTGCTCCTGCAGCTGGAGGCGCTGGTGCGGGTAAGGCGGGTGAAGGAG
Rev 10	CTCACTGTGCCGGCGAGCGGCGCAGGAATCTCTCCTTCACCCGCCTTACC
Fwd 11	CTCGCCGGCACAGTGAGCAAAATCCTGGTTAAAGAGGGCGACACCGTTAA
Rev 12	CTTCCAGAACGAGCACCGTCTGCCCAGCCTTAACGGTGTCGCCCTCTTTA
Fwd 13	ACGGTGCTCGTTCTGGAAGCCATGAAGATGGAGACCGAAATAAACGCCCC
Rev 14	ACAAGCACCTTCTCGACCTTTCCGTCGGTGGGGGCGTTTATTTCGGTCTC
Fwd 15	AAAGGTCGAGAAGGTGCTTGTGAAAGAGAGGGACGCCGTCCAGGGTGGCC
Rev 16	ATCAGTTCCAGGTCGCCGATCTTTATCAGGCCTTGGCCACCCTGGACGGC
Fwd 17	CGGCGACCTGGAACTGATCGAGGGCAGGGCGGCAGCAGCCGCCGTGGGTC
Rev 18	TGAGTGGGGCACGACGATCACCTCTTGCGTGTCCTGACCCACGGCGGCTG
Fwd 19	TCGTCGTGCCCCACTCACTGCCGTTCAAAGTGGTCGTGATCAGCGCGATC
Rev 20	GGCTGATTATTGTGAGCACCACAAGGGCCAAGATCGCGCTGATCACGACC
Fwd 21	TGGTGCTCACAATAATCAGCCTGATCATCCTCATCATGCTGTGGCAGAAG
Rev 22	CCAGCACTTCCGGCAGACCCCCTGGGCTTCTTCTGCCACAGCATGATGAG
Fwd 23	GTCTGCCGGAAGTGCTGGATCAGCAGGAAGCGCCGACGATGATGATAAGG
Rev 24	CTGACTAAGCTTTGGCGCTGCCCTTATCATCATCGTCGGCG

```
  1  AGACAGGCTA GCATGGAAAC TGATACACTC CTCCTGTGGG TGCTTCTCCT
 51  TTGGGTACCG GGCAGTACCG GCGACTACCC TTACGACGTG CCCGACTACG
101  CCGCTGCGGC GGCAATGAAG CTGAAGGTGA CCGTAAACGG CACGGCCTAC
151  GATGTTGACG TCGATGTGGA CAAAAGCCAC GAGAACCCTA TGGGCACAAT
201  TCTGTTCGGT GGCGGTACAG GTGGTGCCCC TGCTCCTGCA GCTGGAGGCG
251  CTGGTGCGGG TAAGGCGGGT GAAGGAGAGA TTCCTGCGCC GCTCGCCGGC
301  ACAGTGAGCA AAATCCTGGT TAAAGAGGGC GACACCGTTA AGGCTGGGCA
351  GACGGTGCTC GTTCTGGAAG CCATGAAGAT GGAGACCGAA ATAAACGCCC
401  CCACCGACGG AAAGGTCGAG AAGGTGCTTG TGAAAGAGAG GGACGCCGTC
451  CAGGGTGGCC AAGGCCTGAT AAAGATCGGC GACCTGGAAC TGATCGAGGG
501  CAGGGCGGCA GCAGCCGCCG TGGGTCAGGA CACGCAAGAG GTGATCGTCG
551  TGCCCCACTC ACTGCCGTTC AAAGTGGTCG TGATCAGCGC GATCTTGGCC
601  CTTGTGGTGC TCACAATAAT CAGCCTGATC ATCCTCATCA TGCTGTGGCA
651  GAAGAAGCCC AGGGGGTCTG CCGGAAGTGC TGGATCAGCA GGAAGCGCCG
701  ACGATGATGA TAAGGGCAGC GCCAAAGCTT AGTCAG
```

FIGURE 5.2 Synthesized BAP-PDGFR gene. DNA encoding the N-terminal reporter includes (base pairs shown in parentheses): 1) NheI (7-12) and HindIII (725-730) restriction sites, 2) a murine Ig κ-chain leader sequence (13-75), 3) a hemagglutinin A epitope tag (76-102), 4) a biotin acceptor peptide (115-504), 5) a platelet-derived growth factor receptor transmembrane domain (517-663), and 6) a linker region (664-723). The nucleotide sequence is codon optimized for expression in mammalian cells.

The pEGFP-N1 vector (Clontech, Palo Alto, CA), which served as a backbone for subsequent cloning, was modified (forward/reverse primers: 5'cactacctgagcacccagtccaagctgagcaaagac3'/5'gtctttgctcagcttggactgggtgctcaggtagtg3') to include a point mutation to GFP. This mutation (denoted A206K in the literature), located at residue 207 of the Clontech vector (due to an insertion that enhances mammalian translation efficiency), prevents non-specific interaction of the fusion proteins (Tsien 1998; Zacharias 2002). The synthesized BAP-PDGFR gene was digested and inserted into the NheI and HindIII sites of the pEGFP-N1 plasmid. Gerbil prestin (AF230376) was isolated (EcoRI and BamHI) from a previously described prestin-GFP fusion (Greeson et al. 2006) and inserted downstream and in-frame with the BAP-PDGFR gene. The resulting fusion construct is referred to as BAP-prestin-GFP and the translated fusion protein is shown in Figure 5.3. The entire fusion, including 5', 3', and interceding junctions were sequence verified using an eight primer set (Baylor Sequencing Core, Houston, TX). Prestin-GFP containing the A206K mutation was used for control activity (nonlinear capacitance) measurements. The pSec-BirA vector (Parrott and Barry 2001), which encodes the biotin ligase of E. coli (BirA) and tags the protein for secretion, was provided as a generous gift from Dr. Michael Barry.

```
   1  METDTLLLWV  LLLWVPGSTG  DYPYDVPDYA  AAAAMKLKVT  VNGTAYDVDV
  51  DVDKSHENPM  GTILFGGGTG  GAPAPAAGGA  GAGKAGEGEI  PAPLAGTVSK
 101  ILVKEGDTVK  AGQTVLVLEA  MKMETEINAP  TDGKVEKVLV  KERDAVQGGQ
 151  GLIKIGDLEL  IEGRAAAAAV  GQDTQEVIVV  PHSLPFKVVV  ISAILALVVL
 201  TIISLIILIM  LWQKKPRGSA  GSAGSAGSAD  DDDKGSAKAS  NSTMDHAEEN
 251  EIPVATQKYH  VERPIFSHPV  LQERLHVKDK  VSESIGDKLK  QAFTCTPKKI
 301  RNIIYMFLPI  TKWLPAYKFK  EYVLGDLVSG  ISTGVLQLPQ  GLAFAMLAAV
 351  PPVFGLYSSF  YPVIMYCFFG  TSRHISIGPF  AVISLMIGGV  AVRLVPDDIV
 401  IPGGVNATNG  TEARDALRVK  VAMSVTLLSG  IIQFCLGVCR  FGFVAIYLTE
 451  PLVRGFTTAA  AVHVFTSMLK  YLFGVKTKRY  SGIFSVVYST  VAVLQNVKNL
 501  NVCSLGVGLM  VFGLLLGGKE  FNERFKEKLP  APIPLEFFAV  VMGTGISAGF
 551  NLHESYSVDV  VGTLPLGLLP  PANPDTSLFH  LVYVDAIAIA  IVGFSVTISM
 601  AKTLANKHGY  QVDGNQELIA  LGICNSIGSL  FQTFSISCSL  SRSLVQEGTG
 651  GKTQLAGCLA  SLMILLVILA  TGFLFESLPQ  AVLSAIVIVN  LKGMFMQFSD
 701  LPFFWRTSKI  ELTIWLTTFV  SSLFLGLDYG  LITAVIIALL  TVIYRTQSPS
 751  YKVLGQLPDT  DVYIDIDAYE  EVKEIPGIKI  FQINAPIYYA  NSDLYSNALK
 801  RKTGVNPALI  MGARRKAMRK  YAKEVGNANI  ANAAVVKVDG  EVDGENATKP
 851  EEEDDEVKYP  PIVIKTTFPE  ELQRFMPQTE  NVHTIILDFT  QVNFIDSVGV
 901  KTLAVMVKEY  GDVGIYVYLA  GCSPQVVNDL  TRNRFFENPA  LKELLFHSIH
 951  DAVLGSHVRE  AMAEQEASAP  PPQDDMEPNA  TPTTPEARDP  PVATMVSKGE
1001  ELFTGVVPIL  VELDGDVNGH  KFSVSGEGEG  DATYGKLTLK  FICTTGKLPV
1051  PWPTLVTTLT  YGVQCFSRYP  DHMKQHDFFK  SAMPEGYVQE  RTIFFKDDGN
1101  YKTRAEVKFE  GDTLVNRIEL  KGIDFKEDGN  ILGHKLEYNY  NSHNVYIMAD
1151  KQKNGIKVNF  KIRHNIEDGS  VQLADHYQQN  TPIGDGPVLL  PDNHYLSTQS
1201  KLSKDPNEKR  DHMVLLEFVT  AAGITLGMDE  LYK
```

FIGURE 5.3 Translated sequence of BAP-prestin-GFP. The BAP-PDGFR reporter encompasses amino acids 1-237 (yellow), prestin 244-987 (teal), and GFP 995-1233 (green). The BAP-PDGFR reporter contains a leader sequence (amino acids 1-21), hemagglutinin tag (22-30), BAP (35-164), PDGFR transmembrane domain (169-216), and cytoplasmic linker (218-237). Biotinylation occurs at Lys 122 (bold K). Proteolytic cleavage sites (underlined) allow cleavage of the fusion following residue 164 or 234 by Factor Xa or Enterokinase, respectively. GFP contains A207K (residue 1201 of overall fusion) modification to prevent formation of non-obligate oligomers.

5.3.2 Plasmid expression and cell culture

HEK293 cells were grown in T75 flasks and 6-well plates containing DMEM supplemented with 10% BCS (Invitrogen, Carlsbad, CA), 1% penicillin-streptomycin, 14.3 mM HEPES, and 16.1 mM $NaHCO_3$, and 10 mg/L (41 μM) d-Biotin (Sigma-Aldrich, St. Louis, MO). Cells were transfected with prestin-GFP, or co-transfected with BAP-prestin-GFP and pSec-BirA plasmids, using 2μg of each plasmid DNA and 3 μL/plamid Fugene 6 transfection reagent (Roche, Indianapolis, IN) according to manufacturer's directions. For electrophysiology and imaging studies, cells were trypsinized and replated onto #1.5 coverslips or MatTek dishes (MatTek Corp., Ashland, MA) 8-12 hours after transfection and then evaluated 48-72 hours post-transfection.

5.3.3 Confocal imaging

Biotinylation of BAP and localization of the BAP-prestin-GFP fusion to the membrane were verified using confocal microscopy 72 hours post-transfection. Transfected HEKs were incubated with 5 μg/mL Alexa-633 conjugated streptavidin (Invitrogen, Carlsbad, CA) for 20 minutes at room temperature. Cells were washed with PBS and imaging was performed on an LSM 510 microscope (Zeiss, Thornwood, New York). GFP and the Alexa-633 conjugated streptavidin (SA-Alexa 633) were excited with 488 nm Argon laser light and 633 nm HeNe laser light, respectively. Using a secondary dichotic and separate band pass filters for each channel, GFP fluorescence was collected between 500-530 nm and SA-Alexa 633 fluorescence was collected between 650-710 nm. The pinhole for both channels was adjusted to produce an optical slice less

than 13 µm (2.9 and 2.1 Airy units for the GFP and SA-Alexa 633 channels, respectively). All imaging was performed using a 63X, 1.4NA objective lens.

5.3.4 Electrophysiology

Kimax-51 capillary tubes (1.5/0.8 mm OD/ID) were heated on a P-97 puller (Sutter, Novato, CA) to form fine tip micropipettes. The micropipettes were filled with pipette blocking solution (130 mM CsCl, 2 mM MgCl$_2$, 10 mM EGTA, 10 mM HEPES) and threaded onto a Ag$^+$/AgCl electrode. Coverslips seeded at low cell density formed the base of a patch clamp chamber in which the cells were bathed in extracellular blocking solution (99 mM NaCl, 20 mM TEA-Cl, 2 mM CoCl$_2$, 1.47 mM MgCl$_2$, 1 mM CaCl$_2$, 10 mM HEPES), and an agar bridge provided electrical continuity with the reference bath containing a Ag$^+$/AgCl reference electrode and pipette blocking solution. Blocking solutions (Deak et al. 2005) were titrated to pH 7.3 and dextrose added to obtain 300 ± 3 mOsm (Osmette A; Precision Systems, Natick, MA). Patch pipettes produced 2-4 MΩ resistance in open-bath and placement was controlled using a Burleigh PCS-6200 Micromanipulator (EXFO Life Sciences, Rochester, NY). On-cell seals in excess of 1 GΩ were obtained from healthy, single cells showing strong GFP fluorescence 48 hours post-transfection. Pipette capacitance was compensated, the cell membrane ruptured to establish whole-cell mode, and only cells with series resistance less than 10 MΩ and membrane resistance in excess of 1 GΩ retained for analysis. We apply an 800 Hz, 10 mV sinewave and measure the current response as DC holding potential is stepped from -140 to +140 mV in 2 mV increments (HEKA EPC 10 Plus Amplifier with 18-bit DAC). Using a software-based phase-sensitive detector, implemented in Patchmaster software (HEKA, Mahone Bay, NS), we determine the real

and imaginary components of the admittance (the complex current response scaled by the command voltage) and calculate membrane capacitance (C_m) and membrane resistance (R_m) (Lindau and Neher 1988). At each DC potential four complete sinusoidal voltage cycles occur and discrete capacitance values are calculated from the latter three. Capacitance versus voltage (DC holding potential) traces are acquired for each cell and fit to the first derivative of the two-state Boltzmann function (Eqn. 5.1) using MATLAB (MathWorks, Natick, MA).

$$C_m = \frac{Q_{max}\left(\dfrac{ze}{kT}\right)}{\exp\left[\left(\dfrac{ze}{kT}\right)(V - V_{1/2})\right]\left(1 + \exp\left[-(V - V_{1/2})\left(\dfrac{ze}{kT}\right)\right]\right)^2} + C_{lin} \qquad \text{Eqn. 5.1}$$

Q_{max} is the maximum nonlinear charge movement provided by prestin. $V_{1/2}$ is the voltage at the peak of the capacitance versus holding potential curve. z is the valence of charge movement by prestin and inversely proportional to the width of the NLC curve. Boltzmann's constant k, absolute temperature T, and the charge carried by an electron e, are all constant values. Since variation in cell size causes differences in the maximal charge transfer (Q_{max}), the charge movement is normalized to C_{lin}, and computed on a cell-by-cell basis. This quantity, designated as charge density, has units of fC/pF (Oliver and Fakler 1999). Representative NLC curves are reconstructed from mean Q_{max}, $V_{1/2}$ and z for either BAP-prestin-GFP or prestin-GFP, and each result is normalized to maximal nonlinear capacitance ($Q_{max}ze/4kT$) of each group.

5.4 Experimental results

5.4.1 Validation of trafficking, biotinylation, and membrane localization

When co-expressed in HEK with BirA, the biotin ligase of E. coli, BAP-prestin-GFP is biotinylated and inserts into the plasma membrane. Confocal imaging shows that a streptavidin (SA) conjugated fluorophore (SA-Alexa 633) cannot permeate the cell membrane and therefore labels the membrane localized fraction of BAP-prestin-GFP in live cells (Fig. 5.4a). BAP-prestin-GFP is not biotinylated in the absence of BirA (data not shown). Thresholding was used to remove pixels with fluorescent intensity values in the lower 5% or 35% (both values approximate) for GFP and SA-Alexa 633 (respectively), and the remaining colocalized signal (pixels with non-zero fluorescent values in each channel) is shown in Figure 5.4b. Nearly all the pixels with SA-Alexa 633 fluorescence coincide with GFP fluorescence, indicating efficient biotinylation of BAP-prestin-GFP. Perfect one-to-one correspondence was not observed due to slight non-specific background staining and PMT detector noise.
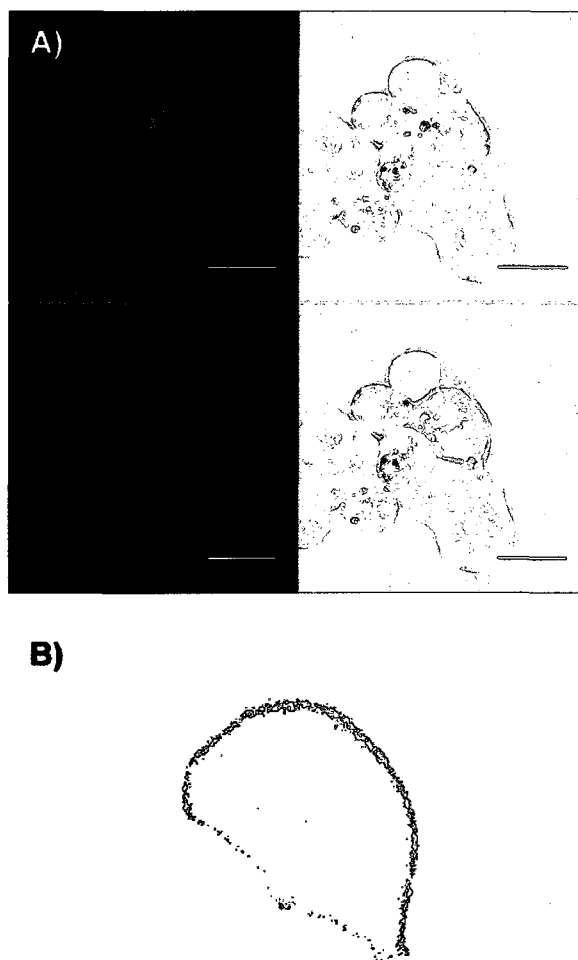
FIGURE 5.4 BAP-prestin-GFP localizes to the cell membrane. (A) Brightfield, GFP, SA-Alexa 633, and overlay images (counter-clockwise from upper right) for HEK cells co-transfected with pSec-BirA and BAP-prestin-GFP plasmid DNA. The streptavidin conjugated dye selectively labels the membrane localized fraction of BAP-prestin and does not non-specifically interact with untransfected HEKs. Scale bar 20 μm. (B) After thresholding to remove low intensity pixels, an overlay of the remaining colocalized signal demonstrates efficient biotinylation of BAP-prestin. 92% of pixels with SA-Alexa 633 fluorescence also have GFP signal, these are displayed in (B).

5.4.2   Prestin activity in the presence of an N-terminal reporter

We next verified prestin function of the BAP-prestin-GFP fusion. The ability of prestin to move charge within the membrane has been established as a reliable measure of motor protein activity (Ashmore 1990; Santos-Sacchi 1991). We use whole-cell patch clamp technique to control the voltage across the cell membrane and assay transmembrane charge movement. In the absence of prestin, HEK cells show uniform, linear capacitance that is proportional to the size of the cell due to the dielectric properties of the membrane. When active prestin is present in the membrane a nonlinear, bell-shaped capacitance versus voltage curve is detected. This charge movement, analogous to the gating current in ion channels, is commonly described as nonlinear capacitance (NLC) and thought to result from prestin conformational change. The NLC plot shown in Figure 5.5 was constructed from mean fit parameters and therefore only displays the mean rise in capacitance (prestin-related charge movement) above the linear capacitance (membrane surface area). BAP-prestin-GFP clearly exhibits motor activity, since it shows bell-shaped NLC. The voltage at peak capacitance ($V_{1/2}$) and valence of charge movement (z) are indistinguishable from prestin-GFP. This shows that the operating range and kinetics of the motor activity were not impacted. Reduced charge density (Q_{max}/C_{lin}) did result from the N-terminal fusion and might reflect lower trafficking and reduced surface expression compared to unmodified prestin-GFP. Coincidently, reduced surface expression is advantageous for some biophysical studies, such as single molecule tracking.
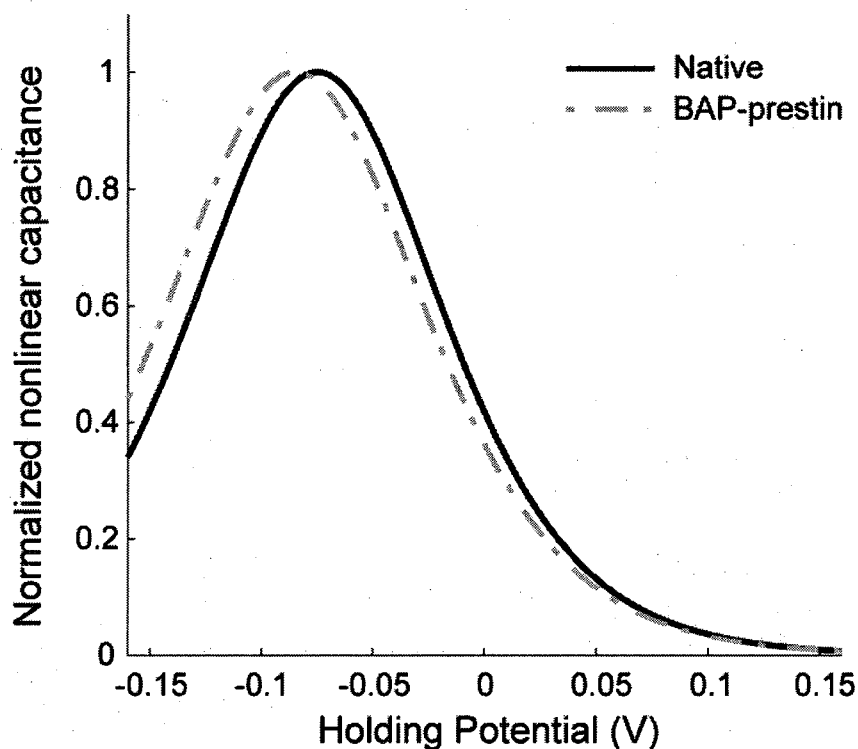
FIGURE 5.5 BAP-prestin-GFP provides motor activity. NLC curves constructed from mean $V_{1/2}$, z, and Q_{max} are normalized to the peak capacitance of each group. BAP-prestin shows normal $V_{1/2}$ and z, and maintains an ability to move charge despite reduction in charge density (Q_{max}/C_{lin}) compared to wild type prestin-GFP ($p < 0.05$). **BAP-prestin-GFP** (n=8): $V_{1/2}$ -84.8 ± 3.7 mV, z 0.66 ± 0.03, Q_{max}/C_{lin} 3.15 ± 0.29 fC/pF. **WT prestin-GFP** (n=12): $V_{1/2}$ -75.1 ± 5.1 mV, z 0.68 ± 0.01, Q_{max}/C_{lin} 18.01 ± 2.87 fC/pF. All values are mean ± SE.

5.5   Discussion and applications

Prestin was identified as the motor protein in cochlear OHCs in 2000 (Zheng et al. 2000) and the physiological significance of motor activity has been clearly demonstrated through knock-out mice lacking prestin (Liberman et al. 2002) and knock-in mice with non-functioning prestin (Dallos et al. 2008), which both exhibit profound deafness. However, the mechanism of prestin voltage to force conversion is not understood. In contrast to other well known linear motors such as myosin, kinesin, and dynein, prestin does not require ATP or calcium for motor function (Kachar et al. 1986; Holley and Ashmore 1988). Since BAP-prestin-GFP membrane localizes and functions, the construct has wide biophysical applications and can be used to advance understanding of prestin activity.

One measure of interest would be the characteristic force produced by an individual motor unit. Whole cell measurements from OHCs show that the cell can produce an axial force of ~5 nN (Iwasa and Adachi 1997), and from estimates of the number of motors in the membrane the individual molecular stall force is on the order of 2.4 pN (He et al. 2006). BAP-prestin-GFP will allow introduction of streptavidin coated microparticles that can be optically trapped to measure force production in patch clamped cells (methods of (Zhang et al. 2007)), and quantification of the membrane localized fraction using fluorescent standards to experimentally determine the force production per prestin molecule. A more general use for BAP-prestin-GFP is the ability to easily label membrane localized prestin in live cells with fluorescent probes having larger molar

absorptivity (extinction coefficient) (Patterson et al. 2001) and higher quantum yield (Panchuk-Voloshina et al. 1999) than fluorescent proteins (XFPs). Conversely, live cell labeling of prestin-GFP is challenging since it requires in-house antibody production because commercially available prestin antibodies have been raised against the intracellular termini, and antibody labeling is more suited for labeling fixed samples. We anticipate that BAP-prestin-GFP will have a variety of applications stemming from the ease of live cell prestin binding via the extracellular biotinylated moiety.

CHAPTER 6

CONCLUSIONS

A succinct summary of the major conclusion for each of our studies is provided below. These results enhance current knowledge about the prestin motor protein and provide new avenues and technologies for further characterization of this crucial molecular component of the auditory system.

6.1 Study of prestin cysteine residues

Our mutational study of prestin cysteine residues provided several valuable insights into prestin structure and function, and methodological improvements for future mutational studies. Of the various NLC perturbations caused by prestin mutation, decreased charge density might be the most physiologically relevant since decoupling of charge movement and electromotility has not been reported. In general, decreased charge density can be explained through impaired prestin function, or decreased surface expression due to impaired trafficking. We describe each of the major contributions of our research below.

1) In our study we introduced a new technique to assess mutations that resulted in reduced charge density. We used NLC to identify mutations that reduced measured charge density and then employed quantitative Western blot of the membrane fraction to differentiate between loss-of-function mutations and those with impaired membrane trafficking. Mutants with normal levels of

glycosylated monomer were likely normally folded, and therefore the sequence alteration accounted for diminished function; these constructs were termed loss-of-function mutations.

2) Analysis of the functional mutants revealed that charge density was linearly related to the concentration of prestin in the membrane. It has been suggested that individual prestin molecules provide quantal contribution to the total measured intramembranous charge movement. We provide evidence of this phenomenon using mutations that do not completely inhibit charge movement, but slightly perturb trafficking.

3) The functional relevance and molecular basis for prestin interactions and oligomerization are not currently understood. Disulfide bonds have been suggested to bridge prestin monomers to form dimers, which can form tetramers through hydrophobic interactions (Zheng et al. 2006). Valine substitutions were made at locations where serine replacement of cysteine impaired charge density (192, 196, and 415) and in each case function was restored, indicating that if disulfide bonding or palmitoylation are present they do not serve a functional role that can be detected via NLC. Moreover, none of the cysteine mutants suppressed prestin dimerization (see Fig. 3.7).

4) Our analysis demonstrated that cysteine 196 and 415 of prestin are critical for charge movement. These sites might be important structural determinants of the Cl$^-$ binding pocket. Interestingly, both residues are unique to prestin in

comparison to its most closely related SLC26 family member, PAT1, which does not exhibit NLC.

5) The prestin crystal structure has not yet been solved, and therefore proposed topologies have been derived from analysis of primary structure (hydrophobicity) and mutational studies. Our analysis contributes to this wealth of data and suggests that cysteines 52, 124, 260, 381, 395, and 679 reside in water-exposed, hydrophilic locations, based on maintenance of normal charge density upon serine (hydrophilic) substitution. Cysteines 192, 196, and 415 are likely buried in the hydrophobic core of prestin since these locations did not tolerate serine, but instead produced normal charge movement with valine (hydrophobic).

6) Notably, our data suggest that cysteine 260 and 381, which are located near the midpoint of purported transmembrane domains, are likely exposed to a hydrophilic local environment. Such exposure might suggest that these residues line an aqueous pore (likely occluded), and this idea is supported by TEM imaging of oligomeric prestin structures which reveal a low density core (see Fig. 2.9).

7) Finally, our results may provide a suitable recipe for development of a functional, membrane-localized, cysteine-less prestin construct. Such a construct could be used for cysteine scanning mutagenesis, a technique in which cysteines are re-introduced at various locations throughout the protein to enable targeting of thiol reactive probes. This technique has been widely

employed in the study of transporters and ion channels. Our findings suggest that serine substitution at residues 52, 124, 260, 381, 395, and 679, and valine substitution at 192, 196, and 415 might be feasible.

6.2   Voltage-dependence of prestin interactions

Prestin interactions have been measured biochemically using Western blot (Matsuda et al. 2004; Zheng et al. 2006; Rajagopalan et al. 2007; Sturm et al. 2007; Detro-Dassen et al. 2008), optically through fluorescence resonance energy transfer (FRET) (Navaratnam et al. 2005; Greeson et al. 2006), and demonstrated *in vivo* through yeast two-hybrid assay (Zheng et al. 2006). Monomer, dimer, trimer, and tetramer prestin populations are commonly observed, but the purpose for these interactions is not currently understood. The key findings from our investigation into the voltage dependence of prestin interactions are summarized below.

1) We provide the first evidence of voltage-dependent prestin self-interactions, demonstrating a decrease in C-terminal interactions upon depolarization of transmembrane potential. The change in FRET could arise from *i*) a voltage-triggered shift in the oligomeric state distribution, *ii*) a change in conformation within intact oligomers from an unchanging distribution, or *iii*) a combination of the two phenomena. Both mechanisms are likely driven by prestin conformational changes, which in turn change self-association by establishing new low-energy states and therefore new favored equilibrium conditions.

2) A variety of factors suggest that the voltage dependence of prestin-prestin FRET is coupled to prestin charge movement. These include the observations that:

    i.   The voltage-induced change in FRET efficiency occurs near $V_{1/2}$ of nonlinear charge transfer.

    ii.   The FRET efficiency change appears to saturate and approach a lower asymptote, specifically near depolarized transmembrane potentials

    iii.   The voltage range over which the transitions occur are highly similar, that is, the valence of the FRET efficiency change (z_{FRET} or $z_{r/Ro}$) is less than 10% different than the valence (z) of prestin NLC.

    iv.   Salicylate concurrently inhibits nonlinear charge transfer and disrupts the voltage-dependent FRET trend

3) NLC has commonly been attributed to a conformation change in prestin, but molecular motion of prestin had not been proven experimentally. An apparent coupling between charge movement and the FRET efficiency change suggests that prestin undergoes conformational change in response to altered transmembrane voltage in such a way that the interactions between their C-termini decrease upon depolarization. Our study therefore provides the first direct experimental confirmation of voltage-induced prestin confirmation change, a central component to current theories of electromotility (area motor and membrane bending models). In a similar manner to NLC forming the

basic electrical signature for electromotility we have identified a fluorescence signature associated with prestin-dependent charge movement.

4) Salicylate has been shown to compete with Cl^- binding and inhibit prestin function. Our work provides exciting insight into the mode of prestin inactivation. Salicylate may disrupt function by inducing a non-functional conformation, characterized by increased C-terminal interactions at depolarized transmembrane potential. Our data is consistent with a fixed, voltage-insensitive prestin conformation induced by salicylate binding.

5) Finally, our work provides support for the use of prestin as a fast, FRET-based, non-invasive transmembrane voltage sensor. This technology would enable *in vivo* detection of resting potential within intact cells, and facilitate measurement of voltage change in response to ligand binding or external stimulation.

6.3   Protein engineering of prestin

We designed and synthesized an N-terminal reporter for prestin that displays extracellular biotinylation, and therefore a convenient binding site for live cell labeling of membrane localized prestin. This reporter, which we call BAP-PDGFR, is biotinylated *in vivo* by mammalian HEK cells in the presence of an exogenous biotin ligase (BirA from E. coli) released in the secretory pathway. We characterized the reporter system and achieved the following results:

1) Our BAP-prestin-GFP construct, which fuses BAP-PDGFR to the N-terminus of prestin and GFP to the C-terminus, was shown by confocal microscopy to insert into the plasma membrane and to efficiently receive biotinylation.

2) BAP-prestin-GFP exhibited motor activity with normal voltage at peak capacitance ($V_{1/2}$) and normal valence of charge movement (z) compared to prestin-GFP (GFP fused to the C-terminus of prestin). BAP-prestin-GFP had reduced charge density (Q_{max}/C_{lin}) compared to prestin-GFP, likely due to lower trafficking and reduced surface expression; however, in light of all the advantages of live cell labeling and the ease of binding prestin via the extracellular biotinylated moiety, the reduced membrane expression is a minor limitation.

3) We anticipate that BAP-prestin-GFP will have a wide variety of biophysical applications and can be used to advance understanding of prestin activity. Additionally, our study was the first use of the BAP-PDGFR reporter for extracellular biotinylation of a multi-pass transmembrane protein.

CHAPTER 7

FUTURE RESEARCH DIRECTIONS

Based upon the major findings of this thesis, an outline is provided for future experimentation. In many cases the discoveries that have been presented in this thesis have opened up new and exciting research opportunities.

7.1   Study of prestin cysteine residues

7.1.1   *Investigation of lipid modification of prestin*

Prestin function is sensitive to membrane cholesterol concentration, which along with sphingolipids forms membrane subdomains commonly referred to as lipid rafts. Prestin is known to populate the lipid rafts (Rajagopalan et al. 2007; Sturm et al. 2007), as determined through membrane fractionation and Western blot analysis. These highly ordered phases of the membrane sequester and concentrate individual receptors and are thought to play an important biological role in signal transduction (Simons and Toomre 2000). Protein palmitoylation is a process that aids localization of proteins to membrane rafts and involves cysteine residues located in close proximity to transmembrane domains, with cysteines near the exoplasmic leaflet being particularly important (Resh 1999; Simons and Toomre 2000). Specifically, the lipid palmitate, a 16-carbon saturated fatty acid, is post-translationally attached to cysteine residues via a thioester covalent bond. As a result it should be investigated whether prestin is palmitoylated.

Incorporation of palmitate can be tracked using tritium labeled lipid ([^{3}H] palmitate) added to the culture media (Chen and Manning 2000) of wild-type prestin-GFP transfected HEK cells. Protein collection, SDS-PAGE, blotting to nitrocellulose, and Western detection of the prestin band can be carried out by standard procedures (described in Chapter 3). To assay for palmitoylation, blots can be re-processed using fluorography. By this method, detection of weak radioactivity is enhanced using a scintillator, a molecule that absorbs radiation and emits fluorescence. To process for fluorography the blot can be spray impregnated with EN^{3}HANCE (Perkin Elmer, Waltham, Massachusetts), air-dried for 60 minutes, and then exposed to Hyperfilm MP (GE Healthcare Bio-Sciences Corp, Piscataway, NJ) at -80°C overnight. If palmitoylation is occurring, a band will be visible in the fluorograph that corresponds to the immunolabeled band for prestin. In the case that palmitoylation is detected, the single cysteine replacement mutants should be tested in order to identify palmitoylation site(s).

7.1.2 Developing a cysteine-less mutant for cysteine scanning mutagenesis

The data provided in Chapter 3 suggest that serine substitution at residues 52, 124, 260, 381, 395, and 679, and valine substitution at 192, 196, and 415 might result in a functional, membrane-localized cysteine-less prestin mutant. If this or future mutation schemes provide a feasible cysteine-less construct it will be possible to perform cysteine scanning mutagenesis, a powerful technique that has been used to obtain detailed information about transporters and ion channels. In this technique the cysteine-less prestin construct serves as a template for additional mutagenesis in which cysteine residues are re-introduced at various locations. Each of the new mutants carries a single cysteine that targets a thiol reactive probe or bulky sulfhydryl reagent to a specific

location in prestin. Thiol reactive fluorescent probes can be used for detailed topological study of prestin. One simple approach would be to introduce cysteines in locations that are hypothesized extracellular loops, express the construct in HEKs, and then use polar membrane-impermeable thiol reactive probes to evaluate the current topological models. Maleimide dyes are suitable for this application. Alternately, cysteine scanning mutagenesis can be used to target bulky sulfhydryl reagents to specific locations in prestin. The goal of this procedure is to identify locations in which the treatment inhibits nonlinear charge movement, assessed via whole-cell patch clamping. Since the reagents sterically hinder conformational change, a series of mutants can be used to screen for functionally important domains within prestin.

Based upon the 12-pass re-entrant loop model of prestin the following mutations provide a cysteine target near the middle of each putative transmembrane domain (TMD): S89C, S115C, S141C, X196C, S224C, X260C, *V297C*, V341C, X381C, L422C, L448C, and *V492C* (X represents residues that were originally cysteine, but were replaced to create the cysteine-less construct). In choosing replacements sites, 1) locations of original (wild type) cysteines, 2) existing serines, or 3) nonpolar residues of similar apparent volume (Leu or Val) (Zamyatnin 1972), were substituted based on availability near the midpoint of the TMD (in the preferred order listed). Serines were given this preference based upon a high tolerance for the substitution in our previously designed constructs (Chapter 3). Valine and leucine were used interchangeably based upon sequence availability, since the former closely matches cysteine size (Zamyatnin 1972) and the latter closely matches cysteine hydrophobicity (Kyte and Doolittle 1982). For each construct that traffics and provides wild type charge movement, NLC should be

assessed before and after local perfusion of sulfhydryl reagent. If a significant decrease in charge movement occurs, it can be concluded that the bulky sulfhydryl reagent bound the target cysteine and inhibited conformational change necessary for prestin activity. p-chloromercuriphenylsulfonate (pCMPS), a highly penetrating organomercurial (van Iwaarden et al. 1992; Kalinec and Kachar 1993; Santos-Sacchi and Wu 2004), or methanethiosulfonate-ethylammonium (MTSEA), an amphipathic molecule capable of crossing the plasma membrane to react with cytoplasmic cysteine side chains, are both suitable sulfhydryl agents for the screen. However, an important control is needed to establish that the sulfhydryl reagents do not affect NLC measures in the cysteine-less mutant, to verify that the compounds do not cause unanticipated secondary effects.

7.2 Voltage-dependent prestin self-interactions

7.2.1 Investigating the mechanism

Our discovery of voltage-dependent prestin self-interactions clearly warrants additional investigation. The decrease in C-terminal interactions upon depolarization of transmembrane potential could arise from:

1) Voltage-triggered shift in the oligomeric state distribution (ex. shift in monomer, dimer, trimer, and/or tetramer populations)

2) Change in conformation within intact oligomers from an unchanging distribution (ex. C-terminal tags move, but populations remain fixed), or

3) Combination of 1 and 2

SDS-PAGE western blots can be used to investigate involvement of the first suggested mechanism. KCl treated prestin transfected HEK cells can be compared to untreated cells, to determine if depolarization alters the normal oligomeric profile (relative amounts of monomer, dimer, trimer, tetramer, etc.). Similar information can be obtained by treating cells with varying the amounts chemical cross-linker (Bis-sulfosuccinimidyl suberate, BS3) prior to Western analysis. Cells treated simultaneously with KCl and BS3 should show less dimer, than those treated with BS3 alone, at any particular BS3 concentration.

7.2.2   *Expanding the testable range*

Our FRET measurement method limited the range of transmembrane voltages that we were able to evaluate. We were unable to explore potentials more hyperpolarized than -140 mV or more depolarized than +60 mV, since sustained current flow often caused reduced membrane resistance (potentially due to electroporation) or seal loss. This difficulty was largely related to the length of time required to complete acceptor (YFP) photobleaching (~9 seconds). Mutations with shifted $V_{1/2}$, the voltage at which elongated and contracted states are equally populated, might be used to investigate transmembrane voltages beyond the range we report. For example, the C395S mutation (characterized in Chapter 3) has a depolarized $V_{1/2}$ compared to wild type prestin, therefore patch clamping this mutant at hyperpolarized potentials increases the probability of prestin in the expanded state compared to the wild type. Specifically, C395S prestin is depolarized ~73 mV compared to WT prestin (see Chapter 3), so we hypothesize that patching this mutant at -140 mV approximates the behavior of WT prestin at -213 mV. Our preliminary data using this strategy indicates that voltage-

dependent FRET does indeed saturate at extreme voltages as reported in Chapter 4. Similarly, we can use the triple mutant K233Q/K235Q/R236Q to evaluate the effects of a hyperpolarizing NLC shift (Oliver et al. 2001; Gao et al. 2007), which increases the probability of a condensed prestin conformation. This mutant can be used to verify saturation of voltage FRET beyond +60 mV and will likely show reduced FRET at all holding potentials compared to wild type prestin.

7.2.3 Investigating the functional significance of voltage-dependent interactions

Our data support a functional role for voltage-dependent prestin self-interactions, since salicylate application concurrently inhibits nonlinear charge transfer and disrupts the voltage-dependent FRET trend. It would be useful to fully map the effect of salicylate inhibition on FRET throughout the range of voltages relevant for nonlinear charge transfer in order to definitively determine if salicylate binding puts prestin in a fixed, voltage-insensitive conformation. Our current evidence shows high C-terminal interactions at both hyperpolarized (-90 mV) and depolarized voltages (+60 mV). It would also be informative to investigate the characteristic FRET for other forms of inhibition such as the loss of function mutants (C196S and C415S, see Chapter 3) or wild type prestin under Cl^- free conditions. Prestin phosphorylation or glycosylation state might also affect self-interaction, whereas the effect(s) on NLC are already known: Mutation to mimic dephosphorylation (S238A) depolarized $V_{1/2}$ (Deak et al. 2005), mutation simulating phosphorylation (238D) hyperpolarized $V_{1/2}$ and reduced z (Deak et al. 2005), and mutation blocking glycosylation (N163Q/N166Q) depolarized $V_{1/2}$ (Matsuda et al. 2004).

7.3   Biotin acceptor peptide tagged prestin

7.3.1   Advantages over standard labeling procedures

We demonstrated the first use of the N-terminal BAP-PDGFR reporter to provide a convenient extracellular binding site for multi-pass membrane proteins. This tool enables easy *in vivo* labeling of proteins that does not rely on the use of antibodies. Since many membrane proteins have not been crystallized it is difficult to obtain monoclonal antibodies, commercial or produced in-house, that have extracellular epitopes that would even make live cell labeling possible. We have shown that BAP-prestin-GFP is readily labeled by streptavidin conjugated fluorescent probes. The construct allows labeling of prestin using brighter, more photostable dyes compared to genetic florescent proteins (XFPs), or labeling using unbleachable quantum dots. This will facilitate studies of prestin diffusion in the membrane via single molecule tracking.

Another advantage over XFP reporters is the ability to selectively label the membrane-localized prestin fraction. In our experience some prestin point mutations impair prestin membrane trafficking and are significantly retained in the golgi apparatus and endoplasmic reticulum. In these cases it is not always possible to separate the cytoplasmic fluorescence from membrane localized signal. Selective labeling of membrane fraction of prestin will enable use of flow cytometry to quantify the membrane concentration of mutants relative to wild type prestin when both carry the BAP-PDGFR reporter. The ability to detect membrane localized prestin also provides an opportunity to

study prestin residence time in the membrane using pulse labeling methods (Howarth et al. 2005).

The rate at which prestin is cycling off the membrane can be determined by labeling the membrane localized population with a streptavidin conjugated quantum dot ($t_1 = 0$), measuring fluorescence (F_{t1}), and then taking another measurement at a later timepoint (F_{t2} at $t_2 > t_1$). The ratio of the fluorescence measurements (F_{t2}/F_{t1}) determines the fraction of prestin remaining in the membrane which can be readily converted into a rate based on the delay between measurements. Similarly, the trafficking rate can be determined by labeling with a streptavidin conjugated quantum dot (SA-QD) and taking an initial fluorescence measurement (F_{t1} at $t_1 = 0$), waiting until a later timepoint ($t_2 > t_1$) then reapplying the SA-QD and measuring the increased fluorescence (F_{t2}). In this case the ratio F_{t2}/F_{t1} determines the fractional increase in membrane-localized prestin, which again is readily converted into a rate based on the delay between measurements. The residence time for prestin can be estimated by labeling membrane-localized prestin with an unconjugated streptavidin ($t_1 = 0$), allowing new biotin-displaying prestin to accumulate in the membrane, and then selectively labeling this population with a SA-QD ($t_2 > t_1$). Fluorescence measurements at t_2 and subsequent time points can be fit to characterize the decay rate, and the time required to clear membrane fluorescence determined by extrapolating the fit. This provides an estimate of residence time (plus or minus the time allowed for initial accumulation). Instead of following the time course in individual cells each of the suggested methods could easily be adapted for flow cytometry.

7.3.2   Using BAP-PDGFR reporter for prestin binding

The effects of oligomerization upon prestin function are unknown. It might be possible to induce artificial clustering of prestin by applying low concentrations of streptavidin to BAP-prestin-GFP expressing cells. Streptavidin (SA) is a tetramer with four biotin binding sites. High concentrations might be expected to singly label all available biotin sites, but lower concentrations could potentially cross-link prestin and shift the oligomeric distribution (monomer, dimer, trimer, tetramer, etc.) toward higher order states. A variety of SA concentrations could be used to treat BAP-prestin-GFP expressing cells and prestin oligomerization analyzed by SDS-PAGE western blot probed with anti-GFP (see Chapter 3 for methods). If a suitable concentration is determined it could be applied extracellularly to live BAP-prestin-GFP expressing HEK and prestin function assessed using patch clamp technique. This would complement a study of forced dimerization that our group has proposed using the ARGENT regulated homodimerization system (ARIAD Pharmaceuticals, Inc, Cambridge, MA) (Spencer et al. 1993). In this system prestin will be fused to the binding domain of human FKBP12 protein, a cytoplasmic protein that serves as the initial intracellular target for the immunosuppressive drugs FK506 and rapamycin. FKBP domains are linked in the presence of a chemical dimerizer, a small synthetic ligand. This is another method by which we can control oligomerization and evaluate the functional consequences.

In Chapter 5 we suggest that BAP-prestin-GFP might be used to experimentally derive the force production per prestin molecule. This is not a trivial procedure, but we suggest some experimental considerations. Streptavidin coated microparticles bound to BAP-prestin-GFP biotin can be trapped using optical tweezers and whole-cell force

production can be measured as the transmembrane voltage is controlled using patch clamp technique (methods of (Zhang et al. 2007)). It might be possible to quantify the membrane-localized fraction through two experiments run in parallel. A calibration curve will be constructed relating the measured absorption to the concentration of a streptavidin conjugated fluorophore (SA-fluor) using a spectrophotometer. Next, BAP-prestin-GFP expressing cells, in suspension, will be labeled in excess SA-fluor (to approximate 1:1 labeling) and absorption repeatedly measured under mixing. The mean absorption value will be corrected to nominal absorption measured in un-labeled BAP-prestin-GFP expressing cells, and then related to SA-fluor concentration via the calibration curve. Assuming that mixing and repeated measures can approximate a homogenous sample, the number of moles of SA-fluor (and therefore the number of particles) will be estimated from the known the sample volume. A second experiment, also run in parallel, will use flow cytometry to count the number of transfected cells. Since transfection efficiencies regularly vary a single source of BAP-prestin-GFP expressing cells should be divided and used for each of the required measurements (un-labeled and SA-fluor labeled cells for spectrophotometry, and cells for flow cytometry). From this data the number of prestin per cell will be calculated (number particles of SA-fluor divided by the number transfected cells) and used to estimate the force production per prestin molecule.

Alternately, it might be possible to quantify the membrane localized prestin solely using confocal microscopy. Fluorescence can be quantified from slides with known SA-fluor suspension concentrations using a fixed optical slice (pinhole size) and region of interest (ROI) area to construct a calibration curve. The ROI area and optical slice should

be larger than typical HEK size, and the optical slice should be thinner than the fluid layer on the calibration slides. BAP-prestin-GFP expressing cells will be labeled in excess SA-fluor (to approximate 1:1 labeling) and fluorescence measured from single cells (without altering laser power, amplifier gain or offset, pinhole, or ROI size) to determine SA-fluor concentration in the membrane. Optical slice and ROI area can then be used to calculate the moles of SA-fluor (and therefore the number of particles) from individual cells. Either of these techniques could also be used to investigate charge movement per prestin molecule.

The extracellularly exposed biotin could also serve as an attachment site for a SA-modified atomic force microscopy probe (Novascan Technologies, Ames, IA). This could enable pull-out studies (Oesterhelt et al. 2000) that would provide useful topological information given the current debate over the number of transmembrane domains. The BAP-prestin-GFP construct may even prove useful for purification of protein from mammalian sources. Resin with immobilized monovalent avidin is readily available (Pierce, Rockford, IL) allowing elution under mild conditions (2 mM biotin in PBS). Prestin can then be cleaved from the BAP-PDGFR segment by digesting the cytoplasmic linker with enterokinase.

APPENDIX

LINDAU-NEHER METHOD OF CAPACITANCE CALCULATION

In whole-cell mode, a sinusoidal command voltage can be imposed and the admittance response analyzed to acquire high-resolution membrane capacitance measurements. Admittance is the complex current response scaled by the command voltage. The form of the complex admittance $Y(\omega)$ is shown below (Eqn. A.1), with the analytical solution for each coefficient (Eqns. A.2 and A.3), when whole-cell capacitance compensation is not performed (but pipette capacitance has been removed through compensation by the amplifier). All variables are as previously defined (see Section 2.6.2) with the addition of angular frequency ω, the frequency of the imposed voltage sinusoid multiplied by 2π radians/cycle.

$$Y(\omega) = A + Bi \qquad \text{Eqn. A.1}$$

$$A = \frac{1 + \omega^2 R_m R_p C_m^2}{R_t (1 + \omega^2 R_p^2 C_m^2)} \qquad \text{Eqn. A.2}$$

$$B = \frac{\omega R_m^2 C_m}{R_t^2 (1 + \omega^2 R_p^2 C_m^2)} \qquad \text{Eqn. A.3}$$

A single sinusoid provides two independent pieces of information, the imposed voltage magnitude and phase, which correspond to the real and imaginary components of the admittance response (A and B, respectively). To solve the three-component system (C_m, R_m, and R_s, see Fig. 2.11), a third piece of independent information is required and obtained by applying the sinusoidal voltage at a superimposed DC holding potential (V_{DC}). The DC holding potential gives rise to a DC current (I_{DC}) that is measured by digital averaging of the current response trace. The following ohmic relationship provides the third independent equation (Eqn. A.4) where E_r is the reversal potential (voltage with zero net current flow, defined by the ionic composition of the pipette and bath solutions).

$$I_{DC} = \frac{V_{DC} - E_r}{R_t}$$

<div align="right">Eqn. A.4</div>

Equations A.2-A.4 can be solved to provide relationships (Eqns. A.5-A.7) for the circuit components of interest: membrane capacitance (C_m), membrane resistance (R_m), and series resistance (R_s). The conductance listed G_t, is the reciprocal of R_t (Lindau and Neher 1988; Pusch and Neher 1988).

$$C_m = \frac{1}{\omega B} \frac{(A^2 + B^2 - AG_t)^2}{(A - G_t)^2 + B^2}$$

<div align="right">Eqn. A.5</div>

$$R_m = \frac{1}{G_t} \frac{(A - G_t)^2 + B^2}{A^2 + B^2 - AG_t}$$

<div align="right">Eqn. A.6</div>

$$R_s = \frac{A - G_t}{A^2 + B^2 - AG_t}$$

<div align="right">Eqn. A.7</div>

The measured admittance response is separated into both in-phase and out-of-phase components, with relation to the voltage stimulus, using a phase-sensitive detector (PSD). Phase-sensitive detection in our experimental setup is implemented in software rather than through the hardware of the amplifier. In summary, the known values include: (1) the real and imaginary admittance components, A and B (respectively), (2) I_{DC}, which is readily measured, (3) E_r, which is near 0 mV and constant due to our pipette and extracellular bath solutions (see Chapters 3-5), (4) V_{DC}, and (5) the angular frequency ω of the imposed voltage sinusoid.

If capacitance compensation is performed, the subtracted current components can be "added back" to the real and imaginary components using Equations A.8 and A.9. The conductance listed G_s is the reciprocal of R_s, and C_{slow} is the whole-cell capacitance compensation (see Sections 2.6.2 and 2.6.3). The compensated admittance components (A_{comp} and B_{comp}) can then be used in Equations A.5-A.7.

$$A_{comp} = \frac{\omega^2 C_{slow}^2 / G_s}{1 + (\omega \, C_{Slow} / G_s)^2}$$ Eqn. A.8

$$B_{comp} = \frac{\omega \, C_{slow}}{1 + (\omega \, C_{slow} / G_s)^2}$$ Eqn. A.9

For the Lindau-Neher technique the signal to noise ratio is constant up to the characteristic frequency, $\omega_c = (R_s C_m)^{-1}$, thus the frequency of the imposed voltage sinusoid is usually selected in the range of 500 Hz to 1.5 kHz (Lindau and Neher 1988).

BIBLIOGRAPHY

Adachi, M. and K. H. Iwasa (1997). "Effect of diamide on force generation and axial stiffness of the cochlear outer hair cell." Biophys J **73**(5): 2809-18.

Adachi, M. and K. H. Iwasa (1999). "Electrically driven motor in the outer hair cell: effect of a mechanical constraint." Proc Natl Acad Sci U S A **96**(13): 7244-9.

Akinlaja, J. and F. Sachs (1998). "The breakdown of cell membranes by electrical and mechanical stress." Biophys J **75**(1): 247-54.

Alberts, B. (2002). Molecular biology of the cell. New York, Garland Science.

Anderson, R. G. (1993). "Caveolae: where incoming and outgoing messengers meet." Proc Natl Acad Sci U S A **90**(23): 10909-13.

Ashmore, J. (2008). "Cochlear outer hair cell motility." Physiol Rev **88**(1): 173-210.

Ashmore, J. F. (1987). "A fast motile response in guinea-pig outer hair cells: the cellular basis of the cochlear amplifier." J Physiol **388**: 323-47.

Ashmore, J. F. (1990). "Forward and reverse transduction in the mammalian cochlea." Neurosci Res Suppl **12**: S39-50.

Audia, J. P., R. A. Roberts and H. H. Winkler (2006). "Cysteine-Scanning Mutagenesis and Thiol Modification of the Rickettsia prowazekii ATP/ADP Translocase: Characterization of TMs IV-VII and IX-XII and Their Accessibility to the Aqueous Translocation Pathway." Biochemistry **45**(8): 2648-56.

Bai, J. P., D. Navaratnam, H. Samaranayake and J. Santos-Sacchi (2006). "En block C-terminal charge cluster reversals in prestin (SLC26A5): effects on voltage-dependent electromechanical activity." Neurosci Lett **404**(3): 270-5.

Bai, M., S. Trivedi and E. M. Brown (1998). "Dimerization of the extracellular calcium-sensing receptor (CaR) on the cell surface of CaR-transfected HEK293 cells." J Biol Chem **273**(36): 23605-10.

Bai, M., S. Trivedi, O. Kifor, S. J. Quinn and E. M. Brown (1999). "Intermolecular interactions between dimeric calcium-sensing receptor monomers are important for its normal function." Proc Natl Acad Sci U S A **96**(6): 2834-9.

Basu, J. (2004). "Protein palmitoylation and dynamic modulation of protein function." Current Science **87**(2): 212-217.

Belyantseva, I. A., H. J. Adler, R. Curi, G. I. Frolenkov and B. Kachar (2000). "Expression and localization of prestin and the sugar transporter GLUT-5 during development of electromotility in cochlear outer hair cells." J Neurosci **20**(24): RC116.

Bijlmakers, M. J. and M. Marsh (2003). "The on-off story of protein palmitoylation." Trends Cell Biol **13**(1): 32-42.

Bordo, D. and P. Argos (1991). "Suggestions for "safe" residue substitutions in site-directed mutagenesis." J Mol Biol **217**(4): 721-9.

Brownell, W. E., C. R. Bader, D. Bertrand and Y. de Ribaupierre (1985). "Evoked mechanical responses of isolated cochlear outer hair cells." Science **227**(4683): 194-6.

Brownell, W. E., A. A. Spector, R. M. Raphael and A. S. Popel (2001). "Micro- and nanomechanics of the cochlear outer hair cell." Annu Rev Biomed Eng **3**: 169-94.

Bull, H. B. and K. Breese (1974). "Surface tension of amino acid solutions: a hydrophobicity scale of the amino acid residues." Arch Biochem Biophys **161**(2): 665-70.

Chambard, J. M. and J. F. Ashmore (2003). "Sugar transport by mammalian members of the SLC26 superfamily of anion-bicarbonate exchangers." J Physiol **550**(Pt 3): 667-77.

Chandler, C. S. and F. J. Ballard (1988). "Regulation of the breakdown rates of biotin-containing proteins in Swiss 3T3-L1 cells." Biochem J **251**(3): 749-55.

Chapman-Smith, A. and J. E. Cronan, Jr. (1999). "In vivo enzymatic protein biotinylation." Biomol Eng **16**(1-4): 119-25.

Cheatham, M. A., K. H. Huynh, J. Gao, J. Zuo and P. Dallos (2004). "Cochlear function in Prestin knockout mice." J Physiol 560(Pt 3): 821-30.

Chen, C. A. and D. R. Manning (2000). "Regulation of galpha i palmitoylation by activation of the 5-hydroxytryptamine-1A receptor." J Biol Chem 275(31): 23516-22.

Coloma, M. J., A. Hastings, L. A. Wims and S. L. Morrison (1992). "Novel vectors for the expression of antibody molecules using variable regions generated by polymerase chain reaction." J Immunol Methods 152(1): 89-104.

Cronan, J. E., Jr. (1990). "Biotination of proteins in vivo. A post-translational modification to label, purify, and study proteins." J Biol Chem 265(18): 10327-33.

Dallos, P., B. N. Evans and R. Hallworth (1991). "Nature of the motor element in electrokinetic shape changes of cochlear outer hair cells." Nature 350(6314): 155-7.

Dallos, P. and B. Fakler (2002). "Prestin, a new type of motor protein." Nat Rev Mol Cell Biol 3(2): 104-11.

Dallos, P., R. Hallworth and B. N. Evans (1993). "Theory of electrically driven shape changes of cochlear outer hair cells." J Neurophysiol 70(1): 299-323.

Dallos, P. and D. Harris (1978). "Properties of auditory nerve responses in absence of outer hair cells." J Neurophysiol 41(2): 365-83.

Dallos, P., X. Wu, M. A. Cheatham, J. Gao, J. Zheng, C. T. Anderson, S. Jia, X. Wang, W. H. Cheng, S. Sengupta, D. Z. He and J. Zuo (2008). "Prestin-based outer hair cell motility is necessary for mammalian cochlear amplification." Neuron 58(3): 333-9.

Dallos, P., J. Zheng and M. A. Cheatham (2006). "Prestin and the cochlear amplifier." J Physiol 576(Pt 1): 37-42.

De Jesus, M. L., J. Salles, J. J. Meana and L. F. Callado (2006). "Characterization of CB1 cannabinoid receptor immunoreactivity in postmortem human brain homogenates." Neuroscience 140(2): 635-43.

Deak, L., J. Zheng, A. Orem, G. G. Du, S. Aguinaga, K. Matsuda and P. Dallos (2005). "Effects of cyclic nucleotides on the function of prestin." J Physiol 563(Pt 2): 483-96.

Detro-Dassen, S., M. Schanzler, H. Lauks, I. Martin, S. M. zu Berstenhorst, D. Nothmann, D. Torres-Salazar, P. Hidalgo, G. Schmalzing and C. Fahlke (2008). "Conserved dimeric subunit stoichiometry of SLC26 multifunctional anion exchangers." J Biol Chem 283(7): 4177-88.

Dong, X. X. and K. H. Iwasa (2004). "Tension sensitivity of prestin: comparison with the membrane motor in outer hair cells." Biophys J 86(2): 1201-8.

Dong, X. X., M. Ospeck and K. H. Iwasa (2002). "Piezoelectric reciprocal relationship of the membrane motor in the cochlear outer hair cell." Biophys J 82(3): 1254-9.

Dutzler, R., E. B. Campbell, M. Cadene, B. T. Chait and R. MacKinnon (2002). "X-ray structure of a ClC chloride channel at 3.0 A reveals the molecular basis of anion selectivity." Nature 415(6869): 287-94.

Edidin, M. (2003). "The state of lipid rafts: from model membranes to cells." Annu Rev Biophys Biomol Struct 32: 257-83.

Evans, E. F. and R. V. Harrison (1976). "Proceedings: Correlation between cochlear outer hair cell damage and deterioration of cochlear nerve tuning properties in the guinea-pig." J Physiol 256(1): 43P-44P.

Fakler, B. and D. Oliver (2003). Functional properties of prestin - How the motormolecule works. Biophysics of the cochlea : from molecules to models. A. W. Gummer. River Edge, N.J., World Scientific Pub. Co.: pp. 110-114.

Fang, J. and K. H. Iwasa (2007). "Effects of chlorpromazine and trinitrophenol on the membrane motor of outer hair cells." Biophys J 93(5): 1809-17.

Fliegert, R., G. Glassmeier, F. Schmid, K. Cornils, S. Genisyuerek, A. Harneit, J. R. Schwarz and A. H. Guse (2007). "Modulation of Ca2+ entry and plasma membrane potential by human TRPM4b." Febs J 274(3): 704-13.

Forge, A. (1991). "Structural features of the lateral walls in mammalian cochlear outer hair cells." Cell Tissue Res 265(3): 473-83.

Frank, G., W. Hemmert and A. W. Gummer (1999). "Limiting dynamics of high-frequency electromechanical transduction of outer hair cells." Proc Natl Acad Sci U S A **96**(8): 4420-5.

Gale, J. E. and J. F. Ashmore (1994). "Charge displacement induced by rapid stretch in the basolateral membrane of the guinea-pig outer hair cell." Proc Biol Sci **255**(1344): 243-9.

Gale, J. E. and J. F. Ashmore (1997). "The outer hair cell motor in membrane patches." Pflugers Arch **434**(3): 267-71.

Gao, J., X. Wang, X. Wu, S. Aguinaga, K. Huynh, S. Jia, K. Matsuda, M. Patel, J. Zheng, M. Cheatham, D. Z. He, P. Dallos and J. Zuo (2007). "Prestin-based outer hair cell electromotility in knockin mice does not appear to adjust the operating point of a cilia-based amplifier." Proc Natl Acad Sci U S A **104**(30): 12542-7.

Garcia-Parajo, M. F., G. M. Segers-Nolten, J. A. Veerman, J. Greve and N. F. van Hulst (2000). "Real-time light-driven dynamics of the fluorescence emission in single green fluorescent protein molecules." Proc Natl Acad Sci U S A **97**(13): 7237-42.

Geisler, C. D. (1998). From sound to synapse : physiology of the mammalian ear. New York, Oxford University Press.

Gelfand, S. A. (1981). Hearing, an introduction to psychological and physiological acoustics. New York, M. Dekker.

Gillis, K. D. (1995). Techniques for Membrane Capacitance Measurements. Single-channel recording. B. Sakmann and E. Neher. New York, Plenum Press: 155-198.

Goldsack, D. E. and R. C. Chalifoux (1973). "Contribution of the free energy of mixing of hydrophobic side chains to the stability of the tertiary structure of proteins." J Theor Biol **39**(3): 645-51.

Goldsmith, P. K., G. F. Fan, K. Ray, J. Shiloach, P. McPhie, K. V. Rogers and A. M. Spiegel (1999). "Expression, purification, and biochemical characterization of the amino-terminal extracellular domain of the human calcium receptor." J Biol Chem **274**(16): 11303-9.

Green, N. M. (1990). "Avidin and streptavidin." Methods Enzymol **184**: 51-67.

Greeson, J. N., L. E. Organ, F. A. Pereira and R. M. Raphael (2006). "Assessment of prestin self-association using fluorescence resonance energy transfer." Brain Res 1091(1): 140-50.

Greeson, J. N. and R. M. Raphael (2009). "Amphipath-induced nanoscale changes in outer hair cell plasma membrane curvature." Biophys J 96(2): 510-20.

Gronwald, R. G., F. J. Grant, B. A. Haldeman, C. E. Hart, P. J. O'Hara, F. S. Hagen, R. Ross, D. F. Bowen-Pope and M. J. Murray (1988). "Cloning and expression of a cDNA coding for the human platelet-derived growth factor receptor: evidence for more than one receptor class." Proc Natl Acad Sci U S A 85(10): 3435-9.

Gulley, R. L. and T. S. Reese (1977). "Regional specialization of the hair cell plasmalemma in the organ of corti." Anat Rec 189(1): 109-23.

Guyton, A. C. and J. E. Hall (2000). Textbook of medical physiology. Philadelphia, Saunders.

Hallworth, R. (1995). "Passive compliance and active force generation in the guinea pig outer hair cell." J Neurophysiol 74(6): 2319-28.

Hamill, O. P., A. Marty, E. Neher, B. Sakmann and F. J. Sigworth (1981). "Improved patch-clamp techniques for high-resolution current recording from cells and cell-free membrane patches." Pflugers Arch 391(2): 85-100.

He, D. Z., B. N. Evans and P. Dallos (1994). "First appearance and development of electromotility in neonatal gerbil outer hair cells." Hear Res 78(1): 77-90.

He, D. Z., J. Zheng, F. Kalinec, S. Kakehata and J. Santos-Sacchi (2006). "Tuning in to the amazing outer hair cell: membrane wizardry with a twist and shout." J Membr Biol 209(2-3): 119-34.

Hodgkin, A. L. and A. F. Huxley (1945). "Resting and action potentials in single nerve fibres." J Physiol 104(2): 176-95.

Holley, M. C. and J. F. Ashmore (1988). "On the mechanism of a high-frequency force generator in outer hair cells isolated from the guinea pig cochlea." Proc R Soc Lond B Biol Sci 232(1269): 413-29.

Hoover, D. M. and J. Lubkowski (2002). "DNAWorks: an automated method for designing oligonucleotides for PCR-based gene synthesis." Nucleic Acids Res 30(10): e43.

Howarth, M., K. Takao, Y. Hayashi and A. Y. Ting (2005). "Targeting quantum dots to surface proteins in living cells with biotin ligase." Proc Natl Acad Sci U S A 102(21): 7583-8.

Huang, G. and J. Santos-Sacchi (1993). "Mapping the distribution of the outer hair cell motility voltage sensor by electrical amputation." Biophys J 65(5): 2228-36.

Huang, G. and J. Santos-Sacchi (1994). "Motility voltage sensor of the outer hair cell resides within the lateral plasma membrane." Proc Natl Acad Sci U S A 91(25): 12268-72.

Iida, K., K. Tsumoto, K. Ikeda, I. Kumagai, T. Kobayashi and H. Wada (2005). "Construction of an expression system for the motor protein prestin in Chinese hamster ovary cells." Hear Res 205(1-2): 262-70.

Iwasa, K. H. (1993). "Effect of stress on the membrane capacitance of the auditory outer hair cell." Biophys J 65(1): 492-8.

Iwasa, K. H. (1994). "A membrane motor model for the fast motility of the outer hair cell." J Acoust Soc Am 96(4): 2216-24.

Iwasa, K. H. (2000). "Effect of membrane motor on the axial stiffness of the cochlear outer hair cell." J Acoust Soc Am 107(5 Pt 1): 2764-6.

Iwasa, K. H. and M. Adachi (1997). "Force generation in the outer hair cell of the cochlea." Biophys J 73(1): 546-55.

Jahn, A. F. and J. Santos-Sacchi (1988). Physiology of the ear. New York, Raven Press.

Kachar, B., W. E. Brownell, R. Altschuler and J. Fex (1986). "Electrokinetic shape changes of cochlear outer hair cells." Nature 322(6077): 365-8.

Kakehata, S. and J. Santos-Sacchi (1996). "Effects of salicylate and lanthanides on outer hair cell motility and associated gating charge." J Neurosci 16(16): 4881-9.

Kalinec, F., M. C. Holley, K. H. Iwasa, D. J. Lim and B. Kachar (1992). "A membrane-based force generation mechanism in auditory sensory cells." Proc Natl Acad Sci U S A **89**(18): 8671-5.

Kalinec, F. and B. Kachar (1993). "Inhibition of outer hair cell electromotility by sulfhydryl specific reagents." Neurosci Lett **157**(2): 231-4.

Kandel, E. R., J. H. Schwartz and T. M. Jessell (2000). Principles of neural science. New York, McGraw-Hill, Health Professions Division.

Kemp, D. T. (1978). "Stimulated acoustic emissions from within the human auditory system." J Acoust Soc Am **64**(5): 1386-91.

Kiang, N. Y., M. C. Liberman and R. A. Levine (1976). "Auditory-nerve activity in cats exposed to ototoxic drugs and high-intensity sounds." Ann Otol Rhinol Laryngol **85**(6 PT. 1): 752-68.

Kim, K. S., J. Neu and G. Oster (1998). "Curvature-mediated interactions between membrane proteins." Biophys J **75**(5): 2274-91.

Krigbaum, W. R. and A. Komoriya (1979). "Local interactions as a structure determinant for protein molecules: II." Biochim Biophys Acta **576**(1): 204-48.

Kyte, J. and R. F. Doolittle (1982). "A simple method for displaying the hydropathic character of a protein." J Mol Biol **157**(1): 105-32.

Lakowicz, J. R. (1999). Principles of fluorescence spectroscopy. New York, Kluwer Academic/Plenum.

Liberman, M. C., J. Gao, D. Z. He, X. Wu, S. Jia and J. Zuo (2002). "Prestin is required for electromotility of the outer hair cell and for the cochlear amplifier." Nature **419**(6904): 300-4.

Lindau, M. and E. Neher (1988). "Patch-clamp techniques for time-resolved capacitance measurements in single cells." Pflugers Arch **411**(2): 137-46.

Ludwig, J., D. Oliver, G. Frank, N. Klocker, A. W. Gummer and B. Fakler (2001). "Reciprocal electromechanical properties of rat prestin: the motor molecule from rat outer hair cells." Proc Natl Acad Sci U S A **98**(7): 4178-83.

Lue, A. J., H. B. Zhao and W. E. Brownell (2001). "Chlorpromazine alters outer hair cell electromotility." Otolaryngol Head Neck Surg **125**(1): 71-6.

Lundstrom, K., A. Vargas and B. Allet (1995). "Functional activity of a biotinylated human neurokinin 1 receptor fusion expressed in the Semliki Forest virus system." Biochem Biophys Res Commun **208**(1): 260-6.

Matsuda, K., J. Zheng, G. G. Du, N. Klocker, L. D. Madison and P. Dallos (2004). "N-linked glycosylation sites of the motor protein prestin: effects on membrane targeting and electrophysiological function." J Neurochem **89**(4): 928-38.

McGuire, R. M., F. A. Pereira and R. M. Raphael (2006). Investigations of the functional/structural implications of embedded cysteine residues in the molecular motor protein prestin. Twenty-Ninth Annual MidWinter Meeting of the Association for Research in Otolaryngology, Baltimore, MD.

McGuire, R. M., F. A. Pereira and R. M. Raphael (2007). Modulation of Prestin Function due to Cysteine Point Mutation. Thirtieth Annual MidWinter Meeting of the Association for Research in Otolaryngology, Denver, CO.

McGuire, R. M., F. A. Pereira, J. J. Silberg and R. M. Raphael (2008). Effects of Cysteine Mutations on Prestin Function and Oligomerization. Thirty-First Annual MidWinter Meeting of the Assocation for Research in Otolaryngolgoy, Phoenix, AZ.

Mio, K., Y. Kubo, T. Ogura, T. Yamamoto, F. Arisaka and C. Sato (2008). "The motor protein prestin is a bullet-shaped molecule with inner cavities." J Biol Chem **283**(2): 1137-45.

Morimoto, N., R. M. Raphael, A. Nygren and W. E. Brownell (2002). "Excess plasma membrane and effects of ionic amphipaths on mechanics of outer hair cell lateral wall." Am J Physiol Cell Physiol **282**(5): C1076-86.

Moseley, R. H., P. Hoglund, G. D. Wu, D. G. Silberg, S. Haila, A. de la Chapelle, C. Holmberg and J. Kere (1999). "Downregulated in adenoma gene encodes a

chloride transporter defective in congenital chloride diarrhea." <u>Am J Physiol</u> **276**(1 Pt 1): G185-92.

Mount, D. B. and M. F. Romero (2004). "The SLC26 gene family of multifunctional anion exchangers." <u>Pflugers Arch</u> **447**(5): 710-21.

Muallem, D. R. and J. F. Ashmore (2006). "An Anion Antiporter Model of Prestin, the Outer Hair Cell Motor Protein." <u>Biophys J</u>.

Murakoshi, M., T. Gomi, K. Iida, S. Kumano, K. Tsumoto, I. Kumagai, K. Ikeda, T. Kobayashi and H. Wada (2006). "Imaging by atomic force microscopy of the plasma membrane of prestin-transfected Chinese hamster ovary cells." <u>J Assoc Res Otolaryngol</u> **7**(3): 267-78.

Navaratnam, D., J. P. Bai, H. Samaranayake and J. Santos-Sacchi (2005). "N-terminal-mediated homomultimerization of prestin, the outer hair cell motor protein." <u>Biophys J</u> **89**(5): 3345-52.

Navarrete, E. G. and J. Santos-Sacchi (2006). "On the effect of prestin on the electrical breakdown of cell membranes." <u>Biophys J</u> **90**(3): 967-74.

Needham, D. and R. S. Nunn (1990). "Elastic deformation and failure of lipid bilayer membranes containing cholesterol." <u>Biophys J</u> **58**(4): 997-1009.

Neher, E. and B. Sakmann (1976). "Single-channel currents recorded from membrane of denervated frog muscle fibres." <u>Nature</u> **260**(5554): 799-802.

Neher, E., B. Sakmann and J. H. Steinbach (1978). "The extracellular patch clamp: a method for resolving currents through individual open channels in biological membranes." <u>Pflugers Arch</u> **375**(2): 219-28.

Oesterhelt, F., D. Oesterhelt, M. Pfeiffer, A. Engel, H. E. Gaub and D. J. Muller (2000). "Unfolding pathways of individual bacteriorhodopsins." <u>Science</u> **288**(5463): 143-6.

Okoruwa, O. E., M. D. Weston, D. C. Sanjeevi, A. R. Millemon, B. Fritzsch, R. Hallworth and K. W. Beisel (2008). "Evolutionary insights into the unique electromotility motor of mammalian outer hair cells." <u>Evol Dev</u> **10**(3): 300-15.

Oliver, D. and B. Fakler (1999). "Expression density and functional characteristics of the outer hair cell motor protein are regulated during postnatal development in rat." J Physiol **519 Pt 3**: 791-800.

Oliver, D., D. Z. He, N. Klocker, J. Ludwig, U. Schulte, S. Waldegger, J. P. Ruppersberg, P. Dallos and B. Fakler (2001). "Intracellular anions as the voltage sensor of prestin, the outer hair cell motor protein." Science **292**(5525): 2340-3.

Ormo, M., A. B. Cubitt, K. Kallio, L. A. Gross, R. Y. Tsien and S. J. Remington (1996). "Crystal structure of the Aequorea victoria green fluorescent protein." Science **273**(5280): 1392-5.

Panchuk-Voloshina, N., R. P. Haugland, J. Bishop-Stewart, M. K. Bhalgat, P. J. Millard, F. Mao and W. Y. Leung (1999). "Alexa dyes, a series of new fluorescent dyes that yield exceptionally bright, photostable conjugates." J Histochem Cytochem **47**(9): 1179-88.

Parrott, M. B. and M. A. Barry (2000). "Metabolic biotinylation of recombinant proteins in mammalian cells and in mice." Mol Ther **1**(1): 96-104.

Parrott, M. B. and M. A. Barry (2001). "Metabolic biotinylation of secreted and cell surface proteins from mammalian cells." Biochem Biophys Res Commun **281**(4): 993-1000.

Parton, R. G. and K. Simons (1995). "Digging into caveolae." Science **269**(5229): 1398-9.

Pasqualetto, E., A. Seydel, A. Pellini and R. Battistutta (2008). "Expression, purification and characterisation of the C-terminal STAS domain of the SLC26 anion transporter prestin." Protein Expr Purif **58**(2): 249-56.

Patterson, G., R. N. Day and D. Piston (2001). "Fluorescent protein spectra." J Cell Sci **114**(Pt 5): 837-8.

Pickles, J. O. (1988). An introduction to the physiology of hearing. London ; San Diego, Academic Press.

Piran, U. and W. J. Riordan (1990). "Dissociation rate constant of the biotin-streptavidin complex." J Immunol Methods **133**(1): 141-3.

Pusch, M. and E. Neher (1988). "Rates of diffusional exchange between small cells and a measuring patch pipette." Pflugers Arch **411**(2): 204-11.

Rajagopalan, L., J. N. Greeson, A. Xia, H. Liu, A. Sturm, R. M. Raphael, A. L. Davidson, J. S. Oghalai, F. A. Pereira and W. E. Brownell (2007). "Tuning of the outer hair cell motor by membrane cholesterol." J Biol Chem **282**(50): 36659-70.

Rajagopalan, L., N. Patel, S. Madabushi, J. A. Goddard, V. Anjan, F. Lin, C. Shope, B. Farrell, O. Lichtarge, A. L. Davidson, W. E. Brownell and F. A. Pereira (2006). "Essential helix interactions in the anion transporter domain of prestin revealed by evolutionary trace analysis." J Neurosci **26**(49): 12727-34.

Raphael, R. M., A. S. Popel and W. E. Brownell (2000). "A membrane bending model of outer hair cell electromotility." Biophys J **78**(6): 2844-62.

Rekas, A., J. R. Alattia, T. Nagai, A. Miyawaki and M. Ikura (2002). "Crystal structure of venus, a yellow fluorescent protein with improved maturation and reduced environmental sensitivity." J Biol Chem **277**(52): 50573-8.

Resh, M. D. (1999). "Fatty acylation of proteins: new insights into membrane targeting of myristoylated and palmitoylated proteins." Biochim Biophys Acta **1451**(1): 1-16.

Rhode, W. S. and L. Robles (1974). "Evidence from Mossbauer experiments for nonlinear vibration in the cochlea." J Acoust Soc Am **55**(3): 588-96.

Rios, C. D., B. A. Jordan, I. Gomes and L. A. Devi (2001). "G-protein-coupled receptor dimerization: modulation of receptor function." Pharmacol Ther **92**(2-3): 71-87.

Robinson, B. H., J. Oei, M. Saunders and R. Gravel (1983). "[3H]biotin-labeled proteins in cultured human skin fibroblasts from patients with pyruvate carboxylase deficiency." J Biol Chem **258**(10): 6660-4.

Romano, C., J. K. Miller, K. Hyrc, S. Dikranian, S. Mennerick, Y. Takeuchi, M. P. Goldberg and K. L. O'Malley (2001). "Covalent and noncovalent interactions mediate metabotropic glutamate receptor mGlu5 dimerization." Mol Pharmacol **59**(1): 46-53.

Romano, C., W. L. Yang and K. L. O'Malley (1996). "Metabotropic glutamate receptor 5 is a disulfide-linked dimer." J Biol Chem **271**(45): 28612-6.

Rotman-Pikielny, P., K. Hirschberg, P. Maruvada, K. Suzuki, I. E. Royaux, E. D. Green, L. D. Kohn, J. Lippincott-Schwartz and P. M. Yen (2002). "Retention of pendrin in the endoplasmic reticulum is a major mechanism for Pendred syndrome." Hum Mol Genet **11**(21): 2625-33.

Rouached, H., P. Berthomieu, E. El Kassis, N. Cathala, V. Catherinot, G. Labesse, J. C. Davidian and P. Fourcroy (2005). "Structural and functional analysis of the C-terminal STAS (sulfate transporter and anti-sigma antagonist) domain of the Arabidopsis thaliana sulfate transporter SULTR1.2." J Biol Chem **280**(16): 15976-83.

Ryan, A. and P. Dallos (1975). "Effect of absence of cochlear outer hair cells on behavioural auditory threshold." Nature **253**(5486): 44-6.

Rybalchenko, V. and J. Santos-Sacchi (2003). "Cl- flux through a non-selective, stretch-sensitive conductance influences the outer hair cell motor of the guinea-pig." J Physiol **547**(Pt 3): 873-91.

Rybalchenko, V. and J. Santos-Sacchi (2008). "Anion control of voltage sensing by the motor protein prestin in outer hair cells." Biophys J **95**(9): 4439-47.

Saier, M. H., Jr., B. H. Eng, S. Fard, J. Garg, D. A. Haggerty, W. J. Hutchinson, D. L. Jack, E. C. Lai, H. J. Liu, D. P. Nusinew, A. M. Omar, S. S. Pao, I. T. Paulsen, J. A. Quan, M. Sliwinski, T. T. Tseng, S. Wachi and G. B. Young (1999). "Phylogenetic characterization of novel transport protein families revealed by genome analyses." Biochim Biophys Acta **1422**(1): 1-56.

Salt, A. N., I. Melichar and R. Thalmann (1987). "Mechanisms of endocochlear potential generation by stria vascularis." Laryngoscope **97**(8 Pt 1): 984-91.

Samols, D., C. G. Thornton, V. L. Murtif, G. K. Kumar, F. C. Haase and H. G. Wood (1988). "Evolutionary conservation among biotin enzymes." J Biol Chem **263**(14): 6461-4.

Santos-Sacchi, J. (1991). "Reversible inhibition of voltage-dependent outer hair cell motility and capacitance." J Neurosci **11**(10): 3096-110.

Santos-Sacchi, J. (1993). "Harmonics of outer hair cell motility." Biophys J **65**(5): 2217-27.

Santos-Sacchi, J. (2003). "New tunes from Corti's organ: the outer hair cell boogie rules." Curr Opin Neurobiol **13**(4): 459-68.

Santos-Sacchi, J., L. Song, J. Zheng and A. L. Nuttall (2006). "Control of mammalian cochlear amplification by chloride anions." J Neurosci **26**(15): 3992-8.

Santos-Sacchi, J. and M. Wu (2004). "Protein- and lipid-reactive agents alter outer hair cell lateral membrane motor charge movement." J Membr Biol **200**(2): 83-92.

Scherer, M. P. and A. W. Gummer (2005). "How many states can the motor molecule, prestin, assume in an electric field?" Biophysical Journal **88**(5): L27-L29.

Senes, A., I. Ubarretxena-Belandia and D. M. Engelman (2001). "The Calpha ---H...O hydrogen bond: a determinant of stability and specificity in transmembrane helix interactions." Proc Natl Acad Sci U S A **98**(16): 9056-61.

Shehata, W. E., W. E. Brownell and R. Dieler (1991). "Effects of salicylate on shape, electromotility and membrane characteristics of isolated outer hair cells from guinea pig cochlea." Acta Otolaryngol **111**(4): 707-18.

Shibagaki, N. and A. R. Grossman (2004). "Probing the function of STAS domains of the Arabidopsis sulfate transporters." J Biol Chem **279**(29): 30791-9.

Shibagaki, N. and A. R. Grossman (2006). "The role of the STAS domain in the function and biogenesis of a sulfate transporter as probed by random mutagenesis." J Biol Chem **281**(32): 22964-73.

Shils, M. E. and M. Shike (2006). Modern nutrition in health and disease. Philadelphia, Lippincott Williams & Wilkins.

Sigg, D., F. Bezanilla and E. Stefani (2003). "Fast gating in the Shaker K+ channel and the energy landscape of activation." Proc Natl Acad Sci U S A **100**(13): 7611-5.

Simons, K. and D. Toomre (2000). "Lipid rafts and signal transduction." Nat Rev Mol Cell Biol **1**(1): 31-9.

Sotomayor, M., D. P. Corey and K. Schulten (2005). "In search of the hair-cell gating spring elastic properties of ankyrin and cadherin repeats." Structure (Camb) 13(4): 669-82.

Souter, M., G. Nevill and A. Forge (1995). "Postnatal development of membrane specialisations of gerbil outer hair cells." Hear Res 91(1-2): 43-62.

Spector, A. A., N. Deo, K. Grosh, J. T. Ratnanather and R. M. Raphael (2006). "Electromechanical models of the outer hair cell composite membrane." J Membr Biol 209(2-3): 135-52.

Spencer, D. M., T. J. Wandless, S. L. Schreiber and G. R. Crabtree (1993). "Controlling signal transduction with synthetic ligands." Science 262(5136): 1019-24.

Sturm, A. K., L. Rajagopalan, D. Yoo, W. E. Brownell and F. A. Pereira (2007). "Functional expression and microdomain localization of prestin in cultured cells." Otolaryngol Head Neck Surg 136(3): 434-9.

Takahashi, S. and J. Santos-Sacchi (2001). "Non-uniform mapping of stress-induced, motility-related charge movement in the outer hair cell plasma membrane." Pflugers Arch 441(4): 506-13.

Tannous, B. A., J. Grimm, K. F. Perry, J. W. Chen, R. Weissleder and X. O. Breakefield (2006). "Metabolic biotinylation of cell surface receptors for in vivo imaging." Nat Methods 3(5): 391-6.

Tanuj Sapra, K., P. S. Park, S. Filipek, A. Engel, D. J. Muller and K. Palczewski (2006). "Detecting Molecular Interactions that Stabilize Native Bovine Rhodopsin." J Mol Biol 358(1): 255-69.

Thomas, P. and T. G. Smart (2005). "HEK293 cell line: a vehicle for the expression of recombinant proteins." J Pharmacol Toxicol Methods 51(3): 187-200.

Toth, T., L. Deak, F. Fazakas, J. Zheng, L. Muszbek and I. Sziklai (2007). "A new mutation in the human pres gene and its effect on prestin function." Int J Mol Med 20(4): 545-50.

Tsien, R. Y. (1998). "The green fluorescent protein." Annu Rev Biochem 67: 509-44.

Tunstall, M. J., J. E. Gale and J. F. Ashmore (1995). "Action of salicylate on membrane capacitance of outer hair cells from the guinea-pig cochlea." J Physiol 485 (Pt 3): 739-52.

van Iwaarden, P. R., A. J. Driessen and W. N. Konings (1992). "What we can learn from the effects of thiol reagents on transport proteins." Biochim Biophys Acta 1113(2): 161-70.

Von Bâekâesy, G. (1960). Experiments in hearing. New York,, McGraw-Hill.

Waldegger, S., I. Moschen, A. Ramirez, R. J. Smith, H. Ayadi, F. Lang and C. Kubisch (2001). "Cloning and characterization of SLC26A6, a novel member of the solute carrier 26 gene family." Genomics 72(1): 43-50.

Wessel, D. and U. I. Flugge (1984). "A method for the quantitative recovery of protein in dilute solution in the presence of detergents and lipids." Anal Biochem 138(1): 141-3.

Wever, E. G. and C. W. Bray (1930). "Auditory Nerve Impulses." Science 71(1834): 215.

Wu, X., B. Currall, T. Yamashita, L. L. Parker, R. Hallworth and J. Zuo (2007). "Prestin-prestin and prestin-GLUT5 interactions in HEK293T cells." Dev Neurobiol 67(4): 483-97.

Yang, F., L. G. Moss and G. N. Phillips, Jr. (1996). "The molecular structure of green fluorescent protein." Nat Biotechnol 14(10): 1246-51.

Zacharias, D. A. (2002). "Sticky caveats in an otherwise glowing report: oligomerizing fluorescent proteins and their use in cell biology." Sci STKE 2002(131): PE23.

Zamyatnin, A. A. (1972). "Protein volume in solution." Prog Biophys Mol Biol 24: 107-23.

Zeng, F. Y. and J. Wess (1999). "Identification and molecular characterization of m3 muscarinic receptor dimers." J Biol Chem 274(27): 19487-97.

Zhang, J., T. Tackaberry, M. W. Ritzel, T. Raborn, G. Barron, S. A. Baldwin, J. D. Young and C. E. Cass (2006). "Cysteine-accessibility analysis of transmembrane

domains 11-13 of human concentrative nucleoside transporter 3." <u>Biochem J</u> **394**(Pt 2): 389-98.

Zhang, R., F. Qian, L. Rajagopalan, F. A. Pereira, W. E. Brownell and B. Anvari (2007). "Prestin modulates mechanics and electromechanical force of the plasma membrane." <u>Biophys J</u> **93**(1): L07-9.

Zheng, J., C. T. Anderson, K. K. Miller, M. Cheatham and P. Dallos (2009). "Identifying components of the hair-cell interactome involved in cochlear amplification." <u>BMC Genomics</u> **10**(1): 127.

Zheng, J., G. G. Du, C. T. Anderson, J. P. Keller, A. Orem, P. Dallos and M. Cheatham (2006). "Analysis of the oligomeric structure of the motor protein prestin." <u>J Biol Chem</u> **281**(29): 19916-24.

Zheng, J., G. G. Du, K. Matsuda, A. Orem, S. Aguinaga, L. Deak, E. Navarrete, L. D. Madison and P. Dallos (2005). "The C-terminus of prestin influences nonlinear capacitance and plasma membrane targeting." <u>J Cell Sci</u> **118**(Pt 13): 2987-96.

Zheng, J., K. B. Long, W. Shen, L. D. Madison and P. Dallos (2001). "Prestin topology: localization of protein epitopes in relation to the plasma membrane." <u>Neuroreport</u> **12**(9): 1929-35.

Zheng, J., W. Shen, D. Z. He, K. B. Long, L. D. Madison and P. Dallos (2000). "Prestin is the motor protein of cochlear outer hair cells." <u>Nature</u> **405**(6783): 149-55.